PART 6c

Calorimetry

TABLE OF CONTENTS, PART 6c

LIST OF FIGURES, PART 6c

LIST OF FIGURES, PART 6c
(Continued)

LIST OF TABLES, PART 6c

6c.0 Summary of Calorimetry

A summary of this work appears in section 6.0.

6c.1 Introduction

This investigation is a part of the study [11, 19, 26, 27, 35, 42, 47] conducted at the Institute of Gas Technology to obtain the necessary information needed to design an efficient coal hydrogasification plant.

Until this investigation was undertaken, the heatof the coal hydrogasification reaction was determined only by calculation. These calculations became more precise as more data became available; however, no measurements were made to check the validity of the calculated data.

Initially, in the absence of accurate pilot plant yield data, the heat of reaction was estimated by assuming that coal and carbon were equivalent and that the hydrogasification reaction could be approximated by:[18, 36]

$$C + 2H_2 \rightarrow CH_4 \qquad (1)$$

Although very crude, this approach could not be expected to provide an accurate answer; it has proven useful to compare thermal efficiencies of various gasification processes.

In a subsequent approach utilizing pilot plant data, [35] the heat of reaction was calculated from the heats of combustion of the reactants and products. Accurate values for the heats of combustion of various coals could be obtained directly utilizing a Parr-bomb calorimeter, or calculated by the modified Dulong formula; however, these techniques have two limitations. First, the calculation involves the difference between large numbers of the same order of magnitude. As a result, chemical analyses of all reactants and products must be very accurate, and pilot material balances must be quite close to 100 percent or the balance must be forced. If the precision implied is not maintained, large errors can be made in the calculation. As a result, the calculated heat of reaction is dependent on the quality of the analytical data, and on the method used to force the balance.

To illustrate this point further, an example is given below.

$$CaO + 1/2O_2 \overset{\Delta H_R}{\rightleftarrows} CaO_2$$

$-\Delta H_f$, Kcal/g mol (25°F)	151.5 ± 0.5	157.5 ± 0.5	(2)

$$\Delta H_R = (-157.5 \pm 0.5) - (-151.5 \pm 0.5)$$

$$= -6 \pm 0.7 \text{ Kcal/g mol}$$

The heats of formation for CaO and CaO_2 were determined to within 0.32% of the NBS value[22, 38]; however, the resulting uncertainty of the heat of reaction determined by the use of Hess' rule[23] — a relatively simple calculation — is about 12% for this case.

The second limitation is that the calculated heat of reaction is determined for 25°C; therefore, no information is obtained on the reaction heat at actual reaction temperature.

Normally, if the heat of reaction could be determined at one temperature, the heat of reaction at various temperatures could be calculated from heat capacity data. Although some heat capacity data are available in the literature for coals and cokes, none are available for the particular coals used here, which prohibits a mathematical projection.

For these reasons, therefore, in the IGT work, thermal data are determined directly, at the pressure and temperature where a reaction occurs.

In considering the heterogeneous reactions in which a gas contacts and reacts with a solid thereby producing reaction products it is necessary to consider all the factors controlling reaction rates. The heat of reaction is not just a function of temperature and pressure but also a function of particle size, feed gas composition and particle distribution. Therefore, other factors to be considered are gas film diffusion, ash diffusion or the chemical reaction to determine the controlling step. For this study the typical HYGAS coal particle size ranging from −20 to +325 mesh was selected for testing and hydrogen was used as the feed gas.

The results obtained from this investigation are sufficient for a specific application but should not be used for general analysis or correlation for all applications. To achieve a generalized correlation suitable for providing design information to any coal gasification process, the following areas require further investigation:

- Effect of particle size of various coals and chars on the heat of reaction,
- Various feed mixtures representing the compositions existing in the coal gasification processes must be studied for the temperatures and pressures in which they operate, and
- Feed particle residence time distribution must be studied because the heat of reaction depends on the degree of gasification on each particle because it is impossible to obtain uniform feed particle size.

6c.2 Instrument Description

6c.2.1 Heat-of-Reaction Calorimeter

The heat-of-reaction calorimeter is designed and constructed to measure the heat of reaction for a temperature range of 100° to 1500°F, and a pressure range of 0 to 1500 psia. The calorimeter can measure heats of both gas-solid

and gas-liquid reactions. Means also are provided to take the gas sample produced by the reaction. Figure 6c-1 is the assembly drawing of this instrument. Figure 6c-2 is a photograph of the control console.

The calorimeter body (Figure 6c-1, item 7), in which the reaction takes place, is a pressure vessel of a super alloy which retains its strength at high temperatures and pressures*. The body is surrounded by resistance elements. The guard isplaced in a water-cooled outer can and all cavities are filled with microquartz to minimize radiant heat loss. In addition, a partial vaccum is applied to the entire unit outside of the calorimeter body to minimize convection heat loss. The heating elements are operated by a proportional controller; temperatures are monitored by platinum resistance and/or chromel-alumel thermocouples. Figure 6c-3 shows the position of all thermocouples. All operating instruments are remote controlled so that the calorimeter is shielded from temperature influence by the operator and the control console.

Prior to reaction, the sample is stored in a cold zone (70° to 72°F) in the neck of the calorimeter (Figure 6c-1, item 2). When the calorimeter has reached thermal equilibrium with the heater guard and pressure has stabilized, the sample is lowered into the calorimeter body. The temperature change of the calorimeter body is monitored and related to the heat of reaction by the calibration constant.

In order to prevent convection and conduction losses up the neck, a transition heater (Figure 6c-1, item 9) is placed above the body. The heater is maintained at a temperature which will keep the body temperature constant. Convection losses are further minimized by baskets of insulation (Figure 6c-1, item 8); however, this insulation proved unnecessary after it had been installed. The sample is lowered into the body by a remotely-operated motor-driven mechanism (Figure 6c-1, item 1) which is stopped automatically by a cam-operated switch.

6c.2.2 Drop Calorimeter

The IGT drop calorimeter is designed to measure the heat capacity of a solid. The calorimeter consists basically of a furnace to heat the test sample, a receiver into which the sample is dropped, an isothermal environment surrounding the insulated receiver, a drop mechanism, the control instrumentation and readout instrumentation, all contained in one cabinet.

The instrument assembly drawing in Figure 6c-4 shows the general design features and the arrangement of the major components.

The furnace (Figure 6c-4, item 1) is a tubular, wound resistance element surrounded by insulation and contained in an air-cooled shell. The furnace is mounted vertically on a support post (item 2) which permits the furnace to be rotated, providing access to the receiver (item 3). The furnace heating element is wound in such a way that the unit provides a centrally located constant (± 0.5°F) temperature zone 2 inches in diameter by 5 inches long.

---

* High-chromium/nickel/cobalt Uniloy N-155.

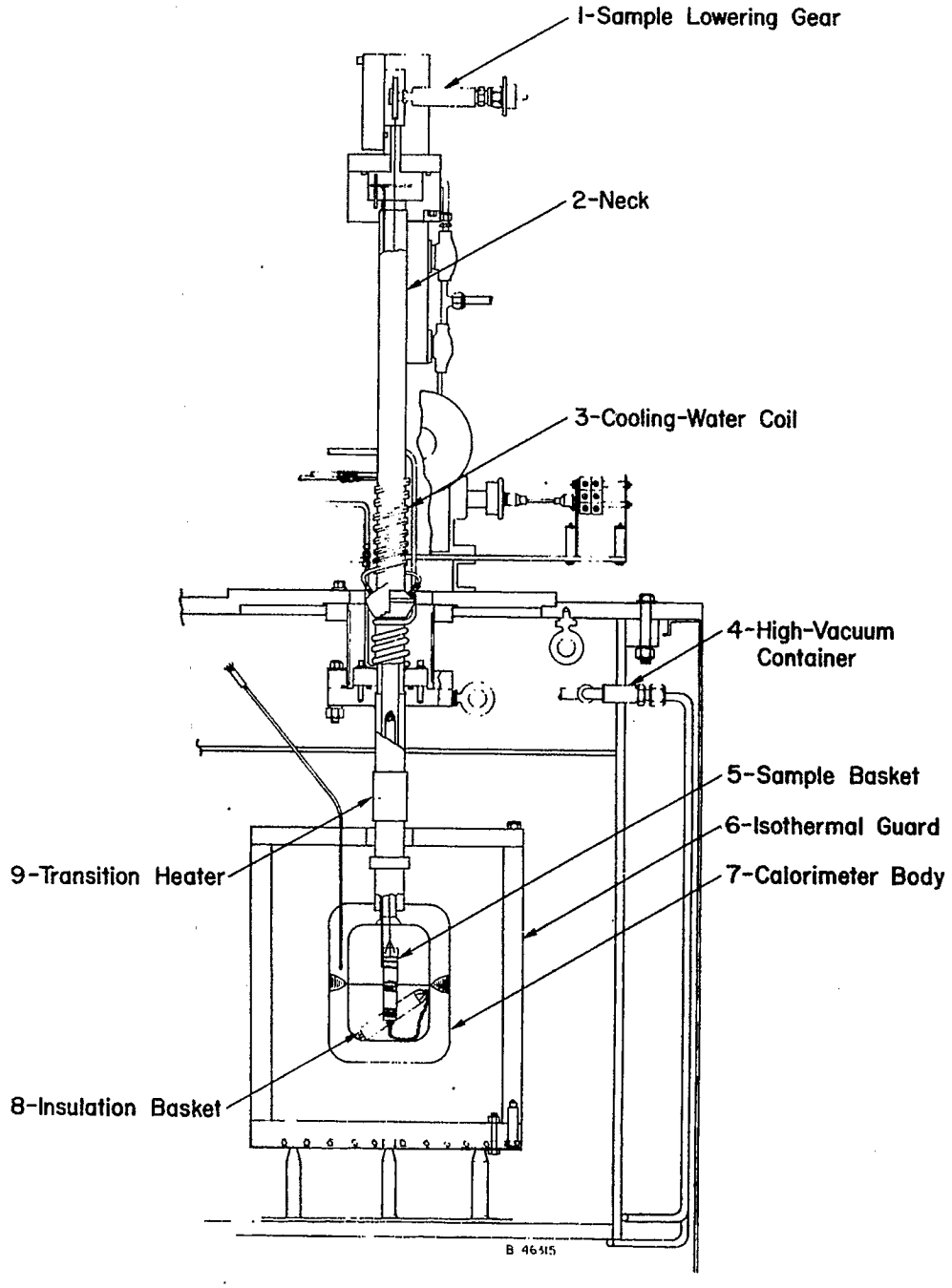

Figure 6c-1. IGT HEAT-OF-REACTION CALORIMETER DESIGNED AND BUILT FOR HYGAS CALORIMETRY RESEARCH

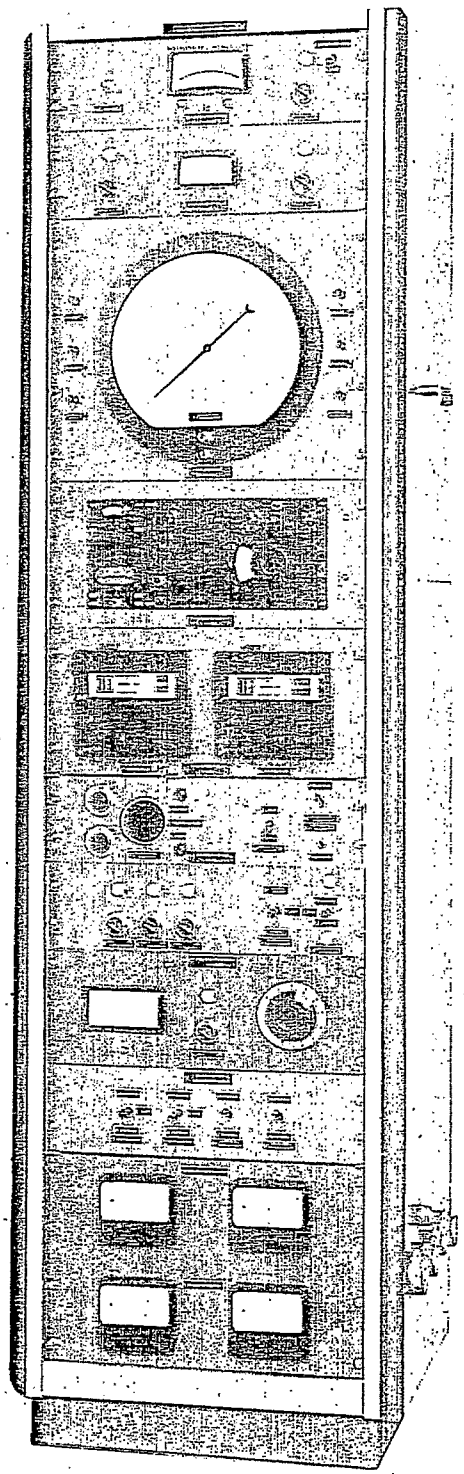

P7506 1397

Figure 6c-2. CONTROL CONSOLE FOR THE IGT HEAT-OF-REACTION AND DROP CALORIMETERS UTILIZED IN THE HYGAS PYROLYSIS RESEARCH

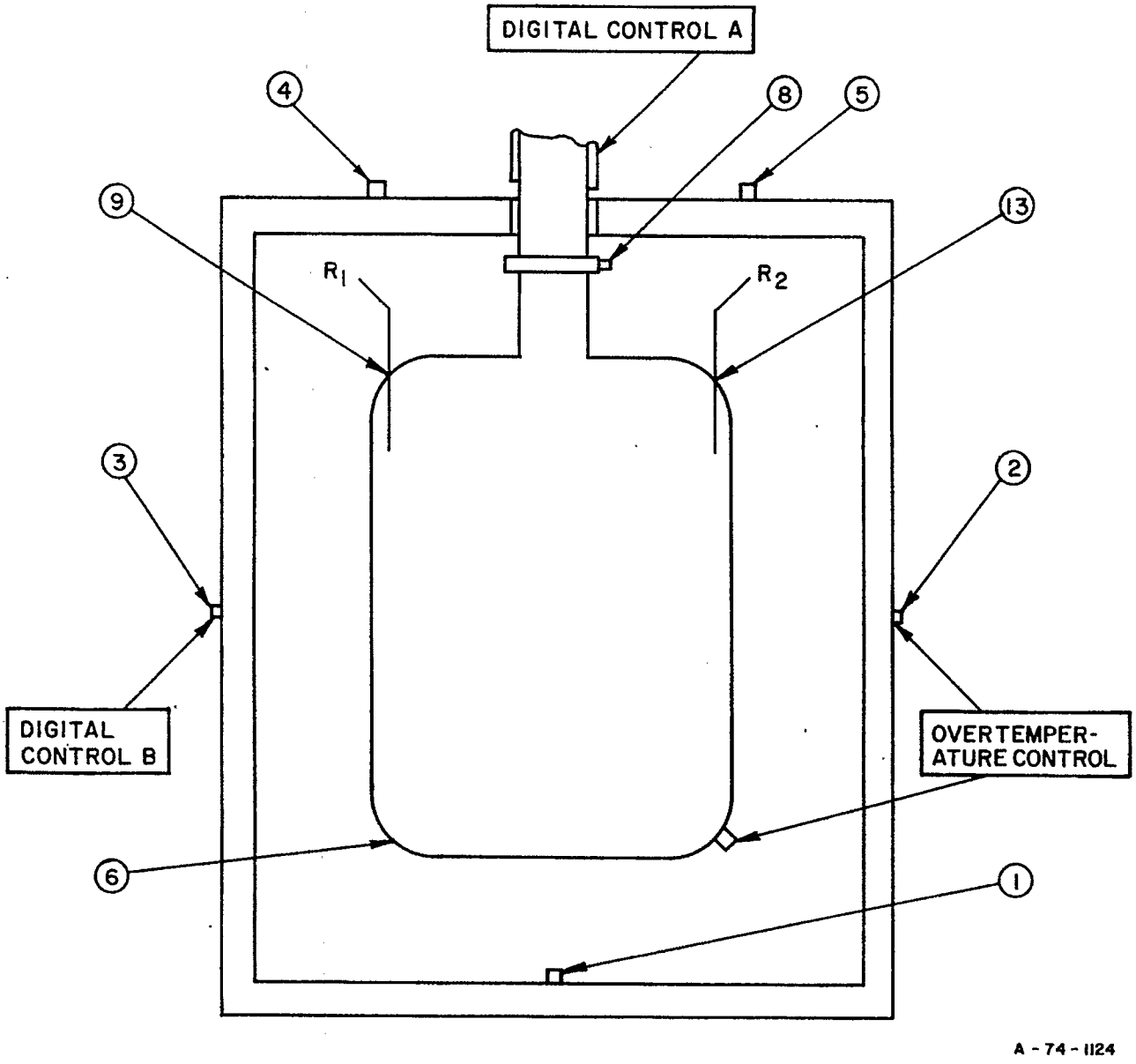

Figure 6c-3. THERMOCOUPLE POSITIONS (NUMBERS) FOR THE HEAT-OF-REACTION CALORIMETER UTILIZED IN HYGAS PYROLYSIS RESEARCH

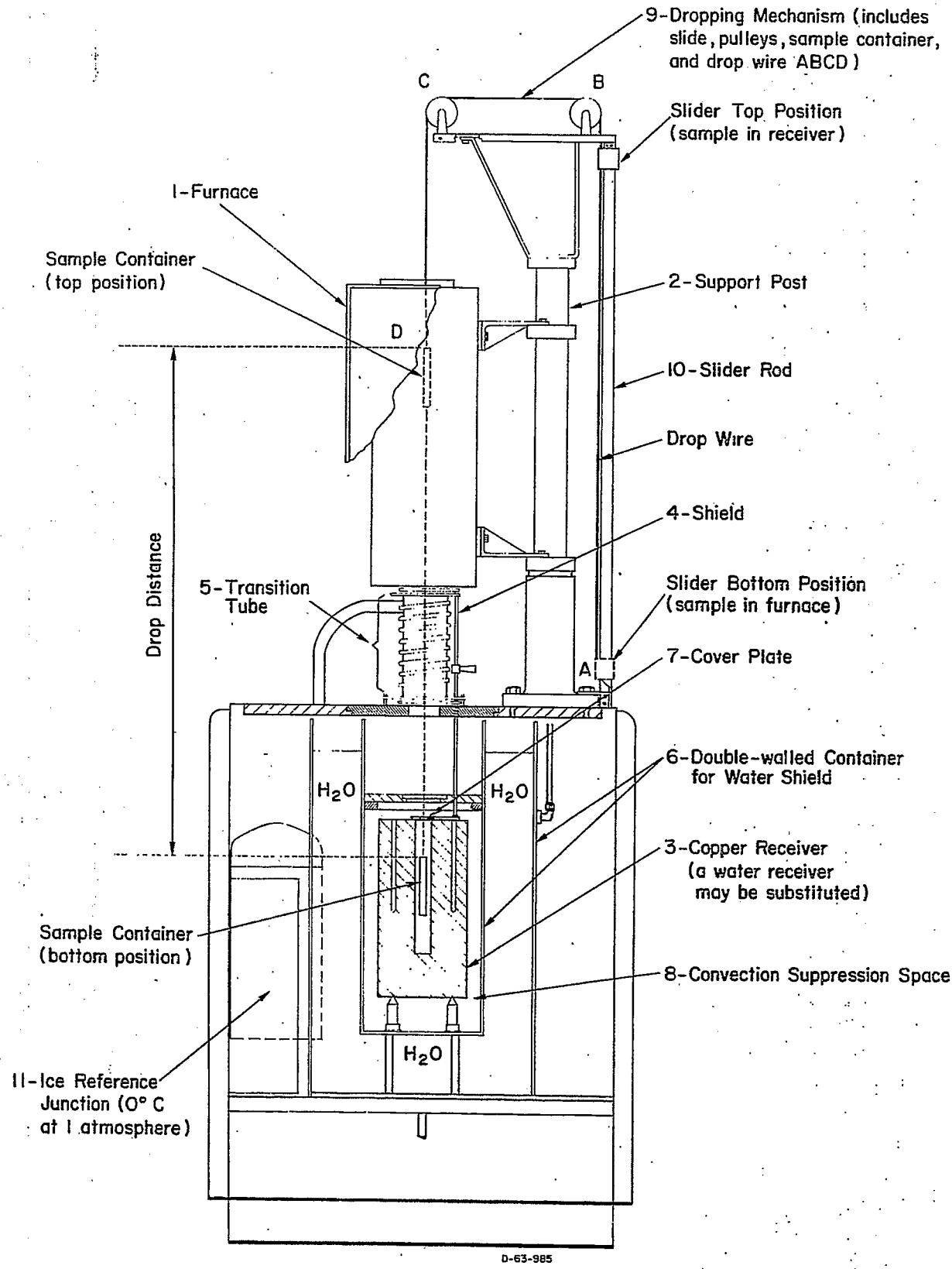

Figure 6c-4. DROP CALORIMETER DESIGNED AND BUILT FOR HYGAS CALORIMETRY RESEARCH

The radiant heat exchange between the furnace and receiver is minimized by use of two shields (item 4) located directly below the furnace. The heat leak from the top of the furnace is reduced by use of a ceramic insulating plug.

The drop calorimeter is designed for use with either a water receiver or a copper receiver (item 3). The use of the water receiver is limited to sample drop temperatures of approximately 300°F. Above this temperature the sample causes violent local boiling as it penetrates the water surface, thus losing a portion of its enthalpy in latent heat. This can cause appreciable inaccuracies in the test data. The copper receiver may be used for all tests from room temperature to 2000°F; however, sample drops below 300°F generally cause a very small rise in the receiver temperature, leading to inaccuracies in the test results.

Either receiver can be placed directly below the furnace and contained within an isothermal environment. Both receivers have provisions for temperature measurement, either by means of a five- or ten-junction thermopile or a differential thermometer. The water bath receiver can be fitted with a stirrer, which gently agitates the water to maintain uniform temperature throughout.

A transition tube (item 5) located between the furnace and the receiver, ensures that the effects of heat loss from the sample during its drop are equal for all drops, independent of room drafts.

The receiver is surrounded by an isothermal environment. This environment consists of a double-walled container (item 6) and a cover plate (item 7). The annulus between the walls of the container is filled with water to dampen the effects of ambient temperature change. If severe ambient temperature changes are encountered, ice water may be used in this annulus to maintain the receiver environment at 0°C. The area inside the container (item 8) and immediately surrounding the receiver is so sized that it suppresses natural convection, thus reducing heat loss from the side of the receiver. A convection shield covering the receiver opening eliminates heat loss from the receiver cavity during a test.

The dropping mechanism (item 9) located above the furnace consists of a double-pulley arrangement and a drop wire. The drop wire extends over the pulleys and is guided along a vertical slide-rod (item 10) located adjacent to the furnace support. This system allows return of the sample to the furnace after each test while offering a minimum of resistance to the wire when the sample is dropped.

The controls and readout instrumentation are located in the control console (Figure 6c-2) which also operates the IGT heat of reaction calorimeter. This console contains separate controllers for each of the two IGT calorimeters. Two cables connect the drop calorimeter to the control console.

The readout instrumentation consists of chromel-alumel thermocouples which measure the sample temperature in the furnace; a five- or ten-junction copper/constantan thermopile or differential thermometer which measures the temperature rise in the receiver; and a time-buzzer which indicates 30-second time intervals.

The sample thermocouple and the receiver thermopile are both referenced to a mixture of ice and water at 32°F (Figure 6c-4, item 11) and may be read on a potentiometer. A jack at the front of the cabinet connects a potentiometer to the thermocouples. A selector switch on the front panel permits the use of the potentiometer to monitor temperatures of either the sample thermocouple or the receiver thermopile without altering circuitry.

6c.3 Test Procedures

6c.3.1 Heat of Reaction Calorimeter

Before power is supplied to the control console, all switches are turned off. After power is supplied, the vacuum pump and vacuum gage are turned on, and the main vacuum valve is fully opened. If there are no leaks in the vacuum system, the gage should indicate about 50 microns after 4 hours of pumping.

The calorimeter is pressure-tested to 1500 psia for leaks using an inert gas such as N_2 or He. After pressure testing and venting, the calorimeter is evacuated to 5 microns using the sample vacuum pump.

All thermocouples are checked for continuity, and should read about room temperature. The coolant water valve is then opened to permit a flow of about 1 gallon per minute to circulate through both coolant and circuit lines. The overtemperature control is set at 100°F above the expected operating temperature. The heaters on the guard are now ready to be tested. The Digiset temperature controller is dialed to 0 and the current limit on the power supply, SCR, is turned full counterclockwise (a detailed discussion is presented in the instrument manual). The controller switch on the console is switched to the "up" position; the guard voltage should indicate about 120v. The "reaction cal heater circuit" switch is placed in the "down" position causing the guard voltage to drop to a low level indicating a small current on the ammeter. The controller is now dialed up slowly until the indicator needle swings through the null position to the left. If there are no shortcircuits and the heaters are connected properly, the voltage current ratio should be 2Ω.

During the beginning of the heatup, the voltage and current should not exceed 60v and 25α on the guard and 50v and 8α on the transition zone. Excessive power input will cause a shortcircuit or burn up the heaters.

When the calorimeter has achieved steady state, it is pressurized by the desired gas. Care is necessary, due to potential hazards if established procedures are not followed and if work is not closely monitored. For example, although a safety relief valve is set to release at 1600 psia, a gas such as hydrogen released into the laboratory would be hazardous.

After pressurization, a period of 4 to 6 hours must elapse before the calorimeter reaches equilibrium. All thermocouples are closely monitored throughout the stabilizing period. The system vacuum may reach 75 to 100 microns as a result of hydrogen diffusion through the wall of the calorimeter. If the vacuum is more than 100 microns, two checks must be made, one for leaks and a second to determine that the vacuum pump is functioning properly.

Two hours after steady state has been reached, the sample is lowered into the calorimeter body. The temperature is then monitored by the thermocouples (Figure 6c-3, items 6, 7, 9, and 13) and/or by the resistance thermometers (Figure 6c-3, R_1 and R_2). Readings should be taken every minute for the first 3 minutes, every 3 minutes for the next 9 minutes, and every 10 minutes thereafter.

The experiment may be stopped at any time by lifting the solid sample into the cold neck zone. The gas sample is collected in the sampling vessel for analysis, and the solid sample is collected after venting off the pressure.

6c.3.2 Drop Calorimeter

When the proper receiver has been chosen (as described in Section 6c-2), it is placed in the internal container of the calorimeter.

The copper receiver contains a circular groove on its base which mates with three Plexiglas support pins in the bottom of the calorimeter. The water receiver is designed to rest in the area bounded by the three support pins.

Once the receiver is in place, the two, five-junction thermopiles are inserted. If the water receiver is used, the junction thermopile is inserted into a glass tube before immersion into the water. The thermopile measures the initial and final temperatures of the receiver as well as the time temperature-change of the receiver. When the water receiver is utilized, the stirrer and motor are placed on the calorimeter cover before the cover is positioned. The differential thermometer then is inserted in the receiver, passing through a hole in the cover.

The furnace is rotated into position so that alignment is ensured between the furnace, the sample protection tube, and the receiver. The sample support wire — a high-temperature wire supplied with the instrument — is passed through the furnace top cover and attached to a carefully weighed sample in the transition zone, while the sample protection tube is temporarily removed.

The support wire is attached at the end of the slider located on the slide rod which is attached to the support post. The length of the support wire ABCD (Figure 6c-4) is measured so that the sample is resting at the receiver bottom when the slider is at the top of the slide rod, and the sample is in the central 2 inches of the furnace when the slider is fixed at the bottom of the slide rod. The difference in elevation of the two positions described comprises the length of the "drop".

When the sample is in the center of the furnace, the radiation shield is closed and the sample protection is set into place. The actual series of tests may now be performed.

The desired sample temperature is set on the temperature controller by dialing the Digiset to the corresponding electromagnetic force. The main power switch is then turned on and the temperature controller guides the furnace to the desired temperature.

When the furnace reaches the desired temperature, the timer switch is turned on and both the sample and the receiver temperature are monitored for approximately 10 to 20 minutes. At a time when the sample temperature is not varying by more than 0.25%, the radiation shield is opened and the sample is released. The sample is released by depressing the sample release lever, which allows the slider to pass freely. When the sample has reached the bottom of the receiver, the radiation shields and receiver cover are closed.

Once the sample is positioned in the receiver, readings are transcribed at 30-second intervals. A sharp change in temperature immediately following the drop and a gradual leveling off of the time temperature plot is characteristic in the drop calorimeter test. The test is continued for about 1 hour after the temperature plot begins to decline.

In the final step, the sample is reweighed, 1) to ensure the reliability of the initial measurement, or 2) to determine whether weight was lost during the test. The pertinent information for each test is recorded on a standard data sheet. A sample of the receiver calibration and a standard test utilizing an Al_2O_3 sample are shown in the sections which follow.

6c.4 Calorimeter Calibration

One of the experimental difficulties introduced by the use of a high-pressure calorimeter is its large wall thickness. The thermal conductivity of the super-alloy Uniloy-155 is about one-sixth that of brass. This 1-in. thick wall and low thermal conductivity cause a large thermal lag which makes the analysis of experimental results unusually tedious.

There are a number of methods to calibrate the calorimeter constant, termed the mass-heat capacity product, or mCp. More commonly used calibration methods include:

1) direct calculation from known mass and heat capacity of calorimeter,
2) chemical reaction calibration,
3) drop method, and
4) electrical calibration.

All these methods were used in the calibration of this instrument and are discussed in the following sections. The background on calorimetry is presented in Appendix 6c-A.

6c.4.1 Direct Calculation from Known Mass and Heat Capacity of Calorimeter Material

This calibration technique is the poorest of the four employed because of the large wall area and its thickness, and the poor thermal conductivity of the metal. The measured calorimeter mCp does not match that obtained by calculation, especially at unsteady-state heat-transfer. Nevertheless, calculations were made and the results can be used as a guide post. The mass of the calorimeter is calculated from the density and dimension. The heat capacity of the calorimeter metal is determined in the drop calorimeter and presented in Figure 6c-5.

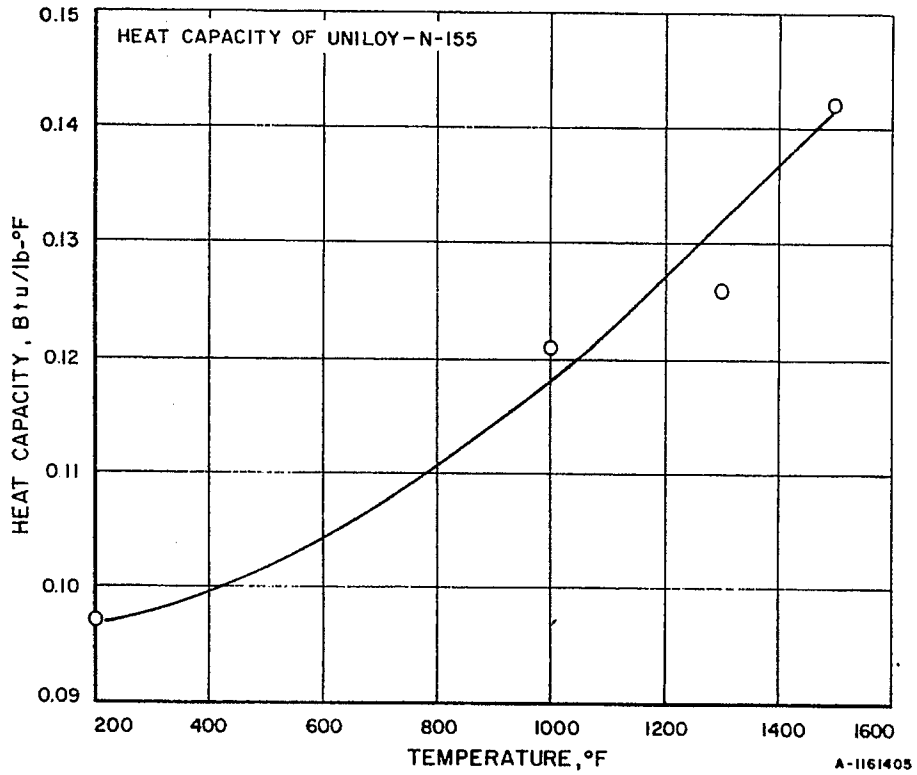

Figure 6c-5. MEAN HEAT CAPACITY OF CALORIMETER (From 70°F to Temperatures Indicated)

The calculated mCp are presented in Figure 6c-6 and compared with the mCp obtained with other methods.

6c.4.2 Chemical Reaction Calibration

This method requires the knowledge of the heat capacity (Cp) of reactants and products, and an accurate mass balance, a composition analysis, and the heat-of-formation (Hf) of all components. In this work, n-decane was used with hydrogen at 1360 psia and about 1500°F. The results are summarized as follows:

Temperature of calorimeter body	1482°F
Temperature change due to reaction	5.27°F
Initial sample temperature	70°F
Mass of sample	9.18 g 0.0202 lb
Mass of container	13.97 g 0.0308 lb
Mass of basket	18.42 g 0.0406 lb
Cp n-decane	0.6 Btu/°F-lb
Cp glass container	0.26 Btu/°F-lb
Cp basket	0.12 Btu/°F-lb
(H_R) heat of reaction based on H_f mass balance)	3223 Btu/lb

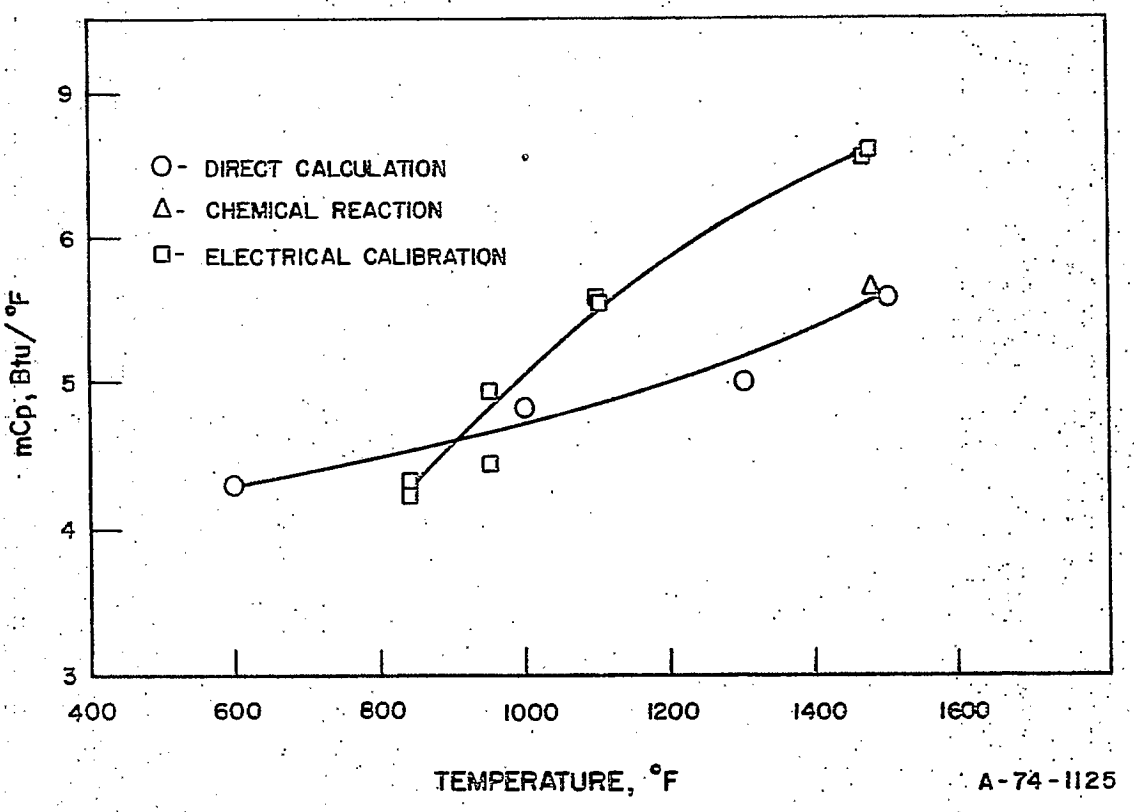

Figure 6c-6. COMPARISON OF VARIOUS CALIBRATION TECHNIQUES FOR THE HEAT-OF-REACTION CALORIMETER UTILIZED IN THE HYGAS CALORIMETRY RESEARCH

The heat balance equation is:

$$m_{sample}\left[H_R - (Cp\,\Delta T)_{sample}\right] - (mCp\,\Delta T)_{container} - (mCp\,\Delta T)_{basket} = (mCp\,\Delta T)_{calorimeter}$$

Solve for:

$$mCp_{calorimeter} = 5.66 \quad Btu/°F \qquad (3)$$

This calibration was carried out at high temperatures for two reasons: 1) the reaction does not take place at lower temperatures, and 2) the mass balance was poor due to the deposit of carbon. However, this calibration serves the following purposes:

1) It tests the effect of an exothermic reaction,

2) It provides a check of the (mCp) calorimeter determined by the other methods, by comparison of the heat-of-reaction of hydrogen and n-decane, and

3) It indicates the sensitivity of the calorimeter and precision of measurement.

6c.4.3 Drop Method

This is the most widely used method to determine $mCp_{calorimeter}$ [21,31,32,45]. The mCp calorimeter is determined by the temperature change of the calorimeter produced by the addition to the calorimeter of a known material of a known mass and heat capacity. Although this method can be used to calibrate for either an endothermic or an exothermic reaction, it is far more accurate for the calibration of endothermic reaction in this case. The results of this calibration are presented in Figure 6c-7. Al_2O_3 was used because the Cp of Al_2O_3 is well established[13] and is in the same range as that of coal. (Detailed discussion is presented in Section 6c.7.)

6c.4.4 Electrical Calibration

With this method, a known mount of electrical energy is put into the calorimeter and the resulting temperature change is observed. Electrical calibration is used only in preparation for calorimetry involving an exothermic reaction. The energy source should be a direct current source with a constant voltage supply, so that the amount of current through the external circuit remains constant regardless of the change of the resistance of the external circuit.

The calorimeter constant is calculated from a heat balance on the calorimeter body, as expressed in the following equation:

$$(mCp\,\Delta T)_{calorimeter} X\,(mCp\,\Delta T)_{heater} = (Pt)_{in} - L \qquad (4)$$

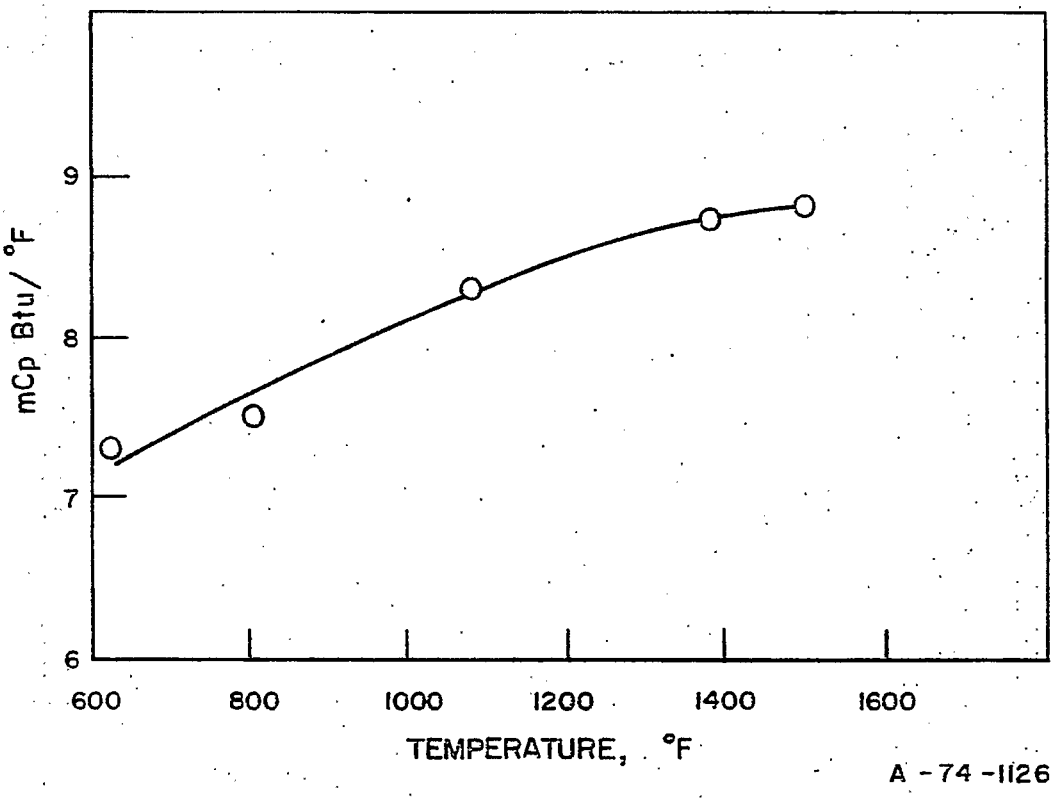

Figure 6c-7. CALIBRATION OF THE DROP CALORIMETER WITH ALUMINUM OXIDE

where

$(Pt)_{in}$ = power input 3.413 IVt

IV= volt amp input

t = heating time

L= losses

The results of this calibration are presented and compared with other results in Figure 6c-6. The calculation procedures are presented in Appendix 6c-B.

6c.5 Heat of Reaction of Hydrogen and Coal

The majority of work involving the heat of reaction of hydrogen and coal was concentrated on the study of a high volatile content bituminous coal from the Ireland mine's Pittsburgh No. 8 seam. Samples involved a size range of −20 to +325 mesh, the pretreated coal, the residue from the low-temperature stage of the hydrogasifier, and the residue from the high-temperature stage of the hydrogasifier. Some studies also were made on West Virginia Sewell coal (Sewell No. 1 mine), West Virginia Block No. 5 coal (Kanawha Mine), Illinois No. 6 coal, Colorado subbituminous coal, and North Dakota lignite.

Because coals decompose when heated, the major problem encountered is prereaction when determining the heat of coal reactions at high temperature and high pressure. Meaningful results can be obtained only if the coal and hydrogen react at conditions at which the desired temperature and pressure are stabilized. Therefore, the method of introducing the sample to the reaction condition is critical.

The coal must not react before the conditions are set, and the pressure must not be disturbed when the coal is introduced.

The present method is to keep the sample at room temperature inside the calorimeter drop tube so that the reaction will not take place prematurely.

Convection shields are installed to prevent a large heat loss from convection, and to ensure that the sample is in a cold zone while the calorimeter is being stabilized at the reaction conditions. The temperature of the sample while it is in the drop tube has been monitored for a period of four days and is established at 70° to 72°F, regardless of the temperature of the calorimeter body.

It was necessary to establish a heat balance around the calorimeter in order to provide sufficiently valid data with which to calculate from experimental data. The heat balance could be calculated by the equation:

$$\Delta\overline{H}_R + h_{in} = (mCp\Delta T)_{calorimeter} + (mCp\Delta T)_{shield} + (mCp\Delta T)_{chain} \quad (5)$$

$$+ (mCp\Delta T)_{basket} + (mCp\Delta T)_{coal}$$

where:

$\Delta\overline{H}_R$ = heat of reaction

h_{in} = heat input from the neck heater

m = mass

C_p = heat capacity

ΔT = temperature change

Each term in Equation 5 must be established by calibration, or must be accurately measured. For exothermic heat of reaction, the effective mCp of the reaction calorimeter was calibrated by a constant heat input technique in a hydrogen atmosphere at 1000 psia and with temperatures from 840° to 1460°F.

After the calorimeter constants were determined, the effective $(mCp\Delta T)$'s of the convection shield, the chain, and the empty sample basket were calibrated in the calorimeter to determine the change of heat input with time, as shown in Equation 6:

$$K(\theta)\int_o^\theta (mCp\Delta T)_{\substack{\text{empty}\\ \text{calorimeter}}} d\theta = \int_o^\theta [(h_{in} - (mCp\Delta T)_{shield} - (mCp\Delta T)_{chain} - (mCp\Delta T)_{basket})]\, d\theta \quad (6)$$

where: $K(\theta)$ = a constant dependent only on time

θ = time

Combining equations 5 and 6, we have:

$$\Delta\overline{H}_R = (mCp\Delta T)_{calorimeter} + (mCp\Delta T)_{coal} - K(\theta) \quad (7)$$

Equation 7 was used to calculate the heat-of-reaction data reported in this paper. The heat transfer analysis of the Heat-of-Reaction calorimeter is presented in Appendix 6c-C.

Table 6c-1 presents the coal and char analyses of Ireland Mine coal before the hydrogen reaction occurs, and of other coals in pretreated state. Table 6c-2 presents the heat of reaction of hydrogen and coal at 1300°F and 1000 psia (simulating conditions of the first stage in the HYGAS pilot plant reactor). Table 6c-3 presents the results at 1500°F and 1000 psia (simulating conditions of the second stage in the HYGAS pilot plant reactor). Table 6c-4 presents the heat of reaction of coals other than that of the Ireland Mine.

Data from a typical experimental run are shown in Figure 6c-8, and the heats of reaction of hydrogen and coal chars at various percentages reacted are presented in Figures 6c-9, 6c-10, and 6c-11.

Table 6c-1. PREHYDROGENATION AND PRETREATED COAL ANALYSES

	Ireland-Mine-Coal Analyses Before Hydrogen Reaction				Analyses of Pretreated Feed From Other Mines				
	Raw Coal	Pretreated Coal	Low-Temp Residue	High-Temp Residue	Illinois	West Virginia Sewell	West Virginia Block No. 5	Colorado	North Dakota Lignite
Proximate Analysis (wt%)									
Moisture	1.3	0.5	0.6	0.6	4.8	1.3	3.0	1.6	[illegible]
Volatiles	34.6	23.3	4.6	3.3	25.4	16.7	23.1	32.5	28.4
Fixed Carbon	52.0	63.5	77.6	71.6	62.3	80.5	66.4	61.1	31.3
Ash	12.1	12.7	17.2	24.5	7.5	1.5	7.5	4.6	6.3
Total	100.0	100.0	100.0	100.0	100.0	100.0	100.0	[illegible]	[illegible]
Ultimate Analysis (wt)									
Carbon	71.2	70.1	76.9	72.52	70.5	84.5	75.3	73.1	64.8
Hydrogen	5.14	3.70	2.05	1.08	3.65	3.37	3.80	3.89	[illegible]
Nitrogen	1.23	1.37	1.01	0.54	1.34	1.54	1.73	1.49	[illegible]
Oxygen	6.03	8.30	[illegible]	[illegible]	13.73	8.60	10.65	16.5	[illegible]
Sulfur	4.19	3.80	2.09	1.24	2.87	0.48	0.79	[illegible]	[illegible]
Ash	12.21	12.73	17.30	24.62	7.91	1.51	7.73	4.64	[illegible]
Total	100.00	100.00	100.00	[illegible]	100.00	100.00	100.00	[illegible]	[illegible]

Table 6c-2. HEAT OF REACTION OF HYDROGEN AND IRELAND MINE COAL AND ANALYSES OF COAL AFTER REACTION (1300°F, 1000 psia)

Run No.	TL-2	TL-3	TL-4	TL-5	TL-8	TL-10	TL-12	TL-16	TL-22	TL-23	TL-24	TL-25	TL-27	TL-29	TL-31	TL-34
Starting Coal	Raw			Pretreated						Raw	Low Temp	Hi Temp	Raw		Low Temp	
Proximate Analysis, wt %																
Moisture	0.4	1.6	2.7	2.9	1.8	3.1	2.9	3.1	1.6	2.5	1.6	1.4	0.9	0.8	1.9	0.8
Volatile Matter	6.9	3.3	3.7	6.6	2.8	--	4.1	6.2	6.4	4.7	7.6	7.7	4.5	4.8	5.8	5.7
Fixed Carbon	73.0	75.0	68.3	74.4	81.0	--	76.6	74.5	77.6	71.4	72.3	71.7	73.3	73.7	71.2	75.1
Ash	19.7	20.1	25.3	16.1	14.4	17.1	16.4	16.2	14.4	21.4	18.5	19.2	21.3	20.7	21.1	18.4
Ultimate Analysis, wt %																
Carbon	73.4	73.8	70.3	81.2	79.1	78.3	77.7	75.0	79.5	71.1	75.3	75.0	74.1	73.4	72.9	75.2
H_2	2.33	2.25	1.24	1.42	1.81	1.50	1.42	1.21	1.34	1.79	1.08	1.11	1.56	1.26	1.17	1.08
N_2	1.17	0.56	--	--	--	0.51	--	--	--	--	--	--	--	--	--	--
O_2	0.78	--	--	--	--	--	--	--	--	--	--	--	--	--	--	--
S	2.50	3.35	--	--	--	2.16	--	--	--	--	--	--	--	--	--	--
Ash	19.82	20.41	26.00	16.60	14.62	17.68	16.9	16.73	14.59	21.90	18.85	19.45	21.49	20.86	21.50	18.52
Temperature, °F.	1000	1342	1438.50	1286.60	1288.35	1290.30	1283.90	1276.63	1296.08	1291.58	1287.54	1290.48	1285.95	1289.10	1287.70	1284.18
Pressure, p.s.i.a.	1002	1009	1008	1000	984	1000	988	960	1000	1000	1000	1000	980	1002	1000	
% Coal Reacted	41.5	52.4	51.7	46.1	48.4	47.3	47.3	48.3	47.1	52.2	24.9	28.8	48.1	46.1	27.3	21.1
% Carbon Gasified		50.7	52.3	37.6	41.7	41.2	41.2	45.0	40.0	52.0	26.0	26.0	55.6	44.2	29.5	23.4
$-\Delta H_R$, Btu/lb coal reacted	1300	1951	1775	1935	2286	1717	1844	1625	2476	1723	1044	3078	1788	1807	2432	2566

Table 6c-3. HEAT OF REACTION OF HYDROGEN AND IRELAND MINE COAL AND ANALYSES OF COAL AFTER REACTION (1300°F, 1000 psia)

Run No.	TL-55	TL-56	TL-57	TL-58	TL-59	TL-60	TL-61	TL-62	TL-64	TL-66	TL-67	TL-68	TL-69	TL-70
Starting Coal	—Pretreated—		—Low Temp—		—Hi Temp—				—Low Temp—		Hi Temp	Pretreated	—Raw—	
Proximate Analysis, wt %														
Moisture	0.9	1.1	[illegible]	0.9	0.9	1.1	1.0	0.9	1.5	1.1	1.4	4.1	1.2	1.2
Volatile Matter	4.4	4.2	[illegible]	5.0	5.0	4.7	4.5	5.1	5.4	5.4	4.4	4.7	4.5	4.3
Fixed Carbon	71.6	78.5	[illegible]	72.3	73.6	70.0	59.8	56.4	71.1	68.7	63.5	73.1	74.6	74.7
Ash	23.1	16.2	[illegible]	21.8	20.5	24.2	34.7	37.6	22.0	24.8	30.7	18.1	19.7	19.8
Ultimate Analysis, wt %														
Carbon	70.3	78.3	[illegible]	73.4	69.1	70.0	59.2	52.6	58.6	65.8	60.6	74.5	65.5	69.7
H_2	0.81	0.84	0.76	0.77	0.78	0.79	0.59	0.50	1.03	0.84	0.85	0.86	0.94	0.83
N_2	0.55	0.50	0.48	--	0.47	0.46	0.38	0.30	0.46	0.51	0.31	0.54	0.73	0.70
O_2	3.77	2.71	2.74	--	8.30	3.61	4.36	8.31	16.60	6.76	6.94	4.01	10.42	6.40
S	1.34	1.24	1.05	--	0.65	0.67	0.39	0.33	0.96	1.26	0.22	1.21	2.50	2.28
Ash	23.23	16.41	23.37	21.97	20.70	24.47	35.08	37.96	22.35	24.83	31.08	18.88	19.91	20.09
Temperature, °F.	1454.00	1458.00	1456.43	1453.12	1450.14	1446.89	1449.67	1450.89	1455.11	1448.98	1447.73	1453.15	1447.67	1448.80
Pressure, p.s.i.a.	988	960	978	1006	1012	1024	1010	1004	966	1018	1012	970	1024	1030
% Coal Reacted	41.5	40.5	30.4	23.3	7.2	8.2	9.7	12.5	22.6	18.3	16.5	41.2	43.1	45.1
% Carbon Gasified	41.3	33.5	26.4	26.8	11.6	11.4	26.3	36.6	41.0	30.1	30.3	37.5	--	--
$-\Delta H_R$, Btu/lb coal reacted	2372	2230	2713	3137	3024	3172	3608	3864	3199	2024	3938	2346	1552	1841

A7506 1641

Table 6c-4. HEAT OF REACTION OF HYDROGEN AND COALS: Analysis of Coal After Measurement

	TL-137 Illinois	TL-138 West Virginia Sewell	TL-140 West Virginia Block No. 5	TL-141 Colorado Subbituminous	TL-143 Illinois	TL-144 West Virginia Sewell	TL-145 West Virginia Block No. 5	TL-146 Colorado Subbituminous
Proximate Analysis (wt %)								
Moisture	3.3	2.3	2.1	4.0	0.9	2.2	1.2	1.0
Volatiles	2.4	3.5	3.5	3.8	1.0	1.0	0.9	2.2
Fixed Carbon	--	90.8	83.3	83.6	81.5	92.8	85.5	87.1
Ash	--	3.4	11.1	8.6	16.6	4.0	12.4	9.7
Total	--	100.0	100.0	100.0	100.0	100.0	100.0	100.0
Ultimate Analysis (wt %)								
Carbon	82.2	91.8	85.19	86.98	80.0	92.1	85.4	87.87
Hydrogen	1.82	1.69	2.33	2.65	0.95	1.06	0.97	1.31
Nitrogen	0.80	0.99	0.85	0.72	0.48	0.67	0.66	0.55
Oxygen	--	1.85			0.53	1.84	0.21	
Sulfur	--	0.23	0.31	0.65	1.28	0.20	0.18	0.50
Ash	--	3.44	11.32	9.00	16.66	4.13	12.58	9.77
Total	100.00	100.00	100.00	100.00	100.00	100.00	100.00	100.00
Temperature (°F)	1215.77	1216.81	1216.30	1214.66	1491.41	1492.63	1490.38	1486.91
Pressure (psia)	1000	1000	1000	1000	1000	1000	1000	1000
$-\Delta H_r$, Btu/lb Coal Reacted	2592.6	2986.0	2396.0	2130.9	2935.8	3089.7	3435.2	2218.6
Reaction Time (min)	60	60	60	60	60	60	60	60
Wt Coal Start (g)	8.5279	6.0182	6.9458	11.0918	7.2292	6.8766	6.5288	10.7320
Wt Coal Finish (g)	4.8869	3.7415	4.0412	5.7835	3.5383	3.7852	3.1999	4.7233
Wt Coal Reacted (g)	3.6410	2.2767	2.9046	5.3083	3.6909	3.0914	3.3289	6.0087
Coal Reacted (%)	43	38	42	48	51	45	51	56

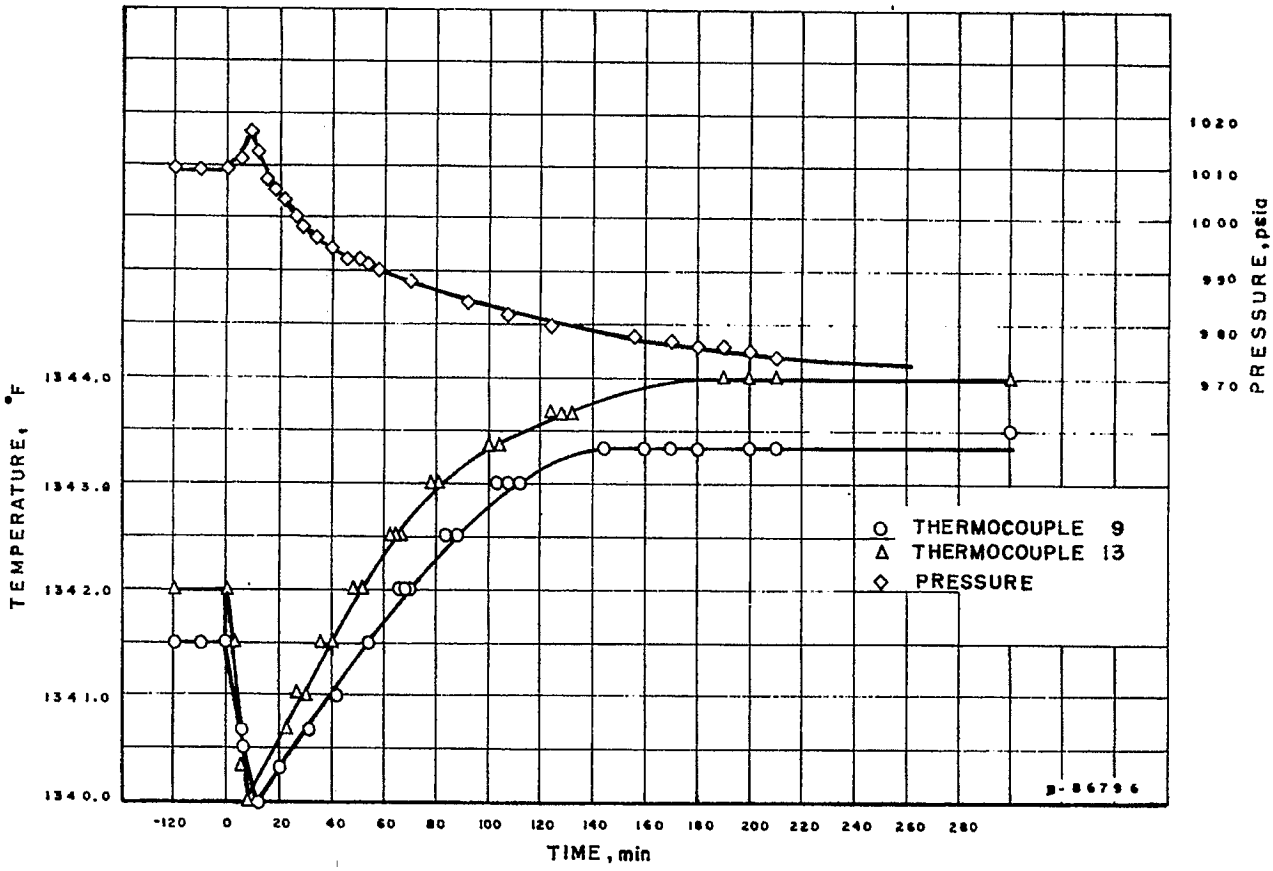

Figure 6c-8. TYPICAL TIME-TEMPERATURE DATA FOR HEAT OF REACTION OF HYDROGEN AND COAL

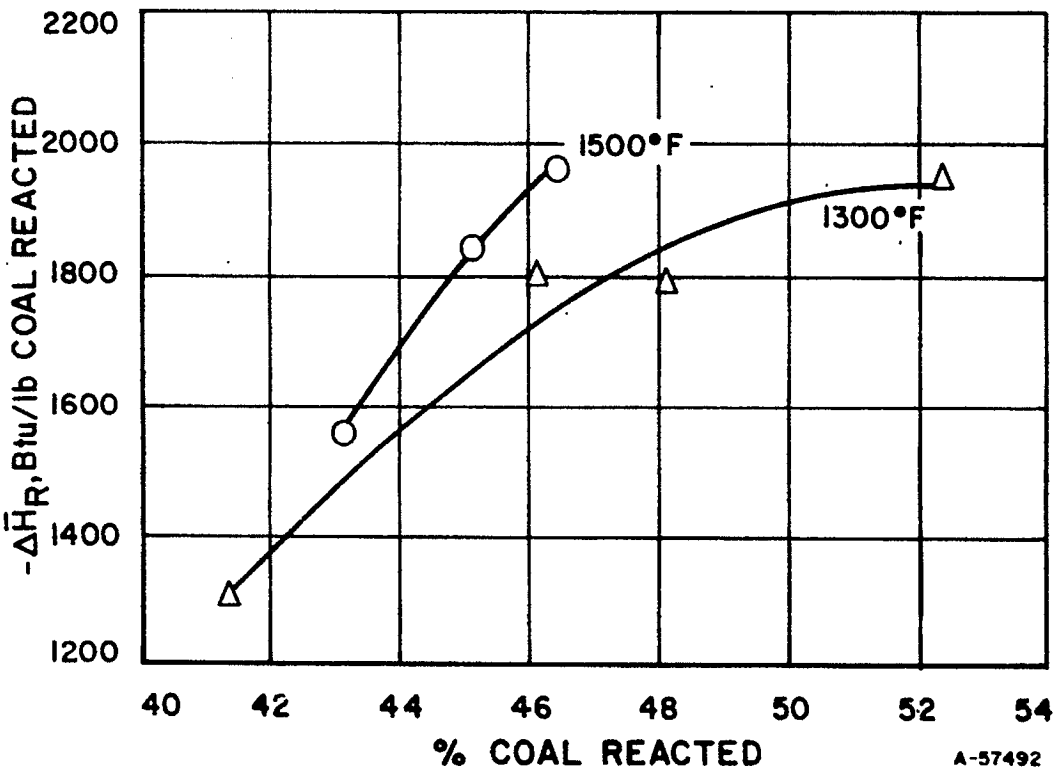

Figure 6c-9. HEAT OF REACTION OF HYDROGEN AND RAW IRELAND MINE COAL

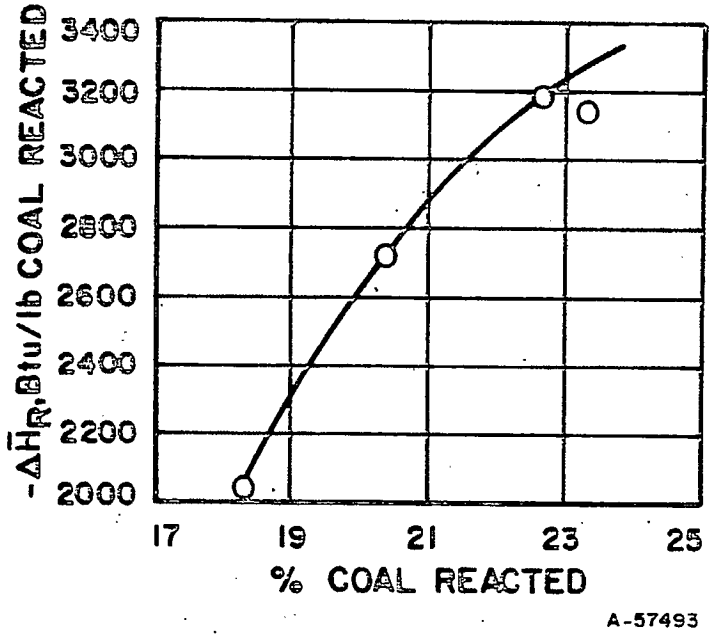

Figure 6c-10. HEAT OF REACTION OF HYDROGEN AND LOW-TEMPERATURE RESIDUE OF IRELAND-MINE COAL REACTED AT 1000 psia AND 1500°F

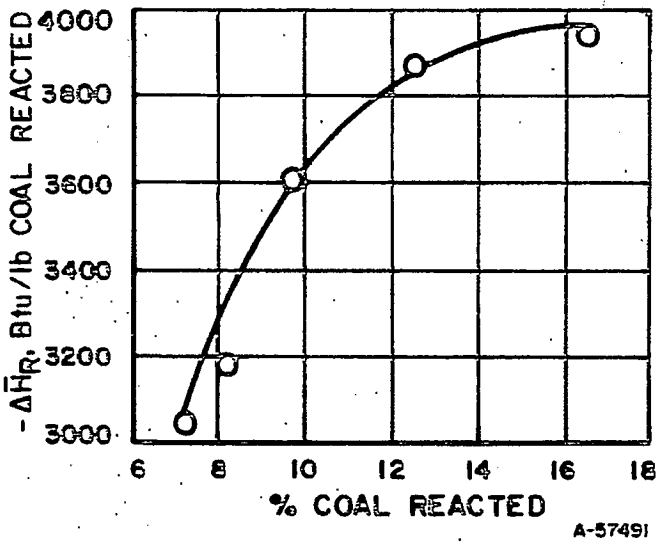

Figure 6c-11. HEAT OF REACTION OF HYDROGEN AND HIGH-TEMPERATURE RESIDUE OF IRELAND-MINE COAL REACTED AT 1000 psia AND 1500°F

Figure 6c-12 compares the heats of reaction of hydrogen and coal obtained from (1) the heat of formation data for $C + 2H_2 \rightarrow CH_4$, and from (2) the pilot plant data, with those obtained from the calorimetry studies. Note that the pilot plant data were based on a 77°F reference temperature, while the present experimental data were obtained at operating conditions. Moreover, the experimental data were obtained from coals at four different stages of reaction including raw coal, pretreated coal, low-temperature gasification residue, and high-temperature gasification residue. Ash balances were used to put these results on a common basis. The ash balance calculations yielded the percent of carbon gasified in each coal or char. Raw coal was assumed to have 0% carbon gasified.

Figure 6c-12 shows the general trend of the heat of reaction. Horizontal lines connecting the data points indicate the percent of carbon gasified before and after the reaction. Using raw coal as an example, the coal before reaction has 0% carbon gasified, after the reaction, 52% of the carbon was gasified. For the raw coal gasification, Figure 6c-13 shows the average heat of reaction was about 1800 Btu/lb coal reacted.

Using the technique for the preparation of Figure 6c-12 the effect of temperature on the heat of reaction of hydrogen and coal is shown in Figure 6c-13.

Accurate heat-of-reaction data are given in Tables 6c-2, 6c-3 and 6c-4. Although the pilot plant data are considerably scattered, the average value is not too different from that obtained by the other methods. The calorimetry data also show some scattering, which is due to the heterogeneous nature of the coal and the characteristics of the calorimeter and the sensing instruments.

Examination of the temperature measurement, the pressure measurement, the temperature distribution in the calorimeter, the total mass balance, and the calibration results obtained from the constant-heat-input method and the experimental runs on hydrogen and n-decane reactions indicate that the data reported in Tables 6c-2, 6c-3 and 6c-4 should not have a deviation greater than 10%.

6c.6 Heat of Pretreatment of Coal

In order to avoid agglomeration, it is necessary to pretreat some raw bituminous coals before the coal enters the gasification reactor. The coal is pretreated in a reactor with air at temperatures between 700° and 800°F (see Part VII of this report). The method used to determine the heat of pretreatment is the same as that used for the heat of reaction. The coal is kept at 70° to 72°F while the air-filled calorimeter is being stabilized at desired conditions. The coal is then dropped into the calorimeter after equilibrium condition has been reached; therefore, the measured heat of pretreatment includes 1) the heat required to warm the coal from 70°F to the reaction temperature, and 2) heat of pyrolysis, if any.

During tests performed in the work reported here, little devolatilization was noticed at 700°F., but the coal devolatilized rapidly at 800°F, as shown by the presence of tars. Thus, because a good portion of the coal weight loss at 800°F resulted from devolatilization and not from the oxidation reaction, the heat of reaction of the pretreatment of coal was also calculated for

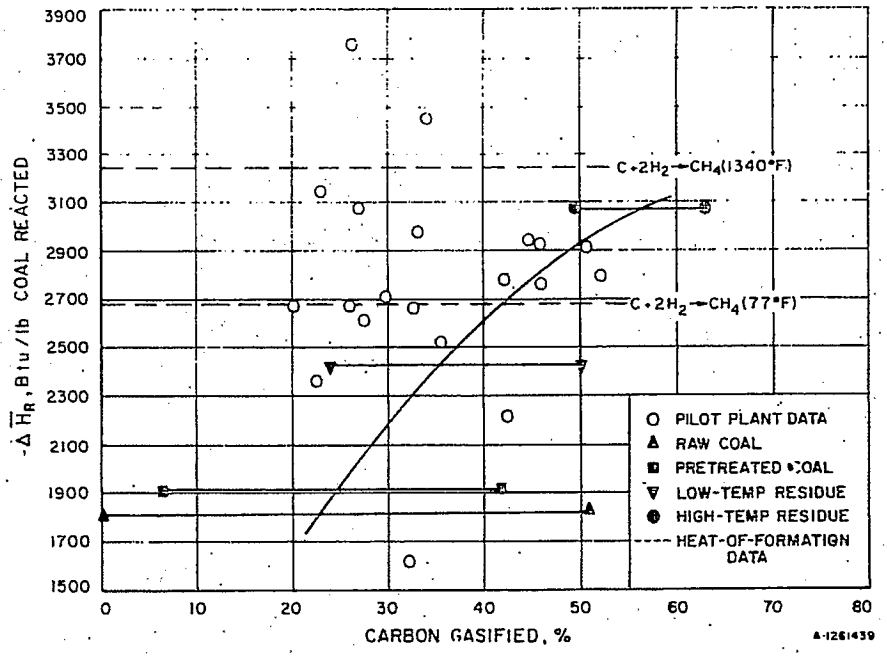

Figure 6c-12. IRELAND MINE COALS COMPARED WITH STANDARD HEAT OF REACTION DATA FOR HYDROGEN AND COAL

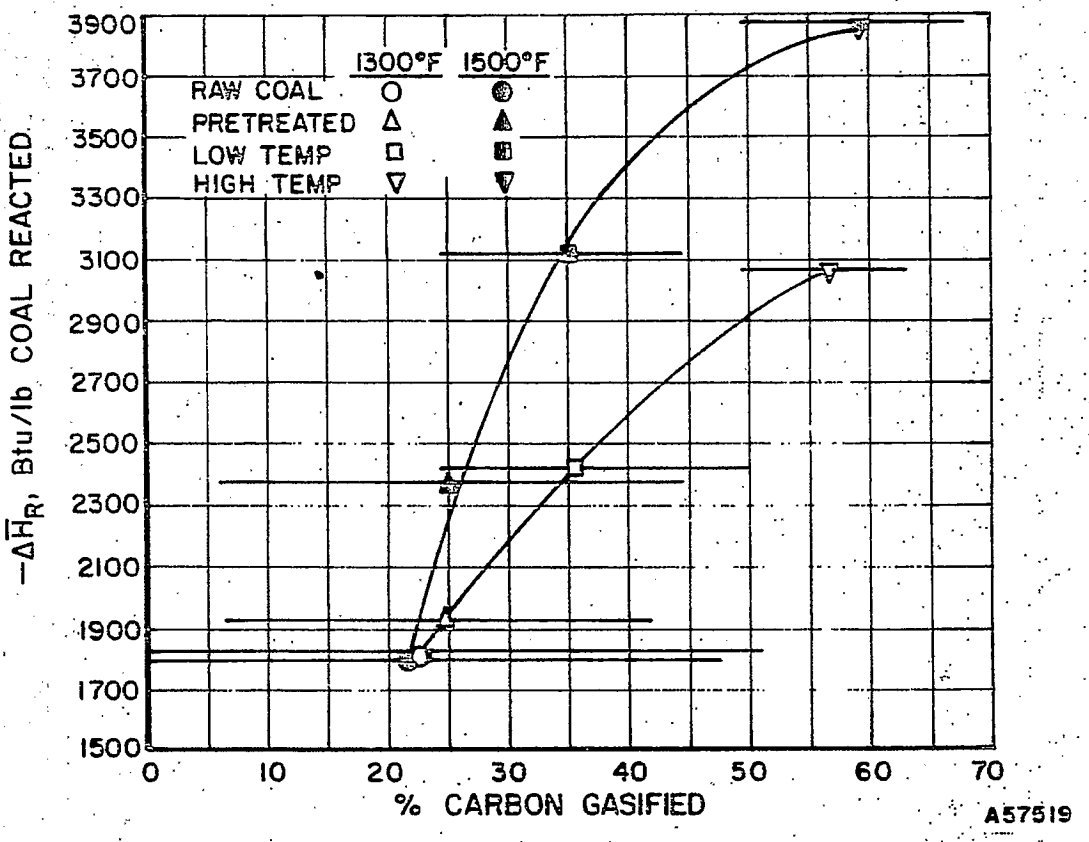

Figure 6c-13. HEAT OF REACTION OF HYDROGEN AND IRELAND MINE COAL AT 1300°F AND 1500°F

800 °F, based on the data obtained at 700 °F, and the heat capacity information of both reactants and products. The results are presented as the dotted line in Figure 6c-14 and in the data of Table 6c-5 where the analysis of coal after reaction is also presented. One should note that, although these experiments were carried out in a static-bed reactor, the IGT pilot plant pretreatment of coal is carried out in a fluidized-bed reactor. At 700 °F, the rate of the devolatilization reaction apparently competes with that of the oxidation reaction. In the static reactor the poor gas-solids contacting favors devolatilization, while the intimate gas-solids contacting in the fluidized-bed reactor favors oxidation. For a fluidized pretreater, therefore, the calculated values of the heat of reaction at 800 °F more nearly approach the actual values.

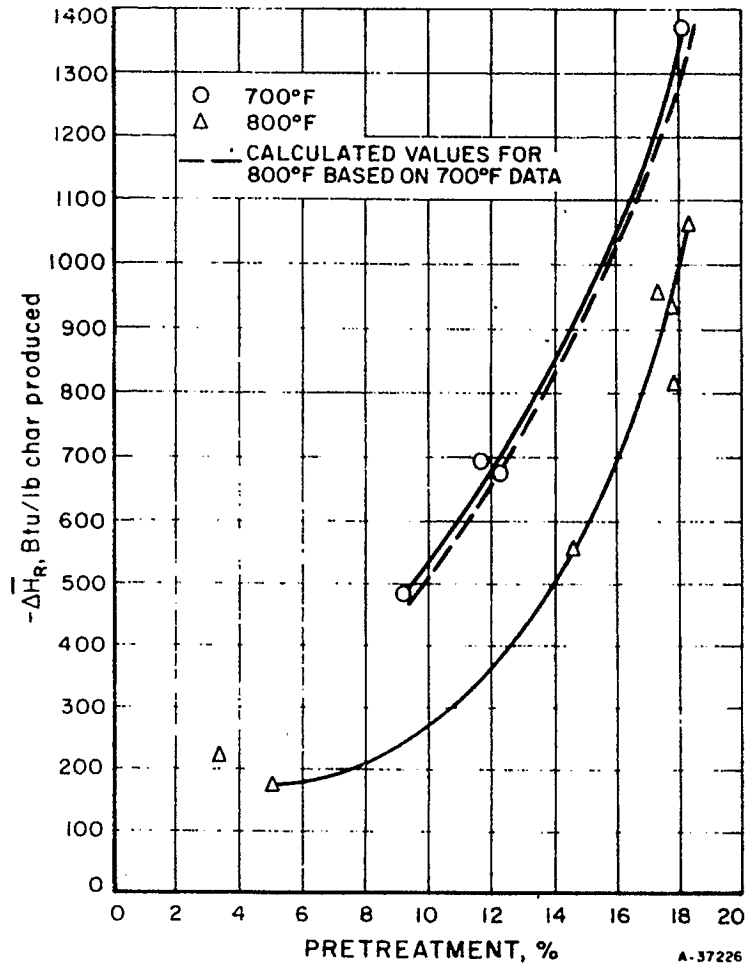

Figure 6c-14. HEAT OF REACTION OF PRETREATMENT OF COAL

Table 6c-5. HEAT OF REACTION OF PRETREATMENT OF IRELAND MINE COAL AND ANALYSES OF COAL AFTER REACTION

Run No.	TL-35	TL-38	TL-40	TL-41	TL-42	TL-43	TL-44	TL-45	TL-46	TL-47	TL-48
Proximate Analysis, wt %											
Moisture	0.5	0.0	0.8	0.3	0.2	0.2	0.2	0.5	0.4	0.5	14.6
Volatile Matter	25.7	20.9	17.6	17.5	18.9	25.8	23.5	18.3	21.3	21.2	19.7
Fixed Carbon	61.1	66.0	67.0	67.9	67.8	60.7	63.0	68.0	64.2	64.8	54.9
Ash	12.7	13.1	14.6	14.3	13.1	13.3	13.3	13.2	14.1	13.5	10.8
Ultimate Analysis, wt %											
Carbon	71.2	71.1	72.2	69.9	71.1	69.9	70.1	74.5	71.5	73.2	83.9
H_2	3.97	3.16	3.29	3.08	3.42	3.86	3.96	3.01	3.32	3.62	2.23
N_2	--	1.03	--	0.96	1.33	1.31	0.87	1.33	1.37	1.41	1.20
O_2	--	7.82	--	7.03	7.13	7.39	7.53	3.49	5.31	3.94	--
S	--	3.83	--	4.70	3.93	4.22	4.19	4.37	4.35	4.25	5.01
Ash	12.73	13.06	14.72	14.33	13.09	13.32	13.35	13.30	14.15	13.58	12.71
Temperature, °F.	702	701	799	800	801	708	707	796	797	794	796
Pressure, p.s.i.a.	170	170	160	120	47	80	110	120	60	120	80
% Pretreatment	11.7	18.1	18.3	17.8	3.47	9.2	12.3	17.8	5.15	17.3	14.6
$-\Delta H_R$, Btu/lb coal reacted	5255	6195	4747	3756	1243	4814	4795	4306	1127	4580	3240
$-\Delta H_R$, Btu/lb char produced	696	1372	1064	817	225	486	674	931	179	956	555

6c.7 Pyro-Heat Capacity of Coal

Many authors have reported the heat capacity of coal and the experimental methods used[1,2,3,5,7,12,20,28,33,46], although few investigations were conducted above 572°F (300°C).

The difficulties of determining the heat capacity of coal experimentally, especially during heating and at high temperatures, have caused disagreement among research workers. Some authors have found that the heat capacity of coal increases with temperature[3,6] and some others have found otherwise.[1,2] The reason for this disagreement could be due to the method one uses to obtain the heat capacity. Because coal contains up to 50 wt-% of volatile matter, the weight of coal alters considerably during heating as the volatile matter escapes. To further complicate the matter, if the coal were allowed to oxidize during heating, one can be sure that the results would not be the same. Even if one takes the escaped volatile matter into consideration, the precision of the measurement will suffer because the treatment of experimental data would depend on the material balance, analytical methods and assumptions.

The reason for the decreasing C_p at increasing temperature above 300°C could be explained by the endothermic reaction of so-called "pyrolysis" or "decarbonization", or "coking."[9,29,46] Coal starts devolatilization quickly at temperatures above 700°F. At 700°F or above, therefore, the experimental measured value is:

$$a = C_p + \Delta H_e$$

where:

C_p is the heat capacity of coal

ΔH_e is the endothermic reaction

If one wishes to determine the true heat capacity of coal, one must have an accurate ΔH_e value. Because coal is an extremely complex substance, it is experimentally impossible to determine ΔH_e accurately. As an example, Agroskin and Goncharov[1,2] proposed to determine the C_p directly as follows:

1) heat the coal to the decarbonizing temperature until coking stops; then,

2) measure the residue for C_p.

Obviously, this residue is no longer the coal one started with, and the measured C_p is, then, not that of the coal, but that of the coke.

In work performed at IGT and reported here, the ΔH_e was determined as follows:

1) Drop the cold coal into the hot calorimeter to determine the C_p and H_e; then,

2) Drop the coke from the previous run to determine the C_p of the coke.

The analyses of volatile matter, coal and char must be very accurate so that a close material balance can be achieved. If the heat capacities of all the volatile matter are known, the heat capacity of coal can be deduced, and the difference of these two runs is then the ΔH_e. This method has the same flaw as that of Agroskin because there is no common base for these two runs. In other words, the C_p of coke is not the same as that of coal. However, one may consider much of this to be purely academic: From an engineering point of view, the "$C_p + \Delta H_e$" term is the one that is needed in actual practice. If one plans to use coal for any purpose at temperatures above decarbonizing temperature, the effect with which he is principally concerned is "$C_p + \Delta H_e$." If coke is to be used, then the C_p for coke should be substituted.

The reported mean heat capacity (Cpm) values at temperatures above 700°F include that of endothermic reaction; therefore, it is called the pyro-heat capacity of coal.

6c.7.1 Experimental Work

In this work, two calorimeters already described in detail were used to measure the heat capacity of coal for temperatures from 600° to 1500°F and for pressures from 0 to 1500 psia. Figure 6c-15 presents a simple schematic drawing of the drop calorimeter, which is suitable for operation at temperatures lower than the decarbonization temperature. Figure 6c-16 presents a simple schematic of the heat-of-reaction calorimeter for operation at high temperatures.

The dried coal sample is contained in a basket which is suspended in the cold neck zone of the calorimeter. The calorimeter body is inside the furnace and maintained at a constant temperature. An inert gas is used to achieve the desired pressure in the calorimeter. The sample is lowered into the calorimeter body after the temperature and pressure of the calorimeter have stabilized for two hours. The cooling rate of the calorimeter is measured by four thermocouples and two resistance thermometers distributed around the calorimeter body. The coal is analyzed before and after the experiment; and a gas sample is taken to be analyzed for the volatile matter which escaped from the coal. Note that the volatile matter is contained within the calorimeter at all times and — knowing the composition, weight, and other variables of the gas and solid — the total material and energy balance can be obtained.

Establishing an energy balance around the calorimeter, we have:

$$-(mCp\,\Delta T)_{calorimeter} = (mCp\Delta T)_{baskets} + (mCp\Delta T)_{coal} \qquad (8)$$

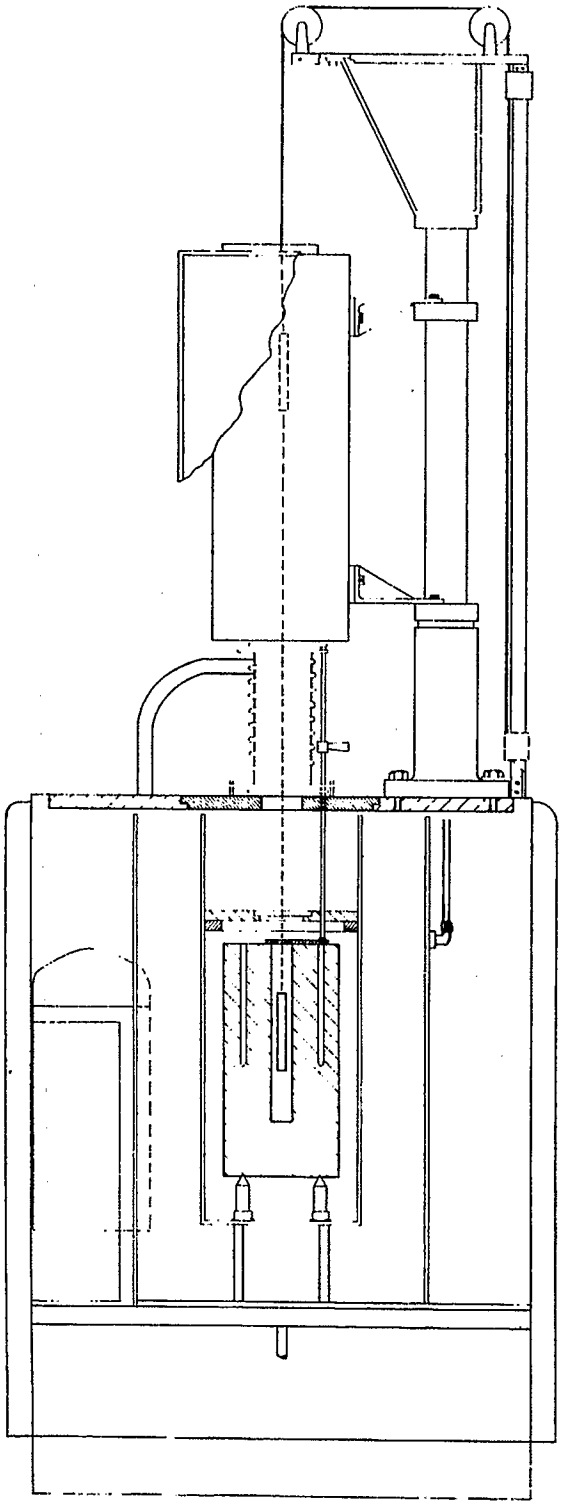

A7506 1434

Figure 6c-15. DROP CALORIMETER

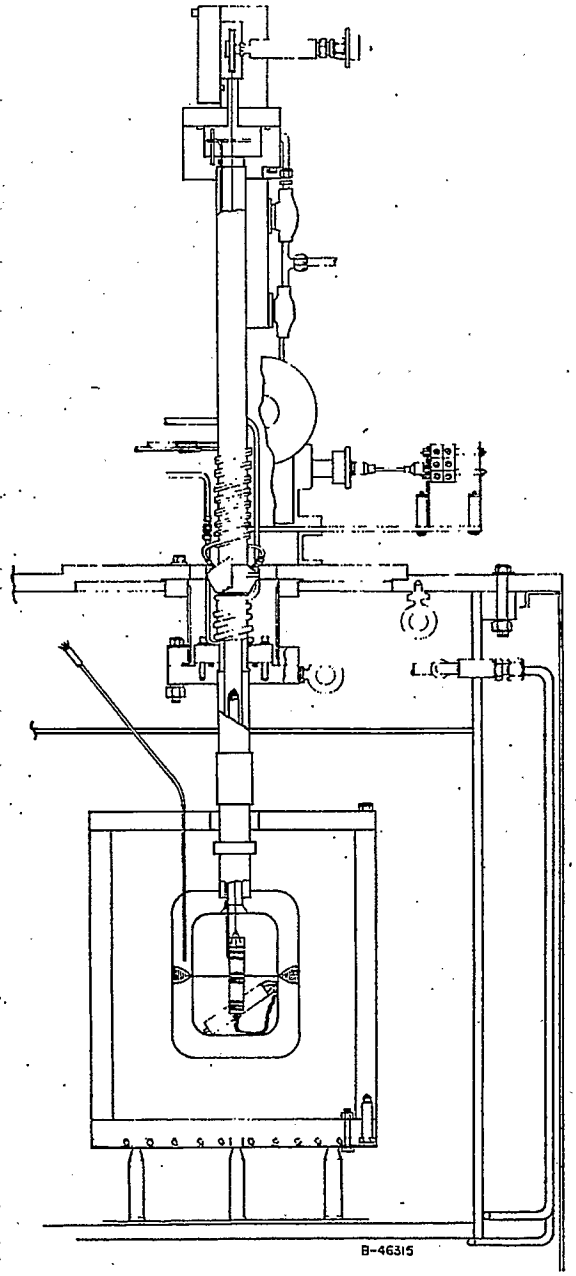

Figure 6c-16. HEAT-OF-REACTION CALORIMETER

The mCp (mass x heat capacity) of the calorimeter was determined by using pure alumina for which the heat capacity is well established for a wide temperature range[13], and the results of calorimeter calibration are presented in Figure 6c-7.

The ΔT of the calorimeter is measured; the mCp of baskets is calibrated as a function of temperature; the initial temperature of coal and basket is measured and the final temperature of coal and basket is assumed to be the same as that of the final calorimeter temperature. The only unknown remaining in Equation 8 is the pyro-heat capacity of coal.

The composition of the coal and chars investigated is presented in Table 6c-6. A typical experimental run is presented in Figure 6c-17. The results of this study are presented in Table 6c-7 and Figure 6c-18. The general trends of the heat capacity of coal are that it increases with increasing temperature, volatile matter, and moisture content, and that it decreases with increasing ash content.

This behavior agrees with determinations by other investigators[3,6,7,12,14,20], because the heat capacity of volatile matter (CH_4, H_2, etc), and of moisture[15] (H_2O) are higher than graphite, and that of ash is lower than graphite. Detailed discussion may be found elsewhere.[6,7,14]

The U. S. Bureau of Mines reported heat content of various coals[14] for temperatures up to 1000°F. The heat capacity deduced from this work ranges from 0.2 to 0.5 Btu/lb-°F, and the general trend is that the C_p increases with increasing temperature.

For comparison, the mean pyro-heat capacities of lignite, coal, pretreated coal and chars are presented in Figure 6c-18 with the data obtained from this work. Each curve is preceded by a number that indicates the weight percent (dry) of volatiles in the various specimens. Each literature source is identified in Figure 6c-18 by the author's name, which may be used to identify the literature source in Section 6c.8, References Cited.

6c.7.2 Correlation

Based on the data obtained from this work and that available in the literature, the heat capacity of coal is assumed to be a function of the volatile matter content and the temperature. The change of heat capacity with volatile matter content at a constant temperature, $(\partial C_p/\partial V_m)_T$, is nearly constant for every temperature. The heat capacity and temperature, $(\partial C_p/\partial T)V_m$, are also nearly constant for every constant volatile matter content within the accuracy of the data. The $(\partial C_p/\partial V_m)_T$ was plotted against temperature. The intercepts of the V_m versus T plot were also plotted against temperature. When an equation is fitted to each of these two plots, the following generalized correlation results:

$$C_{pm} = 0.17 + 1.1 \times 10^{-4} T + (3.2 \times 10^{-3} + 3.05 \times 10^{-6} T)_{V_m} \qquad (8)$$

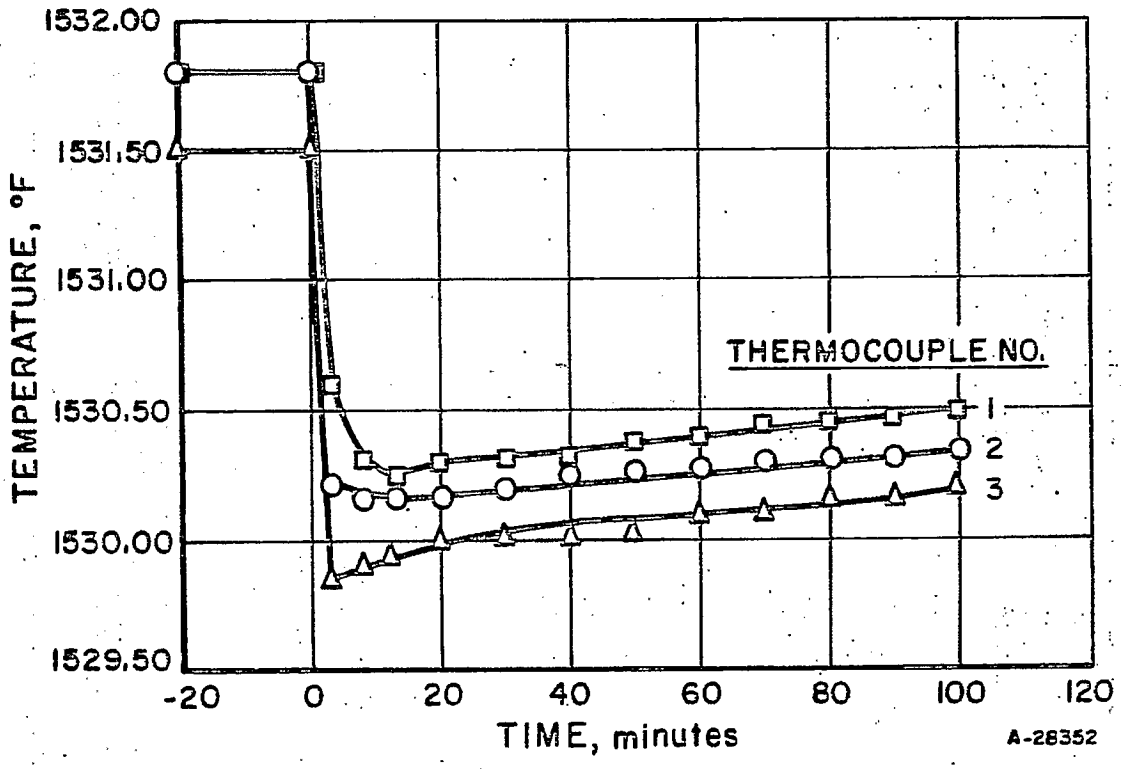

Figure 6c-17. TIME-TEMPERATURE COOLING CURVE FOR RUN NO. 92

Table 6c-6. COMPOSITION OF IRELAND MINE AND LIGNITE COAL AND COAL CHARS USED IN THIS WORK

	Ireland Mine				North Dakota	
	Raw Coal	Pretreated Coal	Low-Temp Residue	High-Temp Residue	Raw Lignite	Lignite Residue
Proximate Analysis, wt %						
Moisture	1.3	0.5	0.6	0.6	34.0	1.1
Volatiles	34.6	23.3	4.6	3.3	28.4	9.2
Fixed Carbon	52.0	63.5	77.6	71.6	31.3	71.9
Ash	12.1	12.7	17.2	24.5	6.3	17.8
Total	100.0	100.0	100.0	100.0	100.0	100.0
Ultimate Analysis, wt %						
Carbon	71.2	70.1	76.9	72.6	64.8	77.2
Hydrogen	5.14	3.70	2.05	1.08	0.7	0.87
Nitrogen	1.23	1.37	1.01	0.54	0.91	0.37
Oxygen	6.03	8.30	0.65	0.00	20.85	3.23
Sulfur	4.19	3.80	2.09	1.24	3.20	0.30
Ash	12.21	12.73	17.30	24.62	9.46	18.03
Total	100.00	100.00	100.00	100.00	100.00	100.00

A7506 1644

Table 6c-7. HEAT CAPACITY OF COAL: Analysis of Coal After Measurement

Run Number	TL-81	TL-82	TL-83	TL-88	TL-89	TL-90	TL-91	TL-92	TL-94
Starting Coal (All Ireland Mine)	Hi Temp	Hi Temp	Hi Temp	Hi Temp	Lo Temp	Lo Temp	Lo Temp	Hi Temp	Pretreated
Proximate Analysis (wt%)									
Moisture	1.2	1.3	1.2	3.3	0.6	0.6	0.6	0.5	1.1
Volatile Matter	1.2	1.0	1.3	0.6	0.7	1.1	1.5	0.5	1.9
Fixed Carbon	78.3	77.8	81.4	65.4	76.9	83.1	80.9	78.2	83.3
Ash	19.3	19.9	16.1	30.7	21.8	15.2	17.9	20.8	13.7
Total	100.0	100.0	100.0	100.0	100.0	100.0	100.0	100.0	100.0
Ultimate Analysis (wt %)									
C	73.1	71.6	78.8	64.3	73.6	81.34	79.28	72.6	82.3
H_2	0.81	0.84	1.10	0.76	0.88	0.88	0.88	0.74	0.75
N_2	0.59	0.56	0.57	0.46	0.67	0.76	0.79	0.56	0.87
O_2	4.86	5.65	2.16	1.55	1.02	--	--	4.04	--
S	1.13	1.22	1.06	1.19	1.89	1.70	1.97	1.17	2.25
Ash	19.51	20.13	16.31	31.74	21.94	15.32	17.08	20.89	13.83
Total	100.00	100.00	100.00	100.00	100.00	100.00	100.00	100.00	100.00
Temperature (°F)	1488.40	1531.33	1494.25	1568.65	1568.73	1566.63	1531.67	1532.30	1566.65
Pressure (psia)	1036He	524	1008	0	0	0	508	504	0
Cp (Btu/lb-°F)	0.297	0.320	0.385	0.384	0.374	0.478	0.334	0.351	0.487

Run Number	TL-95	TL-97	TL-98	TL-100	TL-102	TL-103	TL-104	TL-107	TL-108
Starting Coal (All Ireland Mine)	Raw	Raw	Pretreated	Hi Temp	Lo Temp	Pretreated	Raw	Hi Temp	Lo Temp
Proximate Analysis (wt%)									
Moisture	0.5	0.9	0.7	1.2	2.0	2.4	1.8	1.0	1.1
Volatile Matter	1.1	1.1	1.4	1.8	3.2	4.7	4.1	1.2	2.4
Fixed Carbon	79.8	79.4	80.9	75.6	71.1	77.3	75.2	81.3	76.5
Ash	18.6	18.6	17.0	21.4	23.7	15.6	18.9	16.5	20.0
Total	100.0	100.0	100.0	100.0	100.0	100.0	100.0	100.0	100.0
Ultimate Analysis (wt%)									
C	76.92	69.1	78.8	72.0	71.31	70.7	74.15	79.3	74.2
H_2	0.65	0.83	0.88	1.36	1.31	1.54	1.44	1.38	1.60
N_2	0.49	0.98	0.86	0.6	0.83	0.77	1.15	0.67	0.88
O_2	--	7.31	0.09	2.91	--	8.50	--	0.80	1.09
S	3.24	3.09	2.21	1.42	2.35	2.49	4.05	1.16	2.05
Ash	18.70	18.77	17.16	21.71	24.20	16.00	19.21	16.69	20.18
Total	100.00	100.00	100.00	100.00	100.00	100.00	100.00	100.00	100.00
Temperature (°F)	1568.55	1535.60	1534.45	1337.54	1335.48	1335.66	1334.21	1292.03	1292.68
Pressure (psia)	0	498	508	0	0	0	0	500	500
Cp (Btu/lb-°F)	0.569	0.546	0.489	0.340	0.324	0.554	0.577	0.250	0.320

Table 6c-7, Contd. HEAT CAPACITY OF COAL
Analysis of Coal After Measurement

Run Number	TL-109	TL-110	TL-112	TL-113	TL-114	TL-115	TL-117	TL-[illegible]	TL-11[illegible]	TL-12[illegible]
Starting Coal or Feed (Varied)	Pretreated	Hi Temp	Lignite Residue	Raw	Lignite Residue	Lignite	Hi Temp (Ireland Mine)	L[illegible] Temp	Pretreated	Lignite
Proximate Analysis (wt%)										
Moisture	1.7	2.2	5.4	0.8	1.5	2.5	1.8	2.2	2.5	2.[illegible]
Volatile Matter	3.1	1.6	6.7	3.1	5.9	5.2	2.0	4.[illegible]	9.4	11.8
Fixed Carbon	78.[illegible]	70.4	72.3	79.3	74.9	80.2	77.9	7[illegible].[illegible]	74.4	75.4
Ash	17.2	25.6	15.6	16.8	17.7	12.1	18.3	[illegible].[illegible]	13.7	[illegible].8
Total	100.[illegible]	100.0	100.0	100.0	100.0	100.0	100.0	1[illegible].[illegible]	1[illegible].[illegible]	1[illegible].[illegible]
Ultimate Analysis (wt%)										
C	72.6	69.[illegible]	77.7	75.1	77.1	82.9	77.81	7[illegible].7	73.6	80.2
H_2	1.[illegible]	1.06	1.09	1.74	1.21	1.66	1.90	1.7[illegible]	2.63	2.57
N_2	1.15	0.60	0.36	1.15	0.44	1.02	0.60	[illegible].9[illegible]	1.44	1.1
O_2	5.[illegible]	1.37	4.17	1.81	2.44	1.10	--	0.[illegible]	5.46	4.4[illegible]
S	2.92	1.24	0.22	3.31	0.84	0.88	1.09	1.[illegible]	2.82	[illegible].72
Ash	17.55	26.13	16.46	16.89	17.97	12.44	18.60	21.[illegible]	14.0[illegible]	1[illegible].48
Total	100.[illegible]	100.00	100.00	100.00	100.00	100.00	100.00	1[illegible].[illegible]	100.0[illegible]	1[illegible].[illegible]
Temperature (°F)	1293.67	1292.49	1334.94	1294.35	1334.72	1335.33	1081.18	1[illegible].12	1[illegible].[illegible]	1[illegible].[illegible]
Pressure (psia)	496	496	496	500	0	0	0	[illegible]	0	[illegible]
Cp (Btu/lb-°F)	0.462	0.261	0.348	0.517	0.545	0.607	0.300	[illegible].[illegible]	0.377	[illegible].[illegible]

Run Number	TL-121	TL-124	TL-125	TL-126	TL-127	TL-128	TL-131	TL-132	TL-133	TL-134	TL-135
Starting Coal or Feed (Varied)	Raw Ireland Mine Coal	Hi Temp	Lo Temp	Pretreated	Lignite	Raw	Hi Temp	Lo Temp	Pretreated	Lignite	Raw Ireland Mine Coal
Proximate Analysis (wt%)											
Moisture	2.[illegible]	3.[illegible]	2.1	2.6	3.6	1.0	1.7	1.3	1.8	3.1	0.7
Volatile Matter	8.2	2.4	3.8	18.2	26.0	18.4	2.2	4.0	2[illegible].[illegible]	3[illegible].5	32.0
Fixed Carbon	73.[illegible]	74.7	73.8	65.9	61.1	66.1	63.5	76.7	5[illegible].[illegible]	52.4	55.9
Ash	15.8	19.[illegible]	20.3	13.3	9.[illegible]	14.5	32.6	18.0	18.[illegible]	[illegible].0	11.4
Total	100.0	100.[illegible]	100.[illegible]	100.0	100.0	100.0	100.0	100.0	1[illegible].[illegible]	1[illegible].[illegible]	100.[illegible]
Ultimate Analysis (wt%)											
C	74.[illegible]	76.3	74.0	70.9	72.7	71.4	62.6	74.9	[illegible].7	66.8	70.4
H_2	2.56	1.25	1.82	3.33	3.89	4.10	1.11	1.93	3.41	4.45	4.55
N_2	1.25	0.55	0.83	1.24	1.16	1.28	0.52	0.88	1.[illegible]	[illegible].[illegible]	1.17
O_2	2.44	[illegible].83	0.64	7.50	11.82	4.94	1.25	1.[illegible]	[illegible].4[illegible]	13.[illegible]	8.82
S	2.[illegible]	1.04	1.99	3.35	0.77	3.63	1.34	2.05	3.[illegible]	[illegible].[illegible]	3.20
Ash	15.21	22.83	20.72	13.68	9.66	14.65	33.18	18.25	18.[illegible]	7.21	11.47
Total	100.[illegible]	100.00	100.00	100.00	100.00	100.00	100.00	100.00	1[illegible].[illegible]	1[illegible].[illegible]	1[illegible].[illegible]
Temperature (°F	1077.[illegible]	810.62	811.56	811.48	811.35	810.43	615.94	616.[illegible]	[illegible]15.[illegible]	--	[illegible]1[illegible].[illegible]
Pressure (psia	[illegible]	0	0	0	0	0	0	0	[illegible]		[illegible]
Cp (Btu/lb-°F)	[illegible].548	[illegible].268	0.326	0.369	[illegible].531	0.[illegible]5	[illegible].249	0.271	[illegible].[illegible]2[illegible]	--	[illegible].[illegible]15

A7506 1645A

where:

C_{pm} = mean pyro-heat capacity in Btu/lb - °F; base temperature is 70°F.

T = temperature in °F.

V_m = volatile matter, as-received proximate analysis, dry basis, in weight percent.

Equation 8 can predict all the heat capacity data of coal within the experimental accuracy of the data. The largest deviation is about 10%, while the average deviation is about ±5%. A comparison of the predicted values with the experimental data is shown in Figure 6c-19. To avoid overcrowding, not all the literature values are presented. A nomograph based on the equation 8 is presented as Figure 6c-20.

True heat capacity of coal is also reported in literature. Experimental data from this work were utilized to obtain the true heat capacity so that a comparison on this basis could be made. Because the measured values are mean heat capacities, whose relationship with the true heat capacity is,

$$C_{pm} = \frac{\int_{t_1}^{t_2} C_p \, dt}{t_2 - t_1} \quad (9)$$

and, according to the Mean Value Theorem:

$$f(e) = \frac{f(b) - f(a)}{b - a} \quad , \quad a \leq e \leq b \quad (10)$$

Assuming that the intermediate value of the argument is the average of its extreme values, we have —

$$C_p = \frac{dQ}{dt} \approx \frac{Q_2 - Q_1}{t_2 - t_1} \quad (11)$$

where —

Q is the the amount of heat consumed in heating the coal = C_{pmt}

C_p = true heat capacity

C_{pm} = mean heat capacity

t = temperature

Based on this method, the true heat capacities are calculated and compared with literature values. The results are presented in Figure 6c-21 and in Table 6c-8.

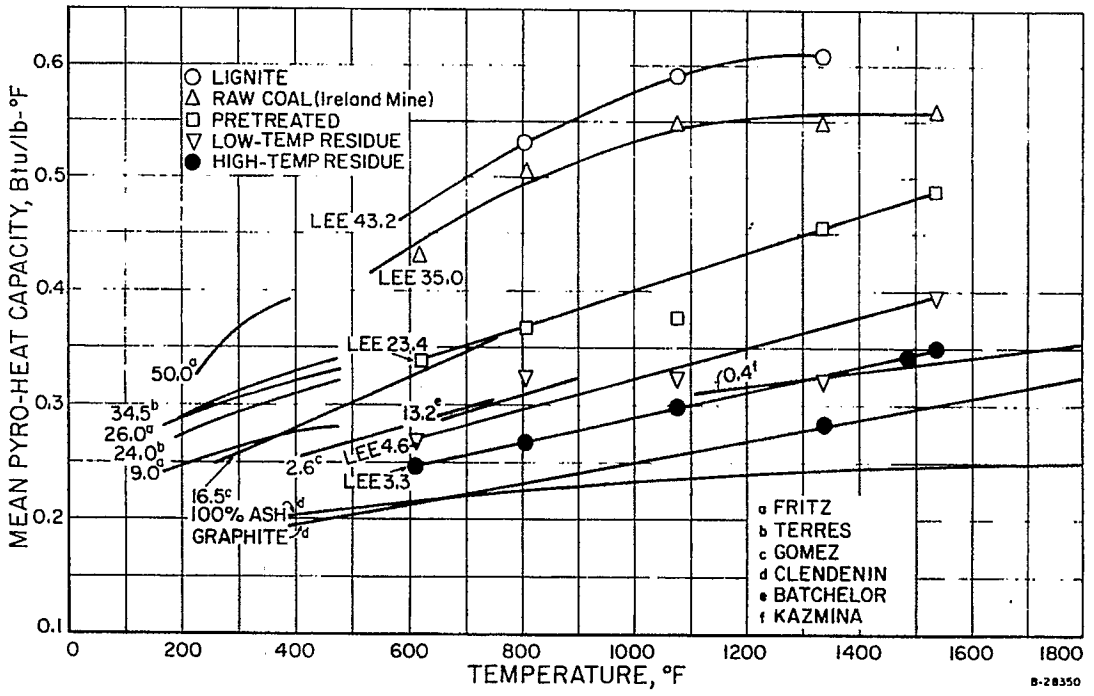

Figure 6c-18. MEAN PYRO-HEAT CAPACITY OF LIGNITE, COAL, PRETREATED COAL, AND CHARS. NUMBERS AT LEFT OF EACH CURVE ARE WT % (DRY) OF VOLATILES IN SPECIMENS. LETTERS DESIGNATE AUTHOR SOURCE.

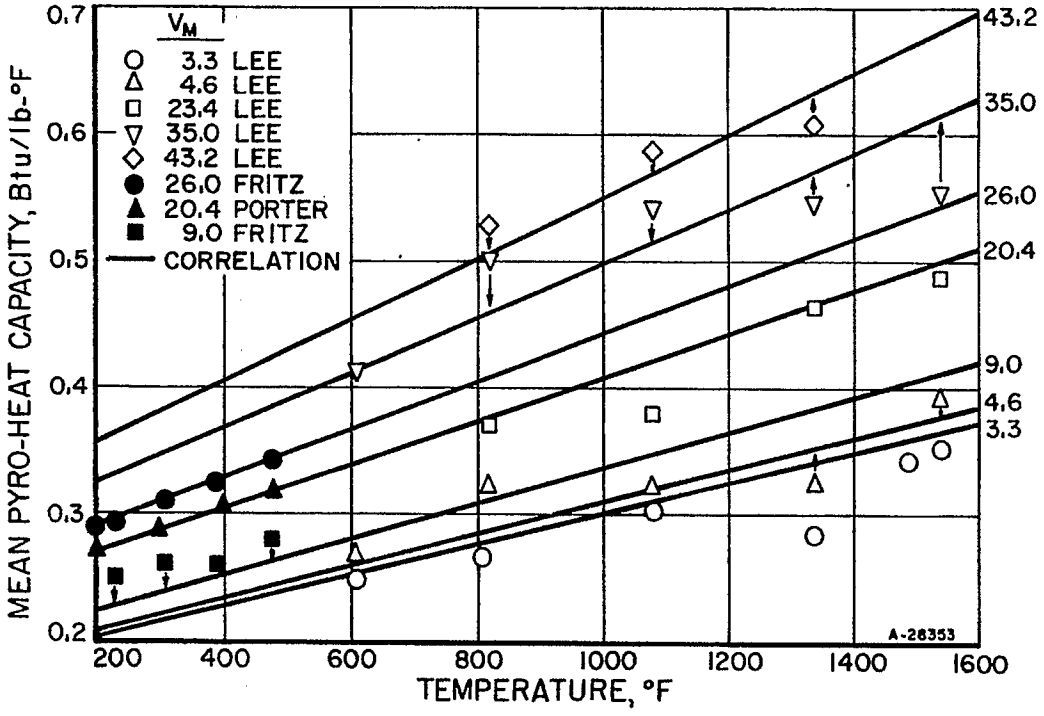

Figure 6c-19. COMPARISON OF CORRELATION WITH EXPERIMENTAL DATA

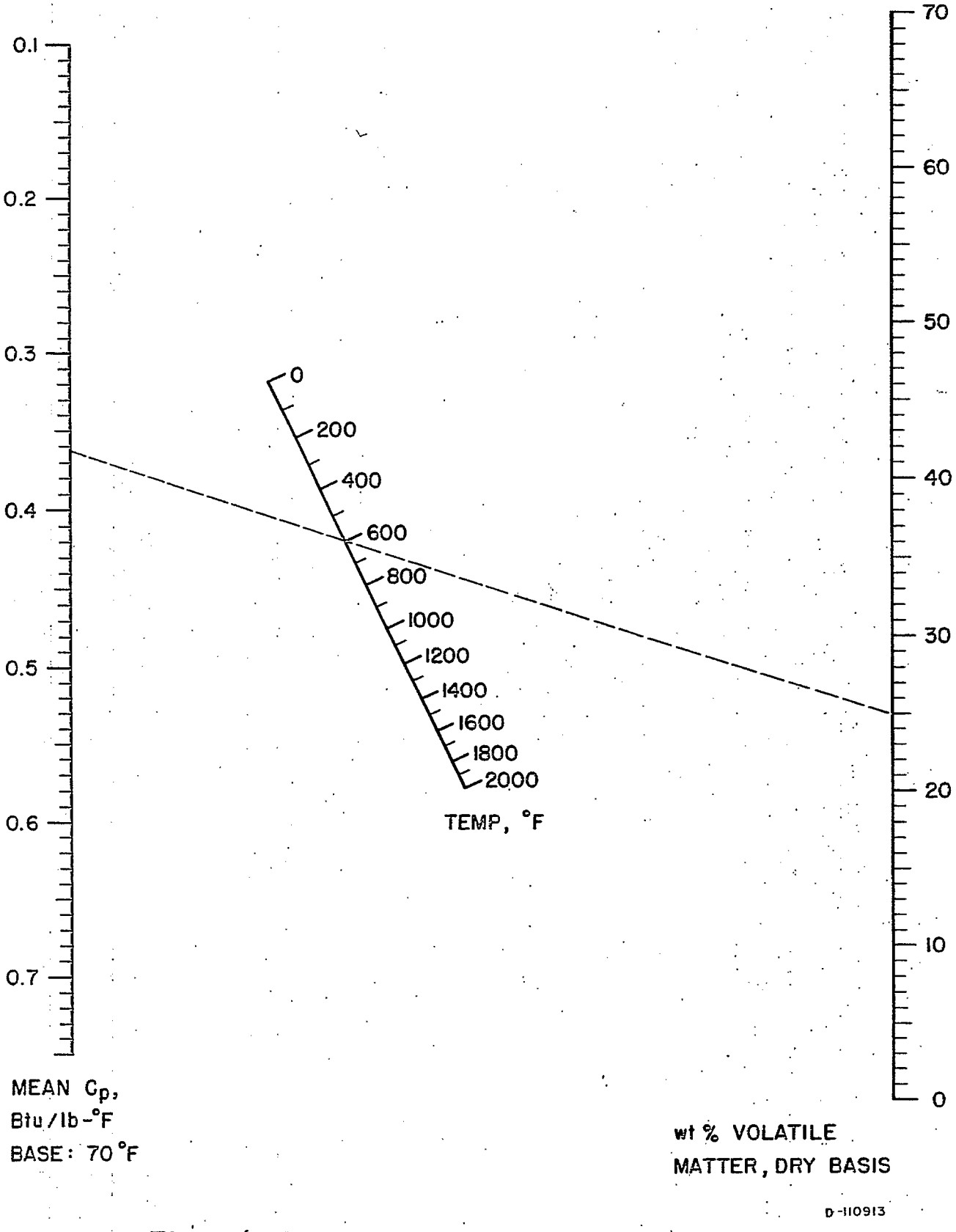

Figure 6c-20. NOMOGRAPH BASED ON EQUATION 8

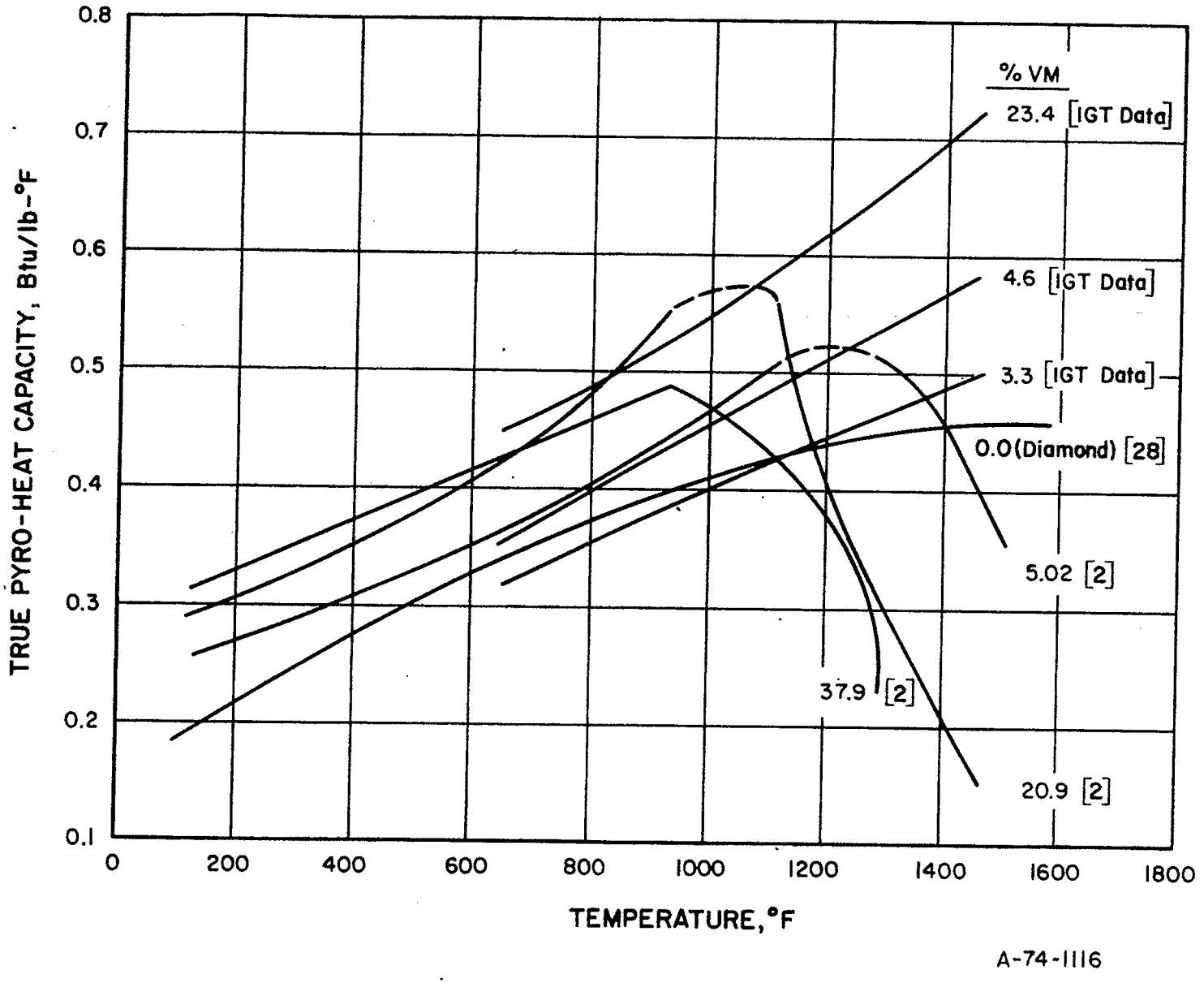

Figure 6c-21. TRUE PYRO-HEAT CAPACITIES OF COALS AND CHARS
(Brackets indicate data source; if not IGT,
please turn to 6c.8, References Cited)

Table 6c-8. CALCULATED TRUE PYRO-HEAT CAPACITY OF IRELAND MINE COAL AND CHARS

	t_2	t_1	t_{ave}	Cpm_2	Cpm_1	Q_2	Q_1	C_p
Raw Coal	1540	1400	1470	0.557	0.557	857.78	779.80	0.56
	1400	1300	1350	0.557	0.555	779.80	721.50	0.58
	1300	1200	1250	0.555	0.552	721.50	662.4	0.59
	1200	1100	1150	0.552	0.545	662.4	599.50	0.63
	1100	1000	1050	0.545	0.531	599.5	531.0	0.68
	1000	900	950	0.531	0.513	531.0	461.7	0.69
	900	800	850	0.513	0.490	461.7	392.0	0.70
	800	700	750	0.490	0.465	392.0	325.5	0.67
	700	600	650	0.465	0.435	325.5	261.0	0.65
Pretreated Coal	1540	1400	1470	0.488	0.465	751.52	651.0	0.72
	1400	1300	1350	0.465	0.448	651.0	582.4	0.68
	1300	1200	1250	0.448	0.432	582.4	518.4	0.64
	1200	1100	1150	0.432	0.415	518.4	456.5	0.62
	1100	1000	1050	0.415	0.400	456.5	400.0	0.56
	1000	900	950	0.400	0.382	400.0	343.8	0.56
	900	800	850	0.382	0.367	343.8	293.6	0.50
	800	700	750	0.367	0.352	293.6	246.4	0.47
	700	600	650	0.352	0.335	246.4	201.0	0.45
Low Temperature Residue	1540	1400	1470	0.395	0.376	608.3	526.4	0.58
	1400	1300	1350	0.376	0.362	526.4	470.6	0.56
	1300	1200	1250	0.362	0.350	470.6	420.0	0.51
	1200	1100	1150	0.350	0.335	420.0	368.5	0.52
	1100	1000	1050	0.335	0.322	368.5	322.0	0.47
	1000	900	950	0.322	0.308	322.0	277.2	0.45
	900	800	850	0.308	0.295	277.2	236.0	0.41
	800	700	750	0.295	0.282	236.0	197.4	0.39
	700	600	650	0.282	0.270	197.4	162.0	0.35
High Temperature Residue	1540	1400	1470	0.348	0.333	535.9	466.2	0.50
	1400	1300	1350	0.333	0.322	466.2	418.6	0.48
	1300	1200	1250	0.322	0.310	418.6	372.0	0.47
	1200	1100	1150	0.310	0.300	372.0	330.0	0.42
	1100	1000	1050	0.300	0.288	330.0	288.0	0.42
	1000	900	950	0.288	0.277	288.0	249.3	0.39
	900	800	850	0.277	0.266	249.3	212.8	0.37
	800	700	750	0.266	0.256	212.8	179.2	0.34
	700	600	650	0.256	0.245	179.2	147.0	0.32

A7506 1646

6c.8 References Cited

1. Agroskin, A. A., Goncharov, E. I., "The Specific Heat of Coal," Coke and Chemistry USSR No. 7, 9-14 (1965)

2. Agroskin, A. A., Goncharov, E. I., "Determination of the Specific Heat of Coals During Carbonization," Coke and Chemistry USSR 11, 16-20 (1965)

3. Batchelor, J. D., Yavorsky, P. M., Gorin, E., "Measurement of the Thermal Properties of Carbonaceous Materials," J.C.E.D. 4, 241-6 (1959)

4. Becker, F., Spalink, F., Z. Physik Chim. None Folge 26, 1 (1960)

5. Binford, Jr., J. S. Strohmenger, J. M., Hebert, T. H., "A Modified Drop Calorimeter, The Heat Content of Aluminum Carbide and Cobalt (II) Flouride Above 25°," J. Phy. Chem. 71, 2404-8 (1967)

6. Clendenin, J. D., Barclay, K. M., Donald, H. J., Gillmore, D. W., Wright, C. C., "Thermal and Electrical Properties of Anthracite and Bituminous Coals," Trans. 7th Annual Anthracite Conference of Lehigh Univ. May 5-6, 1949, Bethlehem, Pa.

7. Coles, G., "The Specific Heat of Coal and Its Relation to Composition," J. of the Soc. of Chem. Industry, XLII, 435-9 (1923)

8. Dainton, F. S., Draper, J., Ivin, K. J., Sheard, D. R., Trans Farraday Soc. 53, 1269 (1957)

9. Dewey, P. H., Harper, 3rd, D. R., "Heat of Combustion of Anthracite Cokes and of Artificial and Natural Graphites," Contribution 71, Carnegie Institute of Tech. and NBS 21, Oct. 1938

10. Duff, A. W., "Physics," Blakiston's, 8th ed. (1959)

11. Feldkirchner, H. L., Huebler, J., "Reaction of Coal With Steam-Hydrogen Mixtures at High Temperatures and Pressures," Ind. Eng. Chem. Process Design Develop. 4, 134 (1965)

12. Fritz, V. W., Moser, H., "Specific Heat, Thermal Conductivity and Thermal Diffusivity of Mineral Coal, Charcoal and Coke," Feneringstechnik u 28, 97-107 (1940)

13. Furukawa, G. T., Douglas, T. B., McCoskey, R. E., Ginnings, D. C., "Thermal Properties of Aluminum Oxide From 0° to 1200°K," J. Res. of National Bureau of Standards, 57, 67-82 (1956)

14. Gomez, M., Gayle, J. B., Taylor, Jr. A. P., "Heat Content and Specific Heat of Coals and Related Products," U.S. Bureau of Mines, Report 6607, 1964

15. Goodman, J. B., Gomez, M., and Parry, V. F., "Determination of Moisture in Low-Rank Coals," Bu. Mines Rept. of Inv. 4969, 1953.

16. Hubbard, W. N., Katz, C., Waddington, G., J. Phys. Chem. 58, 142 (1954)

17. Huebler, J., Schora, F. C., "Coal Hydrogasification," Chem. Eng. Progr. 62, 87 (1966)

18. "JANAF Thermochemical Tables," Distributed by: Clearinghouse for Federal Scientific and Technical Information, Springfield, Va.

19. Kavlick, V. J., Lee, B. S., "Coal Pretreatment in Fluidized Bed," Amer. Chem. Soc. Div. Fuel Chem. Preprints 10, No. 4, 131 (1966) September

20. Kazmina, V. V., "Determination of the Specific Heat of Cokes," Coke & Chem USSR, No. 11, 26-29 (1965)

21. Kleppa, O. J., J. Phys.Chem. 64, 1937 (1960)

22. Kubaschewski, O., Evans, E., "Metallurgical Thermochemistry," Pergamon Press, 234 (1958)

23. Kubaschewski, O., Evans, E., "Metallurgical Thermochemistry," Pergamon Press, 9 (1958)

24. Lacker, J. R., Kianpour, A., Getting, F., Park, J. D., Trans. Faraday Soc. 52, 1500 (1956)

25. LaMer, V. K., Road, C. L., J. Am. Chem. Soc. 52, 3098 (1930)

26. Lee, A. L. Feldkirchner, H. L., Schora, F. C. Henry, J. J., "Heat of Reaction of Hydrogen and Coal," Am. Chem. Soc. Div. of Fuel Chemistry, preprints 11, No. 2 pt. 2, 393-401 (1967)

27. Linden, H. R., "Pipeline Gas From Coal: Status and Future Prospects," Coal Age 71, 64 (1966)

28. Montell, C. L., Industrial Carbon, D. VanNostrand Co., Inc., N.Y. 2nd Ed. 1947, p. 432

29. Morlock, R. J., Naso, A. C., Cameron, J. R., "Heat Requirements for Coking," Presented at the Canadian Coal Conferences, Ottawa, Canada, March 30, 1967

30. Moseley, F., Paterson, D., "The Rapid High-Temperature High-Pressure Hydrogenation of Bituminous Coa.," J. Inst. of Fuel, 523-30 (1967)

31. Neigishi, G. R., J. Am. Chem. Soc. 58, 2293 (1936)

32. Oriani, R. S., Murphy, W. K., J. Phys. Chem. 62, 327 (1958)

33. Porter, H. C., Taylor, G. B., "The Specific Heat of Coal and Its Relation to the Presence of Combined Water in the Coal Substance," I.E.C. 5, 289-93 (1913)

34. Pyrcioch, E. J., Lee, B. S., Schora, F. C., "Hydrogasification of Pretreated Coal for Pipeline Gas Production," Amer. Chem. Soc. Div. Fuel Chem. Preprints 10, No. 4, 206 (1966) September

35. Pyrcioch, E. J., Linden, H. R., "Pipeline Gas by High-Pressure Fluid-Bed Hydrogasification of Char," Ind. Eng. Chem. 52, 590 (1960)

36. Rossini, F. D., et al., "Selected Values of Physical and Thermodynamic Properties of Hydrocarbon and Related Compounds," Pittsburgh: Carnegie Press, 1953.

37. Rossini, F. D., "Experimental Thermochemistry," Vol. I, Interscience, 309 (1956)

38. Rossini, F. D., Wagman, D. D., Evans, W. H., Levine, S., Jaff, I. NBS Circular 500, 386 (1952)

39. Speakman, J. B., Stott, E., Trans. Faraday Soc., 34, 1203 (1938)

40. Swietosjawski, W., "Microcalorimetry," Reinbold, N.Y. (1946)

41. Tai, T. M., Ph.D. Thesis, Univ. S. Carolina, 1966

42. Tajbl, D. G., Feldkirchner, H. L., Lee, A. L., "Cleanup Methanation for Hydrogasification Processes," Amer. Chem. Soc. Div. Fuel Chem. Preprints 10, No. 4, 235 (1966) September

43. Terres, V. E., Dahne, H., Nandi, B., Scheidel, C., Trappe, K., Rauth, P., "The Origin of Fusain Based on Its Specific Heats," Brennstoff-Chemie 366-70 (1956) June

44. Terres, V. E., Dahne, H., Nandi, B., Scheidel, C., Trappe, K., Rauth, P., "The Origin of Fusain Based on Its Specific Heats," Brennstoff-Chemie 269-73 (1956) June.

45. Ticknor, L. B., Bever, M. C., J. of Metals 4, 941 (1952)

46. Voloshin, A. L., Virozub, I. V., Kazmina, V. V., Kurbatova, M. Ya., "Determination of the Heat of Coking Under Laboratory Conditions," Coke & Chemistry USSR No. 3 17-20 (1962)

47. von Fredersdorff, C. G., Vandaveer, F. E., "Substitute Natural Gas From Coal," in Segeler, C. G., Ed., "Gas Engineers Handbook Section 3, Cahp. 9, 3/100-3/123. New York: The Industrial Press, 1965.

APPENDIX 6c-A

Background on Calorimetry

6C-Ai

In order to find a calorimeter for the measurement of the heat of reaction of hydrogen and coal, a survey was made of the then-current technique and equipment. Although none of the existing calorimeters seemed suitable for this work, many design concepts were helpful in constructing the present calorimeter.

An apparatus in which the energy change of sample can be determined is called a calorimeter. When the heat transfer medium is a liquid, the instrument utilized is termed a fluid calorimeter; when the medium is a solid, the instrument is termed a dry calorimeter. If the sample under study flows continuously, the instrument is termed a flow calorimeter; when the sample is static, the instrument is termed a batch calorimeter.

Additionally, an adiabatic calorimeter is one that has no heat transfer between the calorimeter and its surroundings during an experiment. A constant environment calorimeter is one which maintains constant temperature of all calorimeter components during an experiment. Both the adiabatic and the constant environment types of calorimeters are commonly used because the correction factors are much less rigorous than with other types of instruments, although they are by no means simple. Other types of calorimeters are anisothermal[4], Bunsen ice calorimeter[39], diphenyl ether calorimeter[8], flow calorimeters[24,25], and rotational calorimeters[16,40]. A number of heat-of-reaction type calorimeters were presented by Tai[41].

The present calorimeter is designed to be operated either adiabatically or isothermally, although it is easier to operate isothermally. The isothermal operation follows Newton's Law of cooling or heating[10]. In order to use this method, the temperature distribution in the calorimeter must be uniform at all times. This is easier said than done, but with proper design, instrumentation and calibration, temperature uniformity can be approximated within acceptable limits of error.

Referring to Figure 6c-A1, the calorimeter is inside an isothermal can at temperature T_s. Neck heaters are installed to assure that the calorimeter is at temperature T, which is dependent on time only.

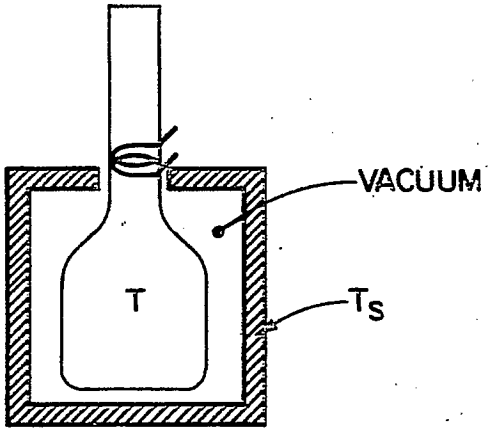

A-74-1119

Figure 6c-A1. CALORIMETER AND ISOTHERMAL CAN

The energy balance of this apparatus gives:

$$MCp \frac{dT}{d\theta} = \frac{dQ}{d\theta} + q_i - q_o \qquad (A\text{-}1)$$

where: $MCp \frac{dT}{d\theta}$ = rate of heat accumulation in the calorimeter due to the mass-heat capacity MCp.

$\frac{dQ}{d\theta}$ = rate of heat generation due to reaction or calibration heaters.

q_i = rate of heat input due to neck heaters or can heaters

q_o = rate of heat loss due to conduction, convection and radiation

If the rate of heat input from the heaters is constant, q_i is constant. The heat loss due to convection and radiation is kept at miniumu by placing the calorimeter in a vacuum jacket, and inserting (installing) convection shields as well as heaters in the neck with this modification for small $T-T_s$, the convection, q_c, and radiation, q_r, losses may be represented by,

$$q_c + q_r = k_1 (T-T_s) \qquad (A\text{-}2)$$

where k is a constant during the period of experiment. The conduction loss is,

$$q_d = k_2 \left[1 + 2 \sum_1^{\infty} \rho^{-\left(\frac{n\pi}{L}\right)^2 \alpha\theta} (2 \cos n\pi - 1)\right] (T-T_s) \qquad (A\text{-}3)$$

where L is the gap between the calorimeter and the can, and α is the thermal diffusivity of this gap and the exponential term approaches zero in this case,

$$q_d = k_2 (T-T_s) \qquad (A\text{-}4)$$

Combining equations

$$MCP \frac{dT}{d\theta} = \frac{dQ}{d\theta} + q_i - k (T-T_s) \qquad (A\text{-}5)$$

where, $k = k_1 + k_2$, and q_i and T_s are constants, then

$$MCp \frac{dT}{d\theta} = \frac{dQ}{d\theta} - k (T-T_o) \qquad (A\text{-}6)$$

where $T_o = \frac{q_i}{k}$, if $q_i = q_o = 0$, then $T_s = T_o$.

for the case $\frac{dQ}{d\theta} = 0$, it becomes the Newton's Law of Cooling,

$$\frac{dT}{d\theta} = -K\,(T-T\theta) \qquad (A-7)$$

where $K = \frac{k}{MCp}$

In actual cases, very few calorimeters follow Newton's Law of cooling because the thermal leakage, k, and equilibrium temperature, T_o, may or may not be constant during the entire period of experiment. In addition, there are problems such as time lagging in sensing instruments, non-uniform temperature distribution in the calorimeter, and unsteady temperature environment. All these factors must be accounted for either by detailed analysis and/or calibration. Detailed discussion of calorimeter analysis may be found in Appendix 6c-C.

APPENDIX 6c-B

Calculation Procedures

6C-B

Based on the discussion in Appendix A, an energy balance can be established either for calibration runs, heat of reaction experiments or heat capacity measurements.

6c-B. 1 Calibration Runs

For calibration of exothermic reaction, the calorimeter constant, MCp is calibrated by an electric heater as shown in Figure 6c-B1.

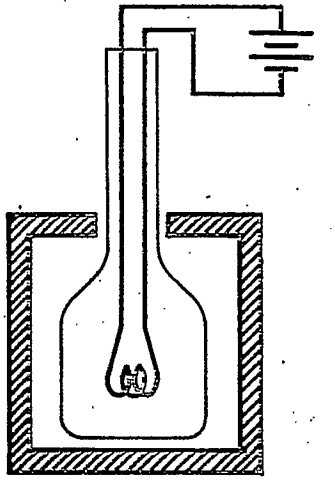

A-74-1120

Figure 6c-B1. ELECTRIC CALIBRATION

The calorimeter temperature and pressure are first stabilized. A measured amount of energy is then put into the heater for a known period of time. The temperature rise of the calorimeter is then measured. An energy balance yields,

$$MCp \frac{dT}{d\theta} = \frac{dQ}{d\theta} + q_i - q_o \qquad (B-1)$$

where $MCp \frac{dT}{d\theta}$ = rate of heat accumulation which, for a given time interval, is equal to:

$$(MCp\Delta T)_{Calorimeter} + (MCp\Delta T)_{heater} + (MCp\Delta T)_{shields} + (MCp\Delta T)_{gas}$$

$\frac{dQ}{d\theta}$ = rate of heat generation; for this time the power is turned on, it is equal to P/θ.

Equation (B-1) then becomes:

$$(MCp\Delta T)_{Calorimeter} + (MCp\Delta T)_{heater} + (MCp\Delta T)_{shields} + (MCp\Delta T)_{gas} = \frac{P}{\theta} + q_i - q_o \qquad (B-2)$$

Because stablized temperature is achieved for at least two hours before each run, and the power input period is very short, it is assumed that $q_i = q_o$ for the period of experiment. Also the M of calorimeter is much greater than that of the heater, shields and gas, it is safe to assume that

$$(MCp\Delta T)_{Calorimeter} >>> [\,(MCp\Delta T)_{shield} + (MCp\Delta T)_{gas} \approx 0.\,]$$

Equation (B-2) is then reduced to:

$$(MCp\Delta T)_{heater} + (MCp\Delta T)_{Calorimeter} = P/\theta \qquad (B-3)$$

where P = VI in watt hr
1 watt hr = 3.413 Btu
θ = time in hours
V = measured voltage in volts
I = measured current in amperes

Example:

$V = 29.5683$ volts
$I = 2.56283$ amps
$\theta = 20$ min $= \frac{1}{3}$ hr
$P/\theta = \frac{1}{3}(29.5683 \times 2.56283) \times 3.413 \frac{\text{Btu}}{\text{watt hr}} = 86.21$ Btu

$$(MCp)_{Calorimeter} = P/\theta - (MCp\Delta T)_{heater}$$

$$= \frac{86.21}{\Delta T} \text{ Btu} - 0.75\text{lb} \times 0.29 \frac{\text{Btu}}{\text{lb}^\circ\text{F}}$$

for $\Delta T = 19.0^\circ$F,

$$(MCp)_{Calorimeter} = \left(\frac{86.21}{19} - 0.221\right) \text{Btu}/^\circ\text{F} = 4.316 \text{ Btu}/^\circ\text{F}.$$

6c-B.2 Heat of Reaction

Let $q_i - q_o = K(\theta)$

where q_i = rate of heat input to calorimeter
q_o = rate of heat loss from calorimeter
$K(\theta)$ = the calibration constant dependent only on time.

Equation (B-1) becomes,

$$MCp \frac{dT}{d\theta} = \frac{dQ}{d\theta} + K(\theta) \qquad (B-4)$$

or $$MCpdT = dQ + K(\theta)d\theta \qquad (B-5)$$

where,

$$MCpdT = -MCp\Delta T)_{shield} + (MCp\Delta T)_{chain} + (MCp\Delta T)_{basket}$$
$$+ (MCp\Delta T)_{gas} + (MCp\Delta T)_{coal} \qquad (B-6)$$

$dQ = \Delta\bar{H}_r$, the heat of reaction (B-7)

and $K(\theta)d\theta$ is obtained from the calibration of the convection shield, chain, empty basket and the gas.

Equation (B-5) is then,

$$-\Delta\bar{H}_r = (MCp\Delta T)_{calorimeter} + (MCp\Delta T)_{coal} - K(\theta) \qquad (B-8)$$

Example: Run 22, Pretreated Coal.

$$(MCp\Delta T)_{calorimeter} = (7.05 \text{ But}/^\circ\text{F})(0.46^\circ\text{F}) = 3.24 \text{ Btu}$$

$$(MCp\Delta T)_{coal} = \frac{4/08 \text{ g}}{453.5924 \text{ g/lb}} \left(0.4 \frac{\text{Btu}}{\text{lb } ^\circ\text{F}}\right)(1200^\circ\text{F}) = 4.23 \text{ Btu}$$

$$K(\theta)d\theta = 2.96 \text{ Btu (From Run 20)}$$

$$-\bar{H}_r = 3.24 + 4.23 + 2.96 = 10.43 \text{ Btu } \left(= 2476 \frac{\text{Btu}}{\text{lb coal reacted}}\right)$$

APPENDIX 6c-C

Heat Transfer Analysis of Heat of Reaction Calorimeter

6c-Ci

6c-C. 1 Introduction

Because the calorimeter is very thick, there is thermal lag in temperature measurement. The time-temperature cooling or heating does not follow Newton's law of cooling. In order to interpolate the experimental results, an analysis pinpointed the temperature difference for the determination of the calorimeter constant and heat of reaction data.

6c-C. 2 Overall Heat Balance

Rate of (Heat in − Heat out) = Rate of Accumulation − Rate of Generation + Unaccounted for Energy

Rate of Heat in = Radiant heat input from Can

$$\approx \epsilon_R \tau A_R (T_C^4 - T_R^4)$$

T_C = Can temperature

T_R = Temperature of Reactor

Rate of Heat our = Loss through the neck of Reactor

$$\approx kA \left.\frac{dT_R}{dx}\right|_{neck}$$

Rate of accumulation in vessel $= \int_o^{V_v} \rho_v C_{p_v} \frac{dT_R}{dt}\, dX$

where the integration extends over the reactor

Rate of accumulation in gas $(H_2) = \int_o^{V_g} \rho_g C_{v_g} \frac{dT_g}{dt} dX$

Rate of accumulation in heater $= m_H C_{p_H} \frac{dT}{dt}$

Rate of accumulation in convection shield $\sim m_s C_{p_s} \frac{dT}{dt}$

Rate of heat generation by electric heater $= E(t) \cdot I(t)$

Unaccounted for terms = Heat loss through the neck in the gas, etc.

6c-C. 3 Steady-State Operation Before the Calibration Run

Assuming that the terms for unaccounted are small, the heat balance is:

$$\epsilon_R \tau A_R (T_c^4 - T_R^4) - k A \left.\frac{dT_R}{dX}\right|_{neck} = 0$$

It is desireable that if steady-state is not present, these terms cancel each other. To investigate this, use the approximation:

$$\frac{dT_R}{dX} \approx \frac{T_R - T_S}{\Delta X}$$

where T_S is the temperature of the surrounding coolant temperature on the neck.

Assume that the temperature of the reactor is raised to T_H ($T_H - T_R \sim 5°F$)

$$T_H^4 \approx T_R^4 + 4T_R^3 \ (T_H - T_R)$$

Substituting into the above balance and assuming that T_C remains constant:

$$\epsilon_R \tau A_R \left(T_C^4 - (T_R^4 + 4T_R^4 (T_H - T_R)\right) - \frac{kA}{\Delta X} \left(T_R - (T_R - T_H) - T_S\right) = ?$$

or

$$\epsilon_R \tau A_R \left(T_C^4 - T_R^4\right) - kA \frac{T_R - T_S}{\Delta X}$$

$$- \epsilon_R \tau A_R 4T_R^3 (T_H - T_R) - \frac{kA}{\Delta X} (T_H - T_R) = ?$$

correction terms

One may see, then, that the correction terms are addictive rather than compensating (or canceling). Because the magnitude of these terms has not been determined, it is difficult to estimate the error introduced by the correction terms.

6c-C.4 Process of Heat Transfer During Calibration

The process of heat transfer during calibration is assumed to take place in the following manner. Two typical temperature profiles are shown in Figure 6c-C1 as a function of time. One temperature is measured at the top of the reactor, the other at the bottom.* The temperature profile is divided into five regimes. These regimes may be described with reference to Figure 6c-C2. The heater is turned on at time 0 but thermocouples will not sense any temperature rise until heat reaches them. Heat is transferred through the gas by conduction and convection. Then heat is transferred through the metal reactor until it reaches the thermocouple. The time delay in the metal has been estimated to be less than 0.08 minute. Because the total time delay is about 2 minutes, we conclude that most of the delay occurs in the gas. Further, most of the heat transferred in the gas to the solid is assumed to be transferred by convection. This assumption could be checked by determination of the thermal diffusivity of hydrogen K. Unfortunately, however, this quantity has not been measured; it should be estimated, but this will not be done here. If the quantity:

$$\frac{k \cdot 2 \text{ min}}{\ell^2} < 0.01$$

* These data are taken from run 1, Pages 1, 2, 3, 4, and 15 of unpublished data book 1.

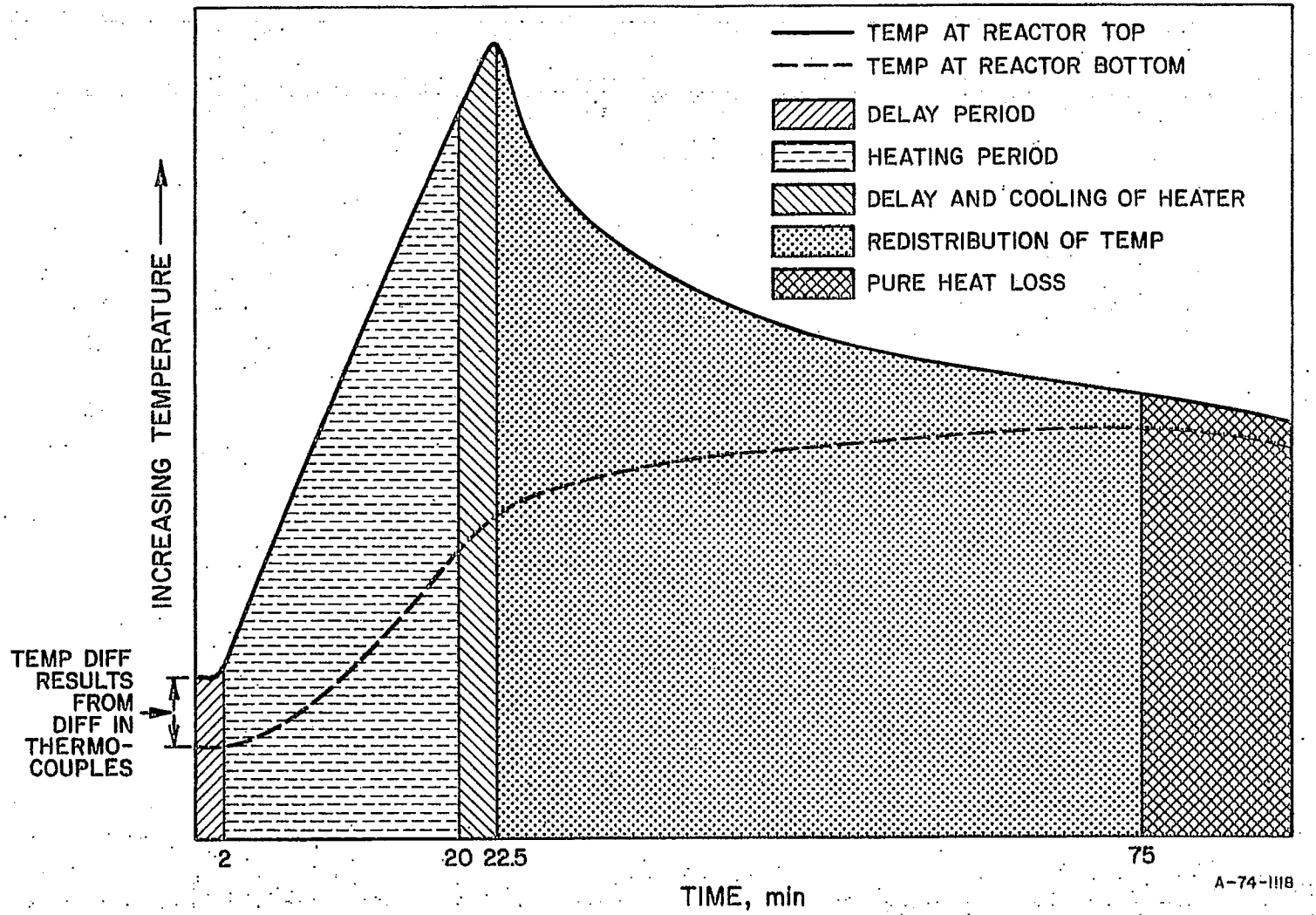

Figure 6c-C1. TYPICAL TEMPERATURE PROFILES AS A FUNCTION OF TIME

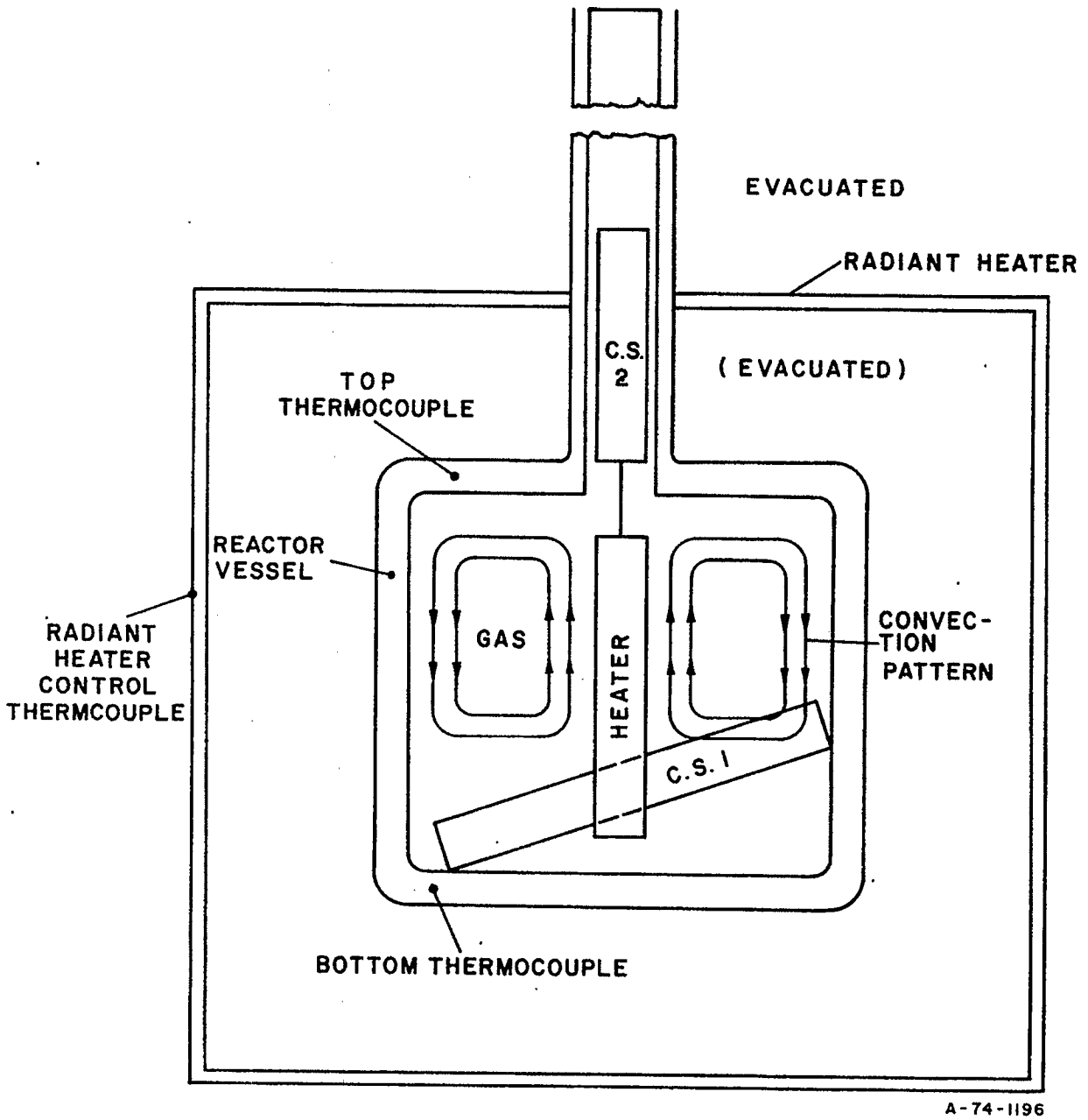

Figure 6c-C2. REACTOR VESSEL

where ℓ is the distance between the heater and the reactor wall, one could conclude that the effect of conduction is negligible and that convection predominates.

Assuming that the conduction in the gas is small, heat transfer takes place by passing from the heater to the gas next to it. This gas is heated and consequently begins to rise to the top of the vessel. When it reaches the top, it begins to transfer heat to the vessel and consequently cools down and begins to fall down along the side of the vessel continually losing heat to the vessel walls. Thus, a stable circulation pattern is set up. The top portion of the vessel is always exposed to the hotter gas while the lower portion is exposed to the cooler gas. This effect explains the divergence between reactor top and reactor bottom temperature curves in Figure 6c-C1 during the heating period.

After the heater is turned off, a certain amount of heat is still in the heaters and a certain amount of delay is observed. The period is almost equal to the delay period at the start of heating.

After these three periods, the vessel has an unequal temperature throughout; and the gas circulation has ceased with the higher temperature gas at the top. The temperature in the vessel is now redistributed principally by conduction on the metal so that the temperature at the bottom increases and the temperature at the top decreases.

Throughout these first four periods, heat has been lost to the surroundings, principally by the mechanism of the correction term previously described.

$$\text{correction term} = -\epsilon_R \tau A_R T_i^3 \, (T - T_i) - \frac{kA}{\Delta X} (T - T_i)$$

where T_i is the initial temperature of the vessel and T is an average temperature at any time.

After the first four periods, this is the predominant heat transfer mode; the effect caused the negative slope of both temperature curves in the last period, in Figure 6c-C1. Because the slope is very small, it is assumed that the heat loss throughout the first four periods is small and may be neglected.

From this analysis, it is seen that the total heat release from the heater in the first two periods is approximately equal to the heat gain by the system from time = 0 to time = 75 minutes. Because the temperature throughout the system is approximately a constant at each of these times is constant, the overall energy balance can be integrated very easilty to obtain:

$$(V_v \rho_v C_{pv} + V_g \rho_g C_{vg} + m_H C_{pH} + m_s C_{ps}) \, (T(75 \text{ min}) - T(0 \text{ min}))$$

$$= \int_0^{20} E(t) \cdot I(t) dt$$

$$- \int_0^{75} \left[\epsilon_R \tau A_R 4T_R^3 (T(t) - T_i) + \frac{kA}{\Delta X} (T(t) - T_i) \right] dt$$

$$+ \int_0^{75} \text{unaccounted for terms}$$

Because we will neglect the last two terms, and because the voltage and current are held constant,

$$MC_{PT} = (V_v \rho_v C_{pv} + V_g \rho_g C_{vg} + m_H C_{PH} + m_s C_{ps}) = \frac{E \cdot I \cdot 20 \text{ min}}{T(75 \text{ min}) - T(0 \text{ min})}$$

where mCp_T is the total heat capacity.

6c-C.5 Maximum Error

An estimate of the error incurred in using $T(75) - T(0)$ may be obtained by extrapolating the temperature slope in the pure conduction region to the beginning of the heating period to obtain a ΔT_E. This extrapolation is indicated in Figure 6c-C-1 and indicates that a maximum error of about 30 percent could be involved in using this value of $\Delta T = T(75) - T(0)$. It is felt that use of $\Delta T + \Delta T_E$ will give a better estimate of mC_{pt}. However, if $T(75) - 7(0)$ is used in the calibration and in the experimental runs, the error in ΔT will tend to cancel if $\overline{H_R}$ is close to $E \cdot I \cdot t$.

6c-C.6 Determination of the Heat of Reaction of an Experimental Run

In this case, the total heat of reaction ($\overline{H_R}$) may be calculated quite simply as

$$\overline{H_R} = \int_0^t H_R(t)dt = (V_v \rho_v C_{pv} + V_g \rho_g C_{vg} + m_H C_{pH} + m_s C_{ps})(T(t) - T(0))$$

where t is the time required to go through the first four periods, and $m_H C p_H$ is an average of the coal, ash, and holder.

It should be noted that with this simplified analysis it is not possible to calculate the heat release as a function of time. Only the total heat of reaction can be calculated.

Many assumptions have been made in the previous development. Fortunately it is possible to check the most important one. This assumption is the existence of the redistribution of temperature. This is done in the following section.

6c-C.7 Time After the Maximum Temperature is Reached (Redistribution of Temperature)

It is apparent from the previous statements that a temperature distribution will exist in the reaction cell after the heater has been turned off. This distribution is due to free convection. For order-of-imagnitude purposes, one may consider this temperature distribution to be a linear function of distance with the maximum temperature occurring at the top of the cell and the minimum occurring at the bottom.

In order to test the hypothesis that the decrease in temperature measured by the top thermocouple results from the redistribution of the heat in the cell walls, the cell walls will be approximated by a slab with a linear temperature distribution with no heat loss or gain from the surroundings. The temperature at the center of the slab is assumed constant because the problem is symmetrical about the center and the following boundary value problem may be formulated (see Figure 6c-C3):

$$T(t, X)$$

$$\rho C_p \frac{\partial T}{\partial t} = k \frac{\partial^2 T}{\partial X^2}$$

$$T(0, X) = (T_{max} - T_{avg}) \frac{X}{\ell} + T_{avg}$$

$$T_{avg} = (T_{max} + T_{min}) \quad (2)$$

$$T(t, 0) = T_{avg}$$

$$T(t, \ell) = T_{max}$$

The solution to this problem is given in Carslaw and Jaeger as:

$$\frac{T - T_{avg}}{T_{max} - T_{avg}} = \frac{2k}{\pi} \sum_{n=1}^{\infty} \frac{(-1)^{n-1}}{n} e^{\frac{-Kn^2\pi^2 t}{\ell^2}} \sin\left(\frac{n\pi X}{\ell}\right)$$

Graphical results for this equation are presented in Carslaw and Jaeger, page 98. The temperature $T(t, \ell)$ is given in terms of $T = \frac{Kt}{\ell^2}$ $K = \frac{k}{\rho C_p}$

In this application:

$$K = 7 \quad \frac{Btu}{hr\ ft\ °F \cdot \frac{3 lb}{in^2} \times \frac{0.103\ Btu}{lb\ °F} \times \frac{12\ in.}{ft} \times \frac{1\ hr}{60\ min.}}$$

$$= .315 \frac{in.^2}{min}$$

$$t = \frac{4\ in.^2}{.315 \frac{in.^2}{min}} \qquad \tau = 51\tau\ min$$

The temperatures at the top, bottom and middle of the reactor are plotted in Figure 6c-C4 and are seen to correspond quite well to the only experimental temperature profiles available. In particular, the time required for redistribution of the temperature is in good agreement. In the absence of any further experimental measurement of $T(t, -\ell)$, HYGAS researchers concluded that the proposed mechanism is reasonable.

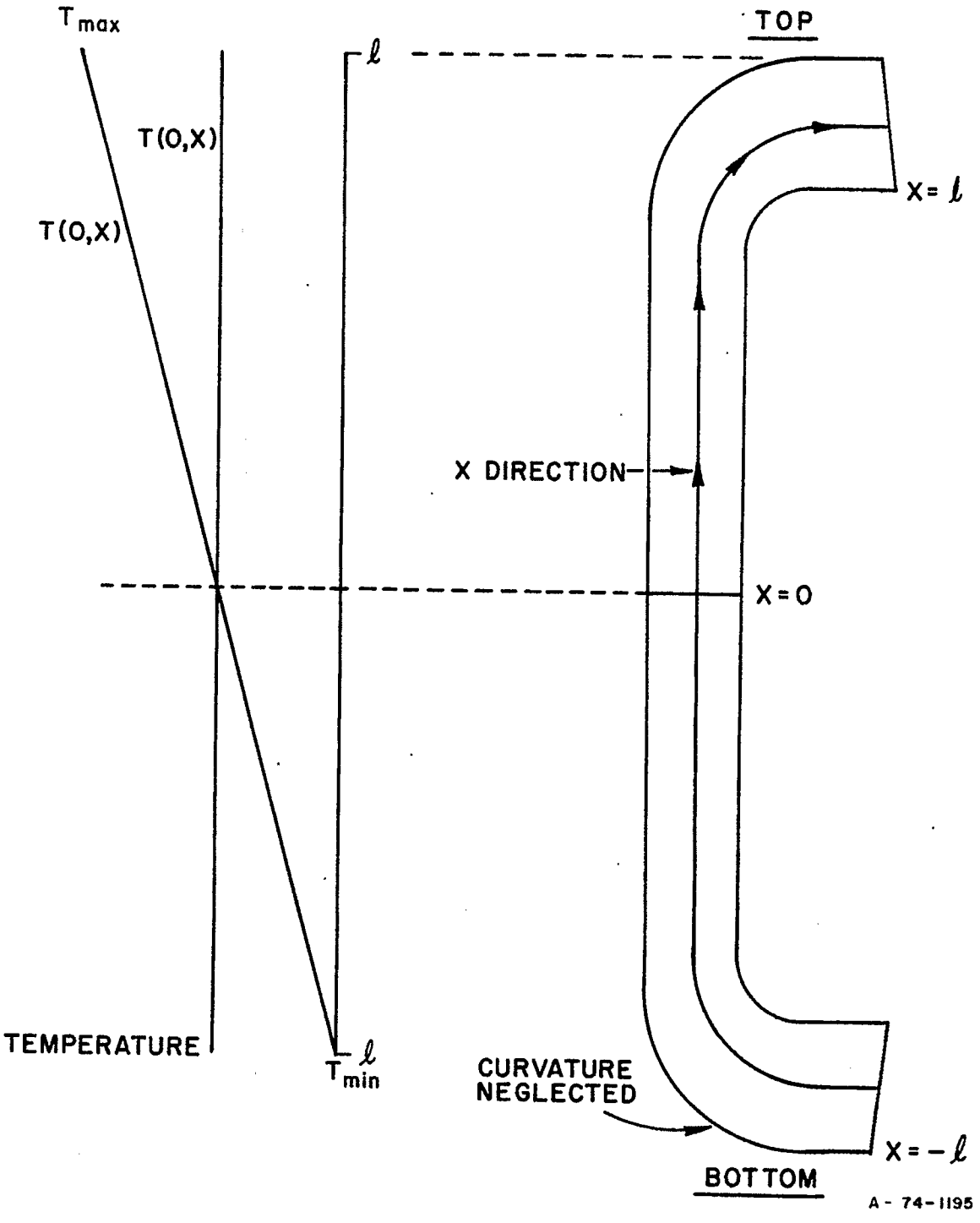

Figure 6c-C3. TEMPERATURE DISTRIBUTIONS IN PERIOD 4

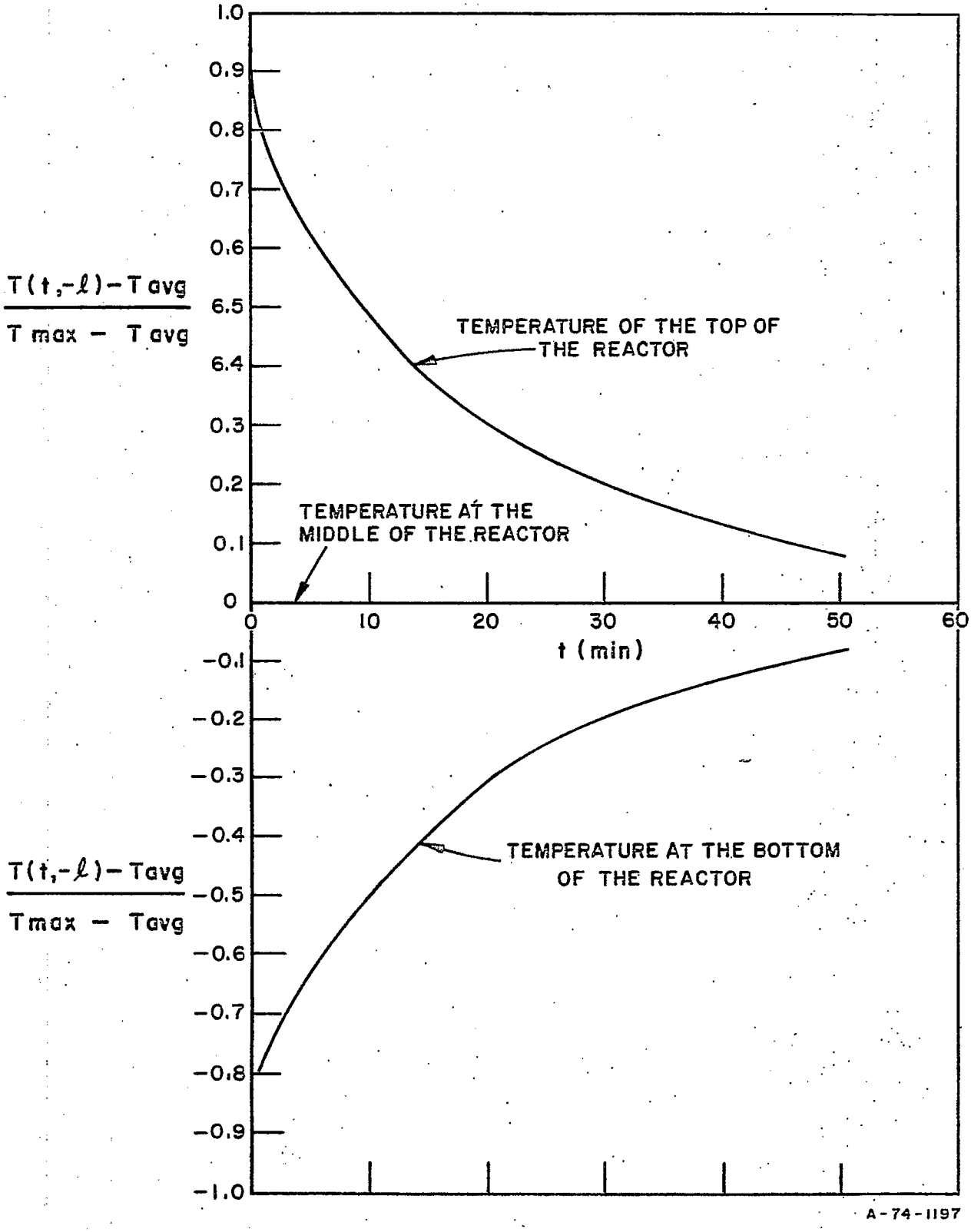

Figure 6c-C4. THEORETICAL TEMPERATURE PROFILES IN PERIOD 4

PART 6d

Kinetics of Coal Gasification

TABLE OF CONTENTS, PART 6d

LIST OF FIGURES, PART 6d

LIST OF FIGURES, PART 6d
(Continued)

LIST OF FIGURES, PART 6d
(Continued)

LIST OF FIGURES, PART 6d
(Continued)

LIST OF TABLES, PART 6d

6d.0 Summary of Kinetics of Coal Gasification

A summary of this work appears in section 6.0.

6d.1 Introduction

A general mathematical model was developed from experimental studies by HYGAS researchers and other laboratories that quantitatively describes the kinetics of pertinent gasification reactions of selected coals in gases containing steam and hydrogen. The purposes for developing this model were to help interpret test results obtained in laboratory and pilot-scale experimental studies and to provide a basis for rational design of intermediate- or commercial-scale reactor systems.

The HYGAS-associated experimental information used in the development and evaluation of the model includes certain of the fluid- and moving-bed test results reported in this report, as well as test results obtained in an experimental study sponsored by Fuel Gas Associates that was conducted from 1966 to 1970. Here pilot-plant-scale fluid beds and a laboratory thermobalance were investigated.

The results obtained with the thermobalance were particularly useful for developing a quantitative kinetic model for coal gasification, as gasification rates could be measured at constant, well-defined gaseous environmental conditions. Such measurements could not be conveniently made with integral fluid- or moving-bed gasification systems where significant gas conversion occurred. Test results from the integral systems considered were therefore primarily evaluated by comparing total gasification rates, determined experimentally, with predicted gasification rates that were computed from the model developed. The predicted rates required reasonable assumptions of gas and solid flow configurations in individual systems. This allowed us to evaluate local rates of gasification throughout a given system, and thus the net rates of gasification for a system as a whole.

Additional selected data available in the literature were also used to develop the model and to quantitatively evaluate parameters in the correlations derived from the model. Investigators at Consolidation Coal Company obtained the literature data used most extensively, using an experimental system that permitted estimation of differential gasification rates of char with steam-hydrogen mixtures in a fluid bed.

In the following discussion, the thermobalance and the type of data obtained with it are described first. Then the overall model of coal gasification adopted in development of quantitative correlations is generally described. Development of the specific kinetic correlations is then discussed. Finally, the consistencies between the predictions of the correlations and test results obtained in various experimental systems in which significant gas conversion occurred are demonstrated.

6d.2 Laboratory-Scale Thermobalance Apparatus

During the past several years, an extensive experimental program at IGT has used a laboratory-scale thermobalance apparatus to obtain kinetic information about coal gasification. Since a significant amount of this information was used in the formulation of the kinetic correlations developed, it is pertinent to generally describe this experimental system. The details of the thermobalance have been described earlier.[1]

The thermobalance is an apparatus capable of continuously weighing a coal sample undergoing gasification in a gaseous environment of desired composition at constant pressure. Temperatures can either be kept constant or varied (10 °F/min = maximum rate).

The nature of gas-solid contacting with this apparatus is shown in Figure 6d-1. The coal sample is contained in the annular space of a wire-mesh basket bounded on the inside by a hollow stainless steel tube and on the outside by a wire-mesh screen. The thickness of the bed is only 2 to 3 particle diameters when using −20+40 USS sieve size particles to facilitate mass and heat transfer between the bed and its environment. With this system, gas flow rates can be used that are sufficiently high (relative to rates of gas evolution from the coal samples used, 0.5-1.5 g) so that gas conversion is negligible. In many of the tests conducted, the wire-mesh basket is initially in an upper cool portion of the reactor in which downward inert gas flow is maintained. During this time, desired temperature and pressure conditions are established in a lower heated portion of the reactor in the presence of a flowing gas of desired composition. A test is initiated by lowering the basket into the heated reaction zone. It takes about 1 minute for the bed to heat up to reaction temperature. Figure 6d-2 shows typical weight loss with time during gasification of low-temperature air-pretreated coal char.

6d.3 General Description of Overall Kinetic Model

In the development of a quantitative kinetic model of coal gasification suitable for use in engineering application, overall reactions that occur rapidly should be distinguished from those that occur much more slowly. Blackwood and McCarthy,[2] for example, have proposed that gasification of coal with hydrogen is a two-stage process in which hydrogen initially reacts very rapidly with the volatile constituents in the coal, followed by a comparatively slow reaction of hydrogen with the residual carbon. These investigators further suggest that these two reactions may be considered as consecutive stages and independent of each other. Similarly, Feldkirchner and Linden[3] have postulated that during the initial period of hydrogasification of coal, pyrolysis rapidly occurs, resulting in devolatilization of the light components, which then undergo hydrogenolysis. This period is then followed by the much slower gasification of the residual char formed.

The models proposed by Blackwood and McCarthy and by Feldkirchner and Linden are similar in that it is assumed that methane could be formed rapidly from the reaction between hydrogen and volatile coal constituents. Although it is not clear whether this reaction is considered to occur in the vapor phase or in the coal substance itself, such an explanation implies that only a limited amount of carbon can be gasified to form methane via this route, since the amount of volatile constituents in a given coal is limited. There is, however, experimental evidence that the total carbon that can be gasified rapidly to methane during the initial reaction stage increases with increasing hydrogen partial pressure in such a manner that, at sufficiently high pressures, virtually all of the carbon in the coal can be gasified to methane. Such behavior has been observed experimentally by Moseley and Paterson,[4] and is suggested by results described by Zahradnick and Glenn.[5] Similar behavior has also been observed in experimental studies at IGT with the thermobalance.

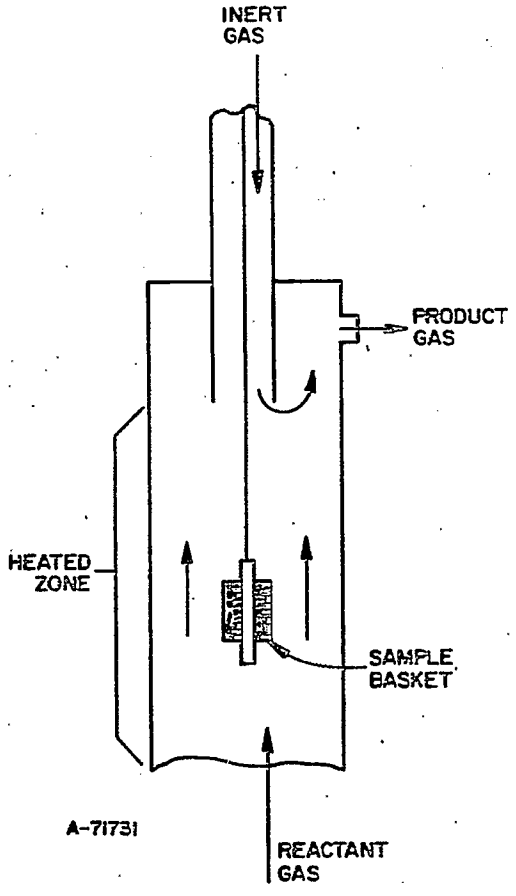

Figure 6d-1. THERMOBALANCE REACTOR

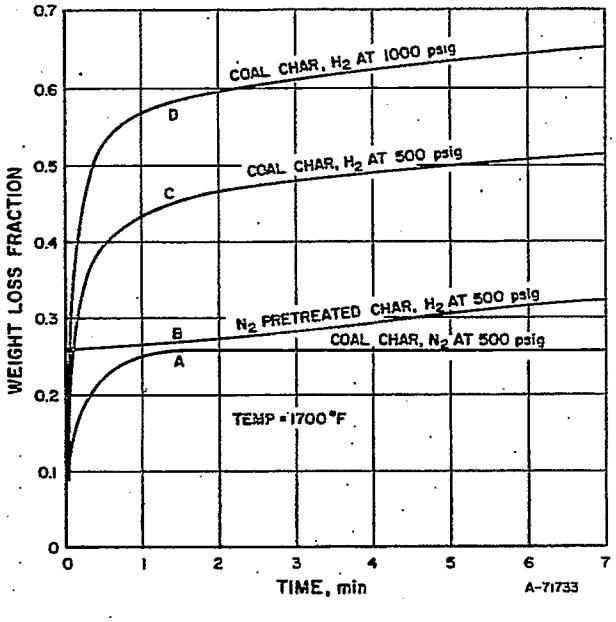

Figure 6d-2. WEIGHT LOSS WITH TIME DURING GASIFICATION OF LOW-TEMPERATURE-AIR-PRETREATED IRELAND MINE BITUMINOUS COAL CHAR

Moseley and Paterson,and Zahradnick and Glenn have proposed similar three-stage models of coal gasification to describe their results. It is assumed that concurrent with the complex phenomena that occur during devolatilization of coal even in an essentially inert gas atmosphere there occurs, when gaseous hydrogen is present, a hydrogen-activated decomposition of some element in the coal structure, which gives rise to an active intermediate that is responsible for the transient high reactivity of coal for methane formation. This reactivity is transient since the active intermediate can also deactivate, possibly due to crosslinking or some polymerization process. Both of these processes are considered to be independent of hydrogen partial pressure, although they likely are activated by the presence of small hydrogen concentrations. Methane formation is catalyzed by the active intermediate, the rate of this step being proportional to the hydrogen partial pressure. The two models proposed differ in that Zahradnick and Glenn assume that the active intermediate is also consumed in the methane formation step, whereas Moseley and Paterson assume that it is unaffected by this step. Zahradnick and Glenn also assume that the formation of the active intermediate is very rapid compared to its subsequent removal via polymerization or due to methane formation, whereas the correlation developed by Moseley and Paterson is consistent either with this assumption or the assumption that the rate of polymerization is much more rapid than the formation rate of the active intermediate.

A significant characteristic of the three-stage model described above is that, at sufficiently high hydrogen pressures, carbon conversion can be virtually complete before the active intermediate is deactivated. Because of the consistency of experimental results now available with this behavior, including results obtained with the thermobalance, such a model has been adopted in the overall development of a quantitative model described in this report. The following three reaction regimes assumed in our model can then be briefly described as follows:

Devolatilization: An extremely rapid process at elevated temperatures, involving the thermal decomposition of coal into devolatilized char and gases containing CO, CO_2, H_2, H_2O, and CH_4 as well as higher hydrocarbons, oils, and tar.

Rapid-Rate Methane Formation: Also an extremely rapid process at elevated temperatures, occurring essentially concurrently with devolatilization whereby methane is formed in the presence of hydrogen in the gaseous atmosphere at rates much greater than methane formation rates obtained with the char resulting from devolatilization.

Low-Rate Gasification: A relatively slower process than those described above, wherein steam and hydrogen interact with char containing negligible volatile matter to form carbon oxides, hydrogen, and methane.

Although both devolatilization and rapid-rate methane formation are considered to occur concurrently, for most practical purposes low-rate gasification can be considered to take place after these rapid processes are essentially completed.

In the development of the model adopted in this study, it has been assumed that the carbon in coal-containing volatile matter is of two distinct types: volatile carbon and base carbon. The volatile carbon is associated with the carbon that can be gasified solely from thermal treatment of the coal. Although it has been observed that this quantity can vary somewhat for extreme values of heat-up conditions, a reasonable approximation of this quantity pertinent to conditions anticipated in many coal gasification processes can be made based on standard coal analyses. Specifically, if —

C_T = total carbon in the feed coal, g/g feed coal

C_B = carbon remaining after standard devolatilization, g/g feed coal

then —

C_V = volatile carbon in feed coal, g/g feed coal

$= C_T - C_B$

With this definition, C_B represents the base carbon content of the feed coal. It is assumed that at temperatures above about 1500 °F, all volatile carbon is rapidly gasified within the devolatilization regime. Base carbon gasification is considered to occur within the rapid-rate methane formation and low-rate gasification regimes.

The definitions given above are consistent with the following simplified view of coal structure. The coal structure can be considered to be comprised of base carbon to which side chains are attached. These side chains contain essentially the components of the volatile matter in the feed coal (including volatile carbon). Thus as coal is heated in a hydrogen-containing atmosphere, pyrolysis reactions cause gasification of the side chains (devolatilization); concurrently the carbon in the base structure is gasified (rapid-rate methane formation) in the presence of the active intermediate which is both formed and deactivated in the base structure. When deactivation of this intermediate is effectively completed, then carbon in the base structure is further gasified relatively slowly within the low-rate gasification regime.

Consistent with the description above, the following definition of base carbon conversion fraction applies when all volatile carbon has been gasified.

$$X = (C_G - C_V)/(C_T - C_V) \qquad (1)$$

where

X = base carbon conversion fraction
C_G = total carbon gasified, g/g feed coal

This definition is used in correlations in a later section, to describe carbon gasification kinetics in the rapid-rate methane formation regime and the low-rate regime.

The results shown in Figure 6d-2 can be interpreted in terms of the three reaction regimes defined above. Curve A corresponds to a test in which a low-temperature, air-pretreated bituminous coal char is exposed to

a nitrogen atmosphere at 500 psig. During the first minute when the sample is heating up in the thermobalance, weight loss corresponds to evolution of volatile matter. After this period no further significant weight loss occurs. The total weight loss of about 26% corresponds closely to the volatile matter in the feed coal as obtained by standard proximate analysis. Within the context of the reaction regimes defined, weight loss in this test is considered to occur entirely in the devolatilization regime where all volatile carbon has been gasified and all base carbon remains in the devolatilized char. When the char resulting from this test is then exposed to hydrogen at 500 psig (Curve B), there is further weight loss due to reaction of the hydrogen with base carbon to form methane. This reaction, which takes place at a much lower rate than devolatilization, is considered to occur in the low-rate reaction regime. With this particular sample, there was no reaction in the rapid-rate methane formation regime because the active intermediate responsible for this reaction was deactivated during prolonged exposure of the sample to nitrogen.

Weight loss due to reaction in the rapid-rate methane formation regime is evident, however, for Curve C, where a sample of the original coal char was exposed only to hydrogen at 500 psig with no initial exposure to nitrogen. There is a weight loss in this test during the first minute or so that is considerably more than the corresponding weight loss obtained during this period when the coal char was exposed to nitrogen (Curve A). The difference in weight loss between Curves C and A during the first minute or so is considered to be due to gasification of base carbon in the rapid-rate regime. It is seen that weight losses of the magnitude exhibited by Curve B during this period are negligible, which justifies the assumption that base carbon in the rapid-rate methane formation regime and in the low-rate gasification regime can be considered gasified consecutively. As will be indicated in a later section, more than 90% of the base carbon to be gasified via the rapid-rate reaction is completed for air-pretreated coal char after about 3 minutes. Thereafter, base carbon is primarily gasified in the low-rate gasification regime.

Curve D is qualitatively similar to Curve C, except that is a greater weight loss from rapid-rate methane formation due to the higher hydrogen pressure. Generally, there are also greater gasification rates in the low-rate gasification regime for higher hydrogen pressures, although this is not clearly evident for the curves shown in Figure 6d-2 because of the relatively short time periods employed.

6d. 4 Rapid-Rate Methane Formation Kinetics

The gasification kinetics of base carbon in the rapid-rate regime have been treated both in terms of the total amount of base carbon that can be gasified via this route (when deactivation is completed at specific reaction conditions) and in terms of the rate of this reaction prior to deactivation of the coal. Generally, for tests conducted at temperatures greater than 1500°F, most of the rapid-rate base carbon is gasified during heat-up of the coal in the thermobalance, so a reasonable definition of actual solid temperatures could not be made. For such tests, the total base carbon gasified via the rapid-rate reaction was estimated by correcting the total weight loss after

about 3 minutes for volatile matter weight loss and the usually small amounts of base carbon gasification that could be attributed to reaction in the low-rate gasification regime. Corrections for reaction in the low-rate gasification regime were based on kinetic correlations developed for this regime, which are discussed in a later section. Generally, after about 3 min, devolatilization is complete for the temperature considered. Weight loss due to devolatilization was assumed to be equal to the volatile matter in the feed coal as determined by standard proximate analysis. Actual values of carbon gasified were computed from total values of weight loss, using empirical correlations that define values of other coal components, particularly hydrogen and nitrogen which are gasified along with base carbon. These correlations were based on analyses of solid residues from tests in which devolatilization was essentially completed. Specifically, these correlations permitted definition of H/C and N/C ratios in char residues as a function of gasification temperature for temperatures greater than 1500°F.

Tests were also conducted on the thermobalance in the range of 700° to 1500°F to obtain a more detailed picture of rapid-rate gasification kinetics since, for these conditions, rates of both devolatilization and rapid-rate methane formation could be specifically measured. Interpretation of weight loss measurements at these conditions, however, in terms of base carbon gasified required a more detailed procedure to define evolution of other coal components, not only as a function of temperature but of time.

6d.4.1 Rapid-Rate Methane Formation Kinetics Above 1500°F

Results similar to those illustrated in Figure 6d-2 have been obtained for a large number of tests conducted on the thermobalance with three particular coals. The analyses of these coals are given in Table 6d-1. The results of these tests have generally shown that for a particular coal and above 1500°F the base carbon conversion fraction due to rapid-rate methane formation, X_r, is a function only of hydrogen partial pressure. This relationship, however, applies only where rapid-rate methane formation is completed and the coal is deactivated with respect to reaction in this regime. Specifically, results have been correlated with the following form of expression:

$$M(X_r) = \int_0^{X_r} \frac{\exp(0.969X^2)\,dx}{(1-X)^{2/3}} = k_r p_{H_2} \qquad (2)$$

where

k_r = kinetic parameter dependent on coal type, atm^{-1}
p_{H_2} = hydrogen partial pressure, atm

The empirical form of this correlation was suggested by equation forms used to describe kinetics in the lower-rate gasification regime, which are discussed in a later section. It is significant, however, that the function, $M(X_r)$, is for all practical purposes equal to the function, $-\ln(1-X_r)$,

for values of X_r as high as 0.99, although $M(X_r)$ approaches a finite value of about 5.8 as X_r approaches 1, whereas $-\ln(1 - X_r)$ approaches infinity at this same limit. Empirical trends of Equation 2 invite comparison with correlations proposed by other investigators to describe total carbon conversion fraction attributed to rapid-rate methane formation as a function of hydrogen partial pressure. Such equations proposed by Zahradnick and Glenn[5] and Moseley and Paterson[4] for this case are as follows:

Zahradnick and Glenn[5]

$$X_r = \frac{ap_{H_2}}{1 + ap_{H_2}}$$

Moseley and Paterson[4]

$$X_r = 1 - \exp(-bp_{H_2})$$

where

a,b = kinetic parameters dependent on coal type, and temperature, atm^{-1}

Table 6d-1. COMPOSITIONS OF COALS EXTENSIVELY USED IN THERMOBALANCE TESTS

Material	Bituminous Coal Char* Pittsburgh No. 8 (Ireland Mine)	Bituminous Coal Montour No. 10	North Dakota Lignite (Mercer County District Glenharold Mine)
	Composition (dry), mass %		
Ultimate			
Carbon	71.1	78.3	66.4
Hydrogen	4.26	3.46	4.48
Oxygen	8.85	9.99	19.63
Nitrogen	1.26		0.78
Sulfur	3.64	1.01	0.79
Ash	10.89	7.24	7.92
Total	100.00	100.00	100.00
Proximate			
Fixed Carbon	60.7	75.2	48.5
Volatile	28.4	17.6	43.6
Ash	10.9	7.2	7.9
Total	100.0	100.0	100.0

* Air-pretreated at about 700°F.

A7506 1647

The empirical trends of these correlations are compared in Figure 6d-3. In representing the equation proposed by Zahradnick and Glenn, values of X_r are plotted against 0.683 a p_{H_2}, in order that a value of $X_r = 0.5$ results when

$$0.693\, a\, p_{H_2} = b\, p_{H_2} = k_r p_{H_2} = 0.693$$

Figure 6d-3 shows that the particular form of correlation adopted in this study (equation 2) is virtually identical to the relationship proposed by Moseley and Paterson, since $M(X_r) \cong -\ln(1 - X_r)$, although significant differences in empirical trends are predicted by the correlation form proposed by Zahradnick and Glenn.

The parameter k_r in equation 2 was found to be independent of temperature above about 1500°F, which is consistent with behavior observed by Blackwood and McCarthy,[2] although Zahradnick and Glenn[5] suggest that a comparable kinetic parameter, "a", used in their correlation, is temperature-dependent.

In Figure 6d-4, values of $M(X_r)$ are plotted versus p_{H_2} for a series of gasification tests conducted with air-pretreated Ireland mine bituminous coal char in hydrogen and hydrogen-methane mixtures. The value of k_r computed as the slope of the line drawn is 0.0092 atm^{-1}. The same value of slope corresponds to the line drawn in Figure 6d-5 for data obtained with Montour No. 10 bituminous coal with hydrogen. An average value of k_r for North Dakota lignite based on three duplicate tests in hydrogen at 500 psig and 1700°F is 0.0087 atm^{-1}.

Figure 6d-6 shows a plot of $M(X_r)$ versus p_{H_2} for tests conducted with the Ireland mine coal char in steam-hydrogen mixtures. The straight line drawn in Figure 6d-6 was constructed with a slope of 0.0092 atm^{-1}. Since this line reasonably represents the data, there is no apparent effect of steam partial pressure on the rapid-rate reaction. It is significant that no rapid-rate reaction occurs in pure steam, as indicated in Figure 6d-7. Results obtained with hydrogen-methane mixtures included in Figure 6d-4 also indicate negligible effects of methane partial pressure on this phenomenon.

6d.4.2 Rapid-Rate Methane Formation Kinetics Below 1500°F

The experimental results described above suggest that equation 2 adequately defines the effect of hydrogen partial pressure on rapid-rate methane formation, which occurs relatively rapidly when solids are heated to temperatures greater than 1500°F in a hydrogen-containing atmosphere. At temperatures less than 1500°F, the rapid-rate phenomenon is more complex. Results obtained on the thermobalance at temperatures from 800° to 1500°F indicate that in this temperature range methane forms during more extended periods of time — at least for the −20+40 USS sieve size particle of air-pretreated Ireland mine bituminous coal char used. This behavior is shown in Figure 6d-8, where total coal char weight loss is plotted versus time for a series of tests conducted at 35.5 atm. The curves were computed from correlations discussed below. For tests conducted at temperatures below about 1280°F, negligible low-rate gasification

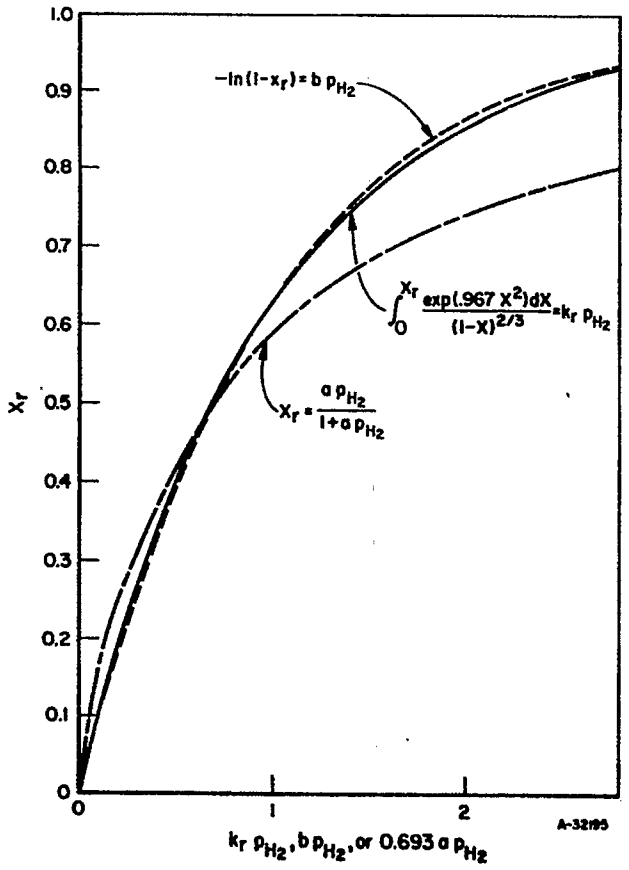

Figure 6d-3. COMPARISON OF EMPIRICAL TRENDS PREDICTED BY DIFFERENT CORRELATION FORMS

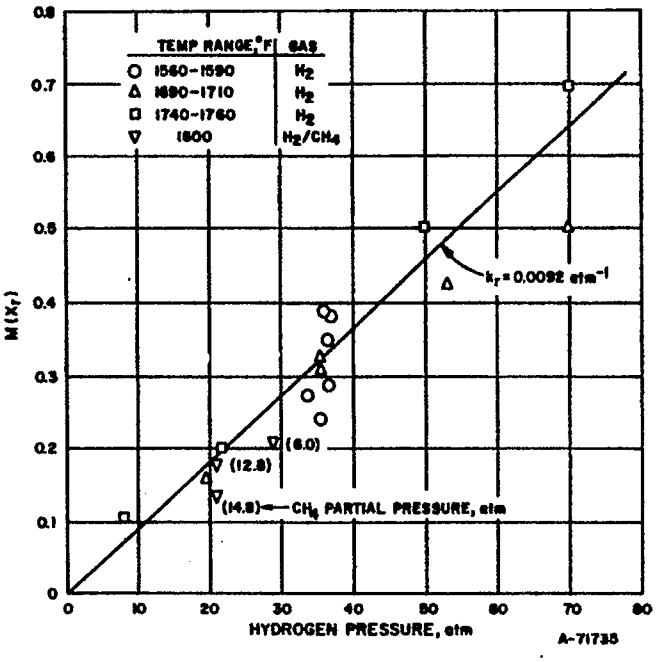

Figure 6d-4. EFFECT OF HYDROGEN PRESSURE ON RAPID RATE METHANE FORMATION FROM GASIFICATION OF IRELAND MINE BITUMINOUS COAL CHAR WITH HYDROGEN AND HYDROGEN-METHANE MIXTURES

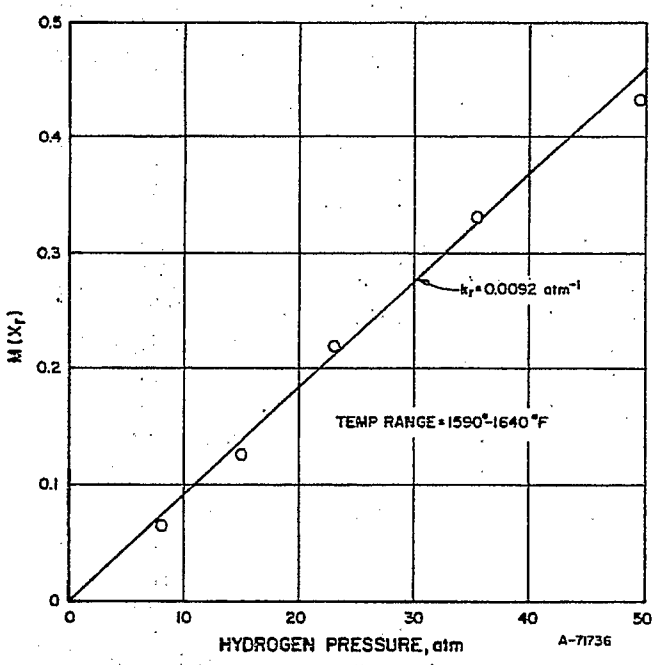

Figure 6d-5. EFFECT OF HYDROGEN PRESSURE ON RAPID-RATE METHANE FORMATION FROM GASIFICATION OF MONTOUR No. 10 BITUMINOUS COAL WITH HYDROGEN

Figure 6d-6. EFFECT OF HYDROGEN PRESSURE ON RAPID-RATE METHANE FORMATION FROM GASIFICATION OF IRELAND MINE BITUMINOUS COAL CHAR WITH STEAM-HYDROGEN MIXTURES

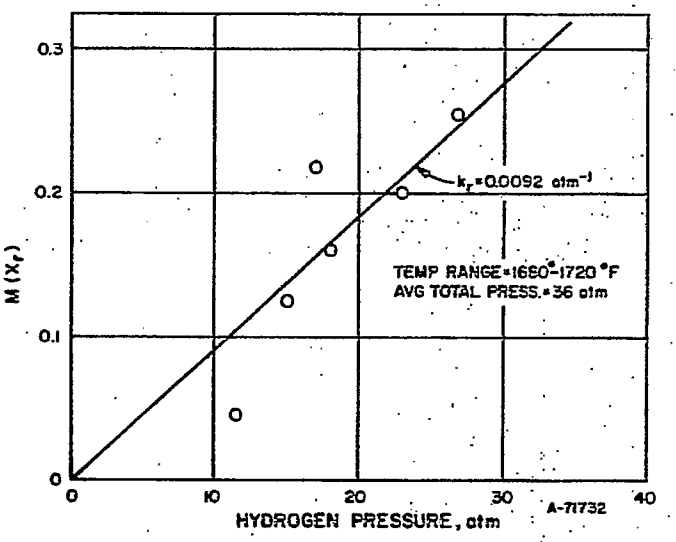

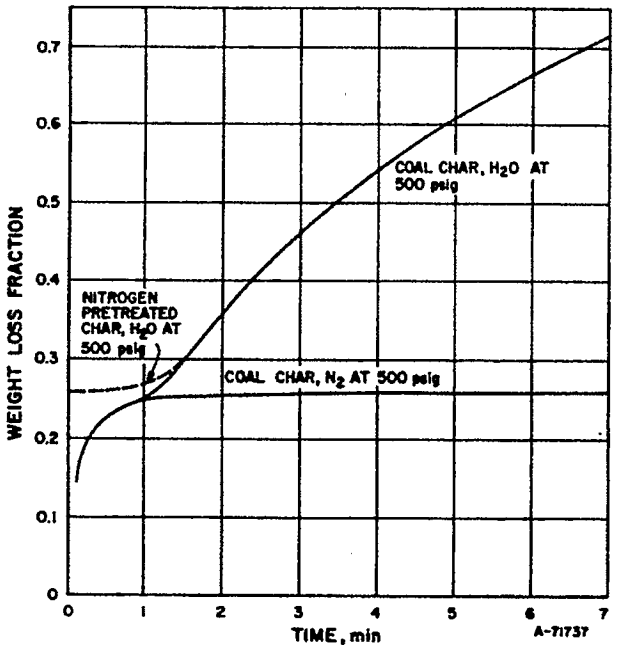

Figure 6d-7. WEIGHT LOSS WITH TIME DURING GASIFICATION OF IRELAND MINE BITUMINOUS COAL CHAR WITH STEAM AT 1700°F

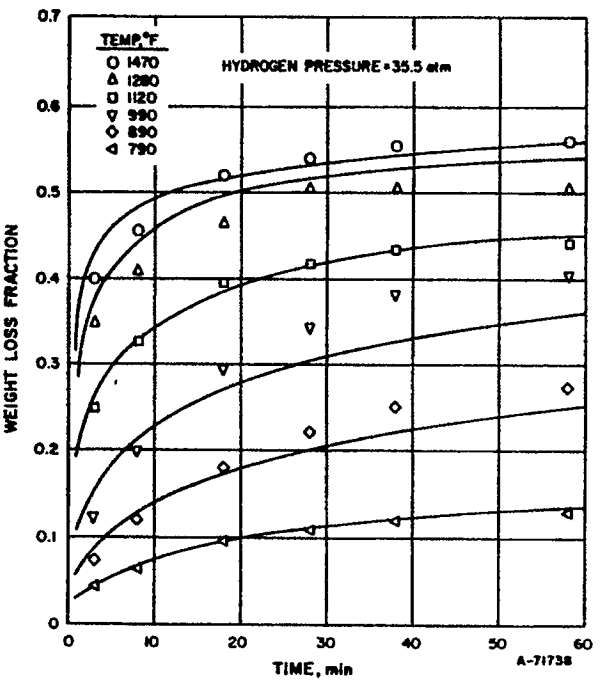

Figure 6d-8. WEIGHT LOSS WITH TIME DURING GASIFICATION OF IRELAND MINE BITUMINOUS COAL CHAR WITH HYDROGEN AT VARIOUS TEMPERATURES

contributes to coal weight loss for test periods of about 1 hour. Above this temperature, however, some of the weight loss is due to low-rate gasification.

The effect of pressure on base carbon gasification in hydrogen at these lower temperatures is illustrated in Figure 6d-9. The difference in weight loss exhibited by a given curve, relative to the weight loss at zero hydrogen partial pressure,* reflects the base carbon gasified. The upward trends which the curves exhibit at temperatures greater than about 1300°F are indicative of the onset of low-rate gasification of the base carbon. Nevertheless, it is seen that there is a significant effect of hydrogen partial pressure on base carbon gasification at all temperatures employed.

Effects of prior treatment conditions on rapid-rate methane formation at lower temperatures are shown in Figure 6d-10. At temperatures greater than about 1000°F, prior treatment in nitrogen tends to deactivate the coal for subsequent rapid-rate methane formation in hydrogen. At temperatures greater than 1500°F, the treatments used result in total deactivation, and base carbon conversion is due solely to low-rate gasification.

Data obtained for rapid-rate methane formation with Ireland mine bituminous coal char at temperatures above 800°F have been correlated from the following model. It is assumed that an active intermediate is formed at conditions conducive to devolatilization and this intermediate can simultaneously deactivate in a manner suggested by Zahradnick and Glenn[5], or by Moseley and Paterson.[4] It is also assumed that base carbon gasification rates are proportional to the concentration of this transient intermediate, as well as to hydrogen partial pressure. The pertinent reaction steps assumed can be represented as follows:

$$R_o \rightarrow R^* \qquad \text{(Step A)}$$

$$R^* \rightarrow R \qquad \text{(Step B)}$$

$$R^* + C + 2H_2 \rightarrow R^* + CH_4 \qquad \text{(Step C)}$$

These steps are essentially the same as those suggested by Moseley and Paterson, although our kinetic description of these steps, discussed below, is quite different from theirs.

It is assumed that steps A and B are essentially activated by hydrogen but become independent of hydrogen partial pressure at relatively low pressure. The species R_o is assumed to convert to the active species R^* via a first-order reaction, but the activation energy for the first-order rate constant corresponding to this reaction is considered to vary for different members of the total family of the R_o species. With this assumption, the rate of step A can generally be represented by the following equation:

$$\frac{dN_{R_o}}{dt} = -N^o_{R_o} \int_0^\infty f(E) k_A \exp\left(-\int_0^t k_A dt\right) dE \qquad (3)$$

* Tests conducted in nitrogen.

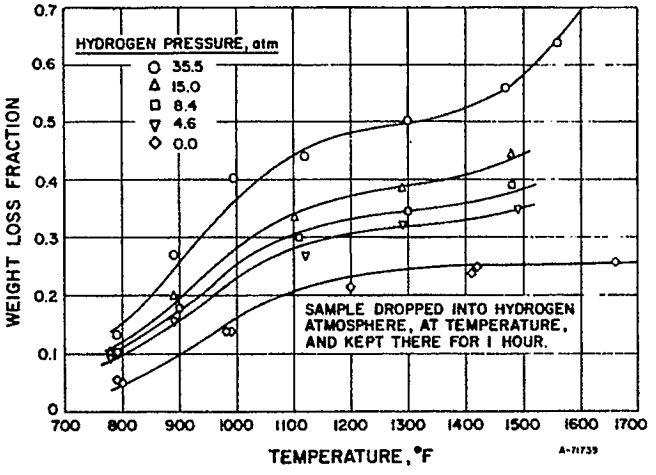

Figure 6d-9. EFFECTS OF TEMPERATURE AND PRESSURE ON WEIGHT LOSS DURING GASIFICATION OF IRELAND MINE BITUMINOUS COAL CHAR WITH HYDROGEN

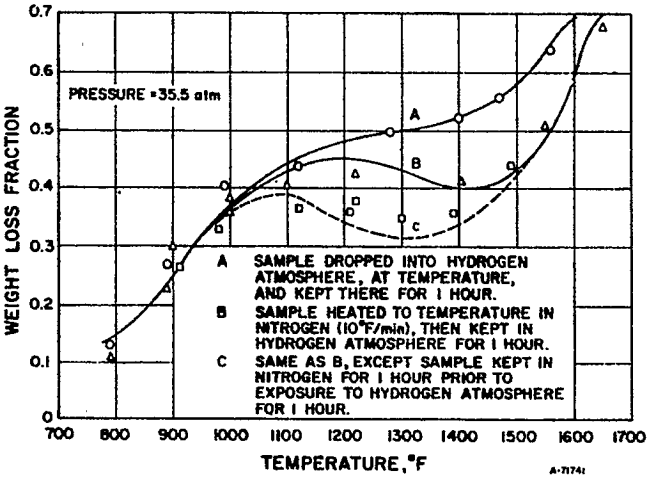

Figure 6d-10. EFFECT OF IRELAND MINE BITUMINOUS COAL CHAR PRETREATMENT IN NITROGEN ON SUBSEQUENT WEIGHT LOSS IN HYDROGEN

where —

$$k_A = k_A^o \exp\left(-\frac{E}{T}\right)$$

and

$f(E)$ = function characterizing distribution of activation energies ($R \cdot E$, where R gas constant), such that

$$\int_0^\infty f(E) \cdot dE = 1$$

N_{R_o} = concentration of R_o species at any time, t, moles/mole base carbon

$N_{R_o}^o$ = initial concentration of R_o species, moles/mole base carbon

t = time, min

T = absolute temperature, °R

k_A = rate constant, min^{-1}

k_A^o = preexponential factor, min^{-1}

E = (activation energy)/R, for Step A, °R

The rate of step B, which is assumed to occur via a first-order process, is described by the expression

$$\frac{dN_R}{dt} = k_B N_R^* \qquad (4)$$

where —

N_R = concentration of R species at time, t, moles/mole base carbon

N_R^* = concentration of R* species at time, t, moles/mole base carbon

k_B = rate constant, min^{-1}

The rate of step C is assumed to be described by the following equation:

$$\frac{dX}{dt} = k_c p_{H_2} N_H (1 - X)^{2/3} N_R^* \exp(-0.969 X^2) \qquad (5)$$

where —

X = base carbon conversion fraction, moles/mole initial base carbon

k_c = rate constant, min^{-1}, atm^{-1}

p_{H_2} = hydrogen partial pressure, atm

N_H = concentration of species, H, on coal, moles/mole base carbon

The concentration of the species H is assumed to be constant in a hydrogen atmosphere. When no prior treatment of the coal is used, then $N_H = N_H^o$. When the coal has been heated, however, as in, for example, nitrogen, then the value of N_H is less than the value of N_H^o, as described below.

Equations 3, 4 and 5 can be solved subject to certain assumptions to yield the following expression for base carbon conversion as a function of pertinent conditions for the case of varying temperature, and constant hydrogen partial pressure.

$$\int_0^X \frac{\exp(0.969\,X^2)}{(1-X)^{2/3}}\,dX = \frac{N_H}{N_H^o} k_r p_{H_2} \left\{ 1 - \frac{4\alpha^{3/2}}{\sqrt{\pi}} \int_{E_1}^{\infty} (E-E_1)^2 \right.$$

$$\left. \cdot \exp[-\alpha(E-E_1)^2] \cdot \left[\exp\left(-k_A^o \int_0^t \cdot \exp\left(-\frac{E}{T}\right) dt \right) \right] dE \right\} \qquad (6)$$

where –

$$k_r = \frac{k_c N_H^o N_{R_o}^o}{k_B}, \qquad (6a)$$

$$f(E) = \frac{4\alpha^{3/2}(E-E_1)^2}{\sqrt{\pi}} \cdot \exp[-\alpha(E-E_1)^2], \text{ for } E \geq E_1, \qquad (6b)$$

and –

$$f(E) = 0, \text{ for } E < E_1 \qquad (6c)$$

where –

E_1 = constant, characteristic of distribution of activation energies, °R

α = constant, characteristic of distribution of activation energies, $°R^{-2}$

In the derivation of equation 6, it was assumed that $k_B >> k_A$ at any temperature and for any value of E, and that the ratio k_c/k_B is temperature-independent.

For gasification of coal in hydrogen at constant temperature, where no prior nitrogen heat treatment is employed, equation 6 can be reduced to the following form:

$$\int_0^X \frac{\exp(0.969\,X^2)\,dX}{(1-X)^{2/3}} =$$

$$k_r p_{H_2} \left\{ 1 - \frac{4\alpha^{3/2}}{\sqrt{\pi}} \int_{E_1}^{\infty} (E-E_1)^2 \exp[-\alpha(E-E_1)^2] \cdot \exp\left[-k_A^o \exp\left(-\frac{E}{T}\right) \cdot t \right] \cdot dE \right\} \qquad (7)$$

This equation was used to correlate data from thermobalance tests with hydrogen, which are shown in Figures 6d-8 through 6d-10. The curves in these figures were computed from the following evaluation of parameters in equation 7:

$$k_r = 0.0092 \text{ min}^{-1}, \text{ atm}^{-1}$$

$$\alpha = 1.352 \ (10^{-7}), \ ^\circ R^{-2}$$

$$E_1 = 16{,}400 \ ^\circ R$$

Other information was also used in computing the curves to account for sample weight loss due to devolatilization. For this purpose, the volatile coal components were divided into three groups: hydrogen, carbon, and residual (oxygen + nitrogen + sulfur). The hydrogen and residual components were assumed to gasify according to the simple reaction:

$$A \text{ (solid)} \rightarrow B \text{ (gas)}$$

The reaction is assumed to be first-order but, again, the activation energies for the first-order rate constants are considered to vary for individual members of each family of components. Thus, assuming distribution function of the form given in equation 6b to describe variations in activation energies, the concentration of hydrogen or the residual component is represented by the expression —

$$N_A = \frac{N_A^\circ \cdot 4\alpha^{3/2}}{\sqrt{\pi}} \int_{E_1}^{\infty} (E - E_1)^2 \ \exp\left[-\alpha(E - E_1)^2\right] \cdot \exp\left[- k_A^\circ \int_0^t \exp\left(-\frac{E}{T}\right) dt \right] \cdot dE \quad (8)$$

where —

N_A = concentration of hydrogen (or residual) component in coal at any time, t, g/g base carbon
N_A^o = concentration of hydrogen (or residual) component in feed coal, g/g initial base carbon
k_A^o = preexponential factor, min^{-1}

Values of the parameters in equation 8, which were used to correlate data obtained with Ireland bituminous mine coal char, are given in Table 6d-2. Results of devolatilization tests conducted in a nitrogen atmosphere indicated that the amount of volatile carbon component gasified is approximately proportional to the amount of residual component gasified; it was assumed that the proportionality constant obtained in nitrogen was also applicable for devolatilization in hydrogen. The value of the proportionality constant obtained with Ireland mine bituminous coal char is as follows:

$$\frac{\text{volatile carbon gasified}}{\text{residual component gasified}} = 0.73 \text{ g/g}.$$

The value of k_r obtained to describe experimental results for gasification below about 1500°F is consistent with results obtained above 1500°F, since equation 7 essentially reduces to equation 2 at the higher temperatures for times greater than a few minutes.

The effect of nitrogen pretreatment on subsequent rapid-rate methane formation was accounted for, assuming the reaction step —

$$H_o \rightarrow H \qquad \text{(Step D)}$$

This reaction is assumed to occur only in the absence of hydrogen, according to the following rate expression:

$$\frac{dN_H}{dt} = -k_D N_H \qquad (9)$$

or —

$$N_H = N^\circ_H \exp\left(-\int_o^t k_D\, dt\right) \qquad (10)$$

where —

$$k_D = k^\circ_D \exp\left(-\frac{E_D}{T}\right) \qquad (10a)$$

For tests in which the coal is preheated in nitrogen for a period $_1$, followed by treatment in hydrogen at constant temperature for a period $_2$, the following equation applied to describe base carbon conversion:

$$\int_0^X \frac{\exp(0.969\,X^2)\,dX}{(1-X)^{2/3}} = k_r p_{H_2} \exp\left[-\int_0^{\theta_1} k^\circ_D \exp\left(-\frac{E_D}{T}\right) dt\right]$$

$$\left\{1 - \frac{4\alpha^{3/2}}{\sqrt{\pi}} \int_{E_1}^{\infty} (E-E_1)^2 \exp\left[-\alpha(E-E_1)^2\right] \cdot \exp\left[-k^\circ_A \exp\left(-\frac{E}{T}\right) \cdot \theta_2\right] dE\right\} \qquad (11)$$

Table 6d-2. KINETIC PARAMETERS USED IN DEVOLATILIZATION CORRELATION (Ireland Mine Bituminous Coal Char)

Solid Component	k°_A, min^{-1}	E_1, °R	α, $°R^{-2}$	N°_A, g/(g feed base carbon
Hydrogen:				
In H_2 atm	$3.564\,(10^{12})$	30,339	$1.31\,(10^{-9})$	0.052
In N_2 atm	$2.572\,(10^{13})$	30,339	$1.31\,(10^{-9})$	0.052
Residual	$2.064\,(10^{18})$	49,684	$4.69\,(10^{-9})$	0.217

A7506 1648

This equation was used to calculate the curves given in Figure 6d-10 using values of k_D^o and E_D given below:

$$k_D^o = 10^5 \text{ min}^{-1}$$

$$E_D = 25{,}632 \text{ °R}$$

Tests with the thermobalance using pure steam, steam-hydrogen, and hydrogen-methane mixtures determined the effects of concentrations of gaseous species, other than hydrogen, on rapid-rate methane formation below about 1500°F. Results with steam and steam-hydrogen mixtures are given in Figures 6d-11 and -12. The curves drawn were computed with the correlations described above, assuming that rapid-rate methane formation is dependent only on hydrogen partial pressure.

In computing values for the curves drawn in Figures 6d-11 and -12, correlations developed to describe low-rate gasification were also used for temperatures greater than about 1200°F. These correlations are described in a later section. The results show, however, that the rapid-rate step does not occur in pure steam and that, in steam-hydrogen mixtures, steam does not inhibit the reaction.

Results with hydrogen-methane mixtures are given in Figures 6d-13 and -14 where, again, the curves drawn were computed from the assumption that methane does not inhibit the rapid-rate step. Although the data obtained at 35.7 atm were somewhat scattered, these results do not indicate any obvious systematic effect of methane concentration on rapid-rate methane formation. It should be noted, however, that the closest approach to equilibrium with respect to the reaction —

$$C \text{ (graphite)} + 2H_2 \rightleftarrows CH_4 \qquad (12)$$

studied with the hydrogen-methane mixtures (given in Figure 6d-14 was obtained for a methane/hydrogen ratio of 0.506 mol/mol at 35.7 atm and 1370°F. The equilibrium constant for the above reaction is about 0.084 atm^{-1} at this condition, whereas the experimental $p_{CH_4}/p_{H_2}^2$ ratio is about 0.021 atm^{-1}. Attempts to make tests with higher methane/hydrogen ratios were complicated by carbon deposition in the coal bed and on the wire mesh basket at long exposure times. This is shown in Figure 6d-15, where for both tests the methane-hydrogen compositions were such as to promote a potential for carbon to deposit according to the reaction given above. In Table 6d-3, experimental weight losses are compared with values calculated from the correlations developed. These data assume no effect of methane concentration on rapid-rate methane formation. They are at relatively short coal residence times where it may be reasonably assumed that only a small amount of carbon deposition occurred. At a coal residence time of 10 minutes, calculated and experimental values agree closely, indicating that even when a carbon deposition potential in hydrogen-methane mixtures (graphite formation) exists, rapid-rate methane formation is unaffected by

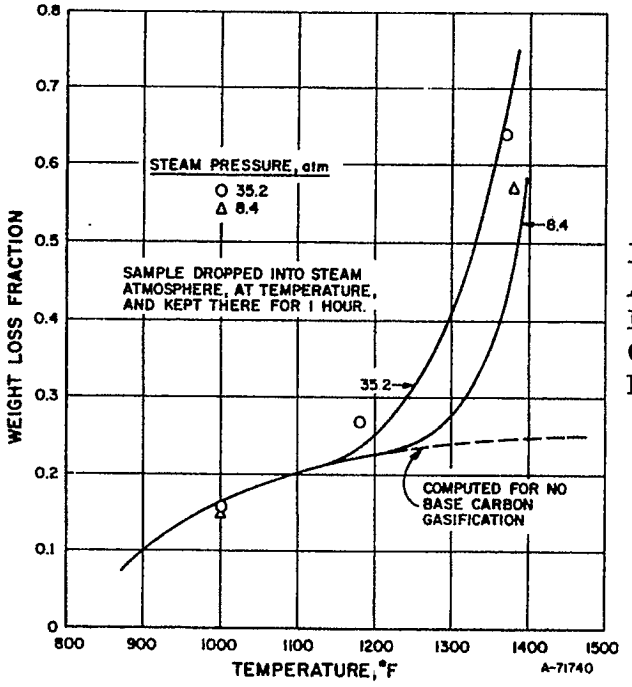

Figure 6d-11. EFFECTS OF PRESSURE AND TEMPERATURE ON WEIGHT LOSSES OBTAINED FROM GASIFICATION OF IRELAND MINE BITUMINOUS COAL CHAR WITH STEAM

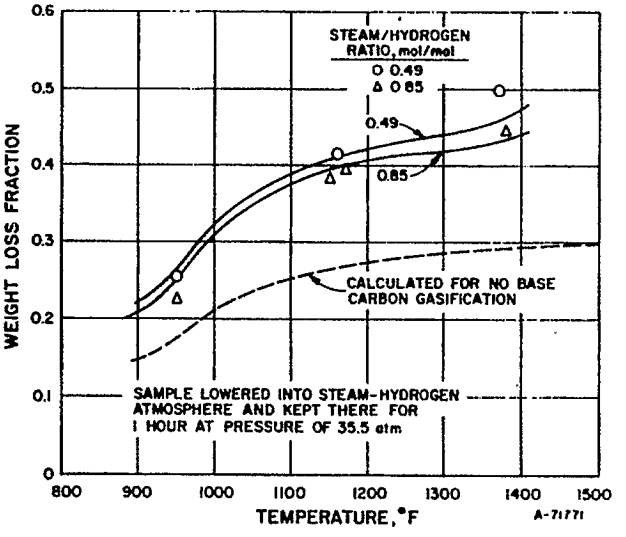

Figure 6d-12. EFFECTS OF TEMPERATURE AND GAS COMPOSITION ON WEIGHT LOSSES OBTAINED FROM GASIFICATION OF IRELAND MINE BITUMINOUS COAL CHAR WITH STEAM-HYDROGEN MIXTURES

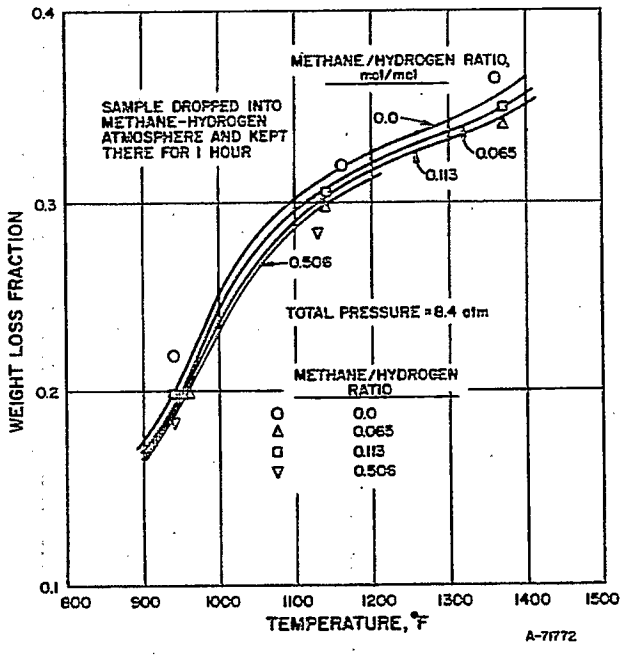

Figure 6d-13. EFFECTS OF TEMPERATURE AND GAS COMPOSITION ON WEIGHT LOSSES OBTAINED FROM GASIFICATION OF IRELAND MINE BITUMINOUS COAL CHAR WITH METHANE-HYDROGEN MIXTURES AT 8.4 atm

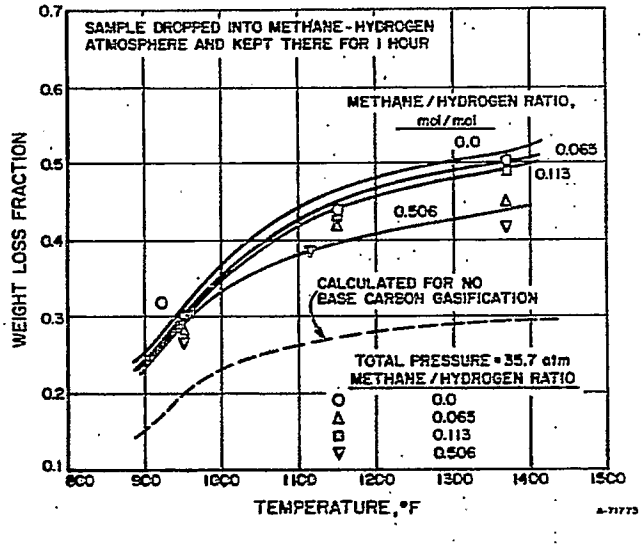

Figure 6d-14. EFFECTS OF TEMPERATURE AND GAS COMPOSITION ON WEIGHT LOSSES OBTAINED FROM GASIFICATION OF IRELAND MINE BITUMINOUS COAL CHAR WITH METHANE-HYDROGEN MIXTURES AT 35.7 atm

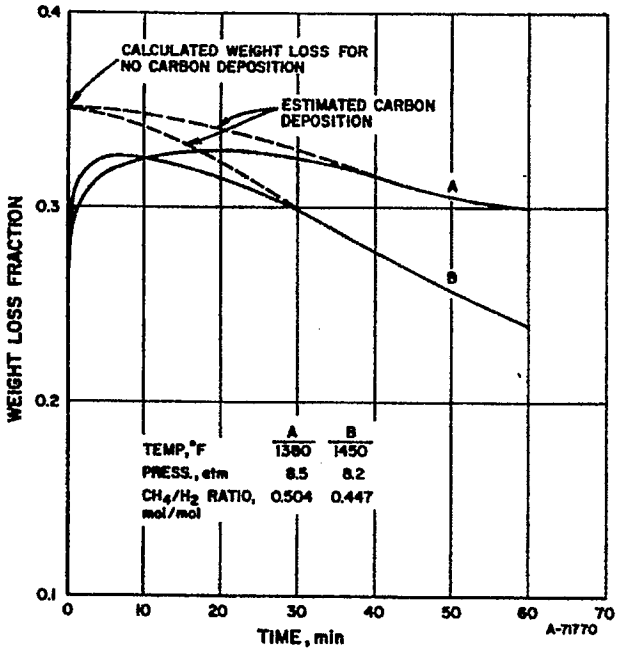

Figure 6d-15. WEIGHT LOSS WITH TIME DURING GASIFICATION OF IRELAND MINE BITUMINOUS COAL CHAR WITH METHANE-HYDROGEN MIXTURES HAVING A POTENTIAL FOR GRAPHITE DEPOSITION

Figure 6d-16. CORRELATION OF FLUID-BED DATA OF BIRCH et al[6], FOR GASIFICATION OF BROWN COAL WITH HYDROGEN

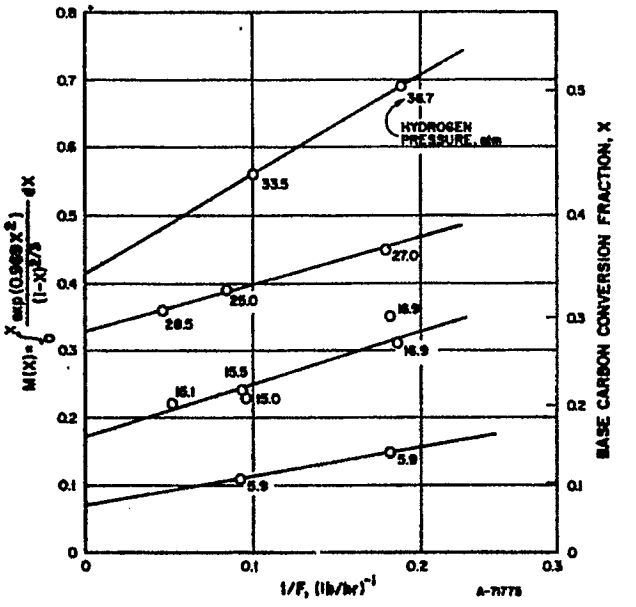

methane partial pressure. This is of particular practical importance since large-scale gasification systems can be designed to permit gas-solid contacting times that are sufficiently long to favor rapid-rate methane formation but which are much too short for the slower graphite deposition to occur. This can then result in methane concentrations in the product gas from an integral reactor considerably in excess of the methane concentration corresponding to equilibrium for the graphite-hydrogen-methane system at reaction bed temperatures.

Table 6d-3. COMPARISON OF CALCULATED WITH EXPERIMENTAL WEIGHT LOSS IN METHANE-HYDROGEN MIXTURES

				Weight Loss Fraction After 10 Minutes		
		Gas Composition			Calculated	
Temp, °F	Press., atm	H_2	CH_4 mole %	Experimental	Base C Gasifn	No Base C Gasifn
1380	8.5	66.5	33.5	0.325	0.318	0.286
1450	8.2	69.1	30.9	0.326	0.324	0.290

A7506 1649

6d.4.3 Consistency of Correlation for Rapid-Rate Methane Formation and Other Data

Data obtained by Birch et al.[6] for gasification of brown coal with hydrogen in a continuous fluid-bed system at about 1570 °F was analyzed using the correlations developed in this study. Values of total base carbon gasified, X, were estimated from the available data according to the expression —

$$X = \frac{n_{CH_4} - n^{o}_{CH_4}}{1 - n_{oil} - n_{CO_x} - n^{o}_{CH_4}} \qquad (13)$$

where —

n_{CH_4} = total moles methane formed/mole carbon fed
n_{oil} = moles of carbon in oil formed/mole carbon fed
n_{CO_x} = total moles carbon oxides formed/mole carbon fed
$n^{o}_{CH_4}$ = estimated value of moles of methane formed due only to devolatilization/mole carbon fed

The above expression assumes that the volatile carbon in the feed coal gasifies to form oil, carbon oxides, and some methane. Although the oils and carbon oxides are reported directly in the run data available, the value of $n^{o}_{CH_4}$ was estimated from methane yields obtained at low hydrogen pressure and where nitrogen was used as the feed gas.

In Figure 6d-16, values of — $M(X) = \int_{o}^{X} \frac{\exp(0.969\,X^2)\,dX}{(1-X)^{2/3}}$

are plotted vs. values of 1/F where —

$$F = \text{DAF feed coal rate, lb/hr}$$

Straight lines are drawn through the data at roughly corresponding hydrogen partial pressures in the product gas, which are extrapolated to values of

$$1/F = 0$$

to obtain values of $M(X) = M(X_r)$ at a condition where low-rate gasification is negligible compared to rapid-rate methane formation. Extrapolated values of $M(X_r)$ at $1/F = 0$ vs. average hydrogen partial pressure are plotted in Figure 6d-17; the straight line drawn corresponds to a value of $k_r = 0.012\ atm^{-1}$. This value is reasonably close to the corresponding value of $k_r = 0.0092\ atm^{-1}$ obtained for Ireland mine bituminous coal char.

Data obtained by Hiteschue et al.[7] for batch gasification of a high-volatile "A" bituminous coal with hydrogen in a fixed bed has also been analysed in terms of the model developed in this study. For this analysis, values of base carbon conversion, X_r, were estimated from the following expression:

$$X_r = \frac{\Delta W - V}{F_c} \qquad (14)$$

where —

ΔW = total weight loss fraction of coal, g/g-feed coal

V = volatile matter in feed coal, g/g-feed coal (from proximate analysis)

F_c = fixed carbon in feed coal, g/g-feed coal (from proximate analysis)

Figure 6d-18 shows values of $M(X_r)$ vs. p_{H_2} for tests conducted at 1470° and 2190°F. Since only values for the hydrogen partial pressure in feed gases were available for use in evaluation of the correlation, the trends exhibited are approximate. Data for solids "time at temperature" of 30 min were used for gasification at 1470°F, since low-rate gasification would be negligible during this time. Data at "zero" residence time were used for results obtained at 2190°F, since low-rate gasification may be significant at this temperature. ("Zero" residence time corresponds to the situation where a sample is heated up to temperature and then is immediately cooled.)

Figure 6d-18 shows that data obtained at both temperatures are consistent with the correlation. The value of k_r corresponding to the line drawn is $0.0105\ atm^{-1}$, which again is quite close to the value of k_r obtained for Ireland mine coal.

Hiteschue et al.[7] also pretreated the "A" bituminous coal with helium for 2 hours at 1110°F, then tested the resultant char at 1470°F. The data obtained in gasification tests with this char are given in Figure 6d-19, where the line drawn corresponds to a value of

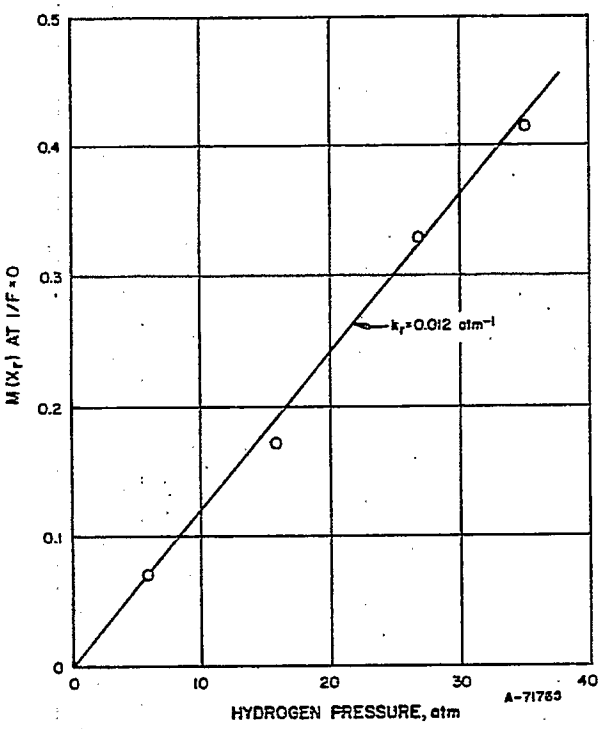

Figure 6d-17. CONSISTENCY OF DATA OF BIRCH et al.[6] WITH KINETIC MODEL FOR RAPID-RATE METHANE FORMATION WITH BROWN COAL

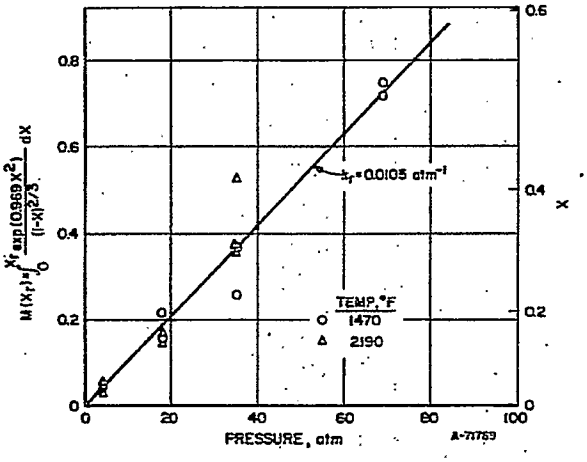

Figure 6d-18. CONSISTENCY OF HITESHUE et al.[7] DATA WITH KINETIC MODEL FOR RAPID-RATE METHANE FORMATION WITH HIGH-VOLATILE "A" BITUMINOUS COAL

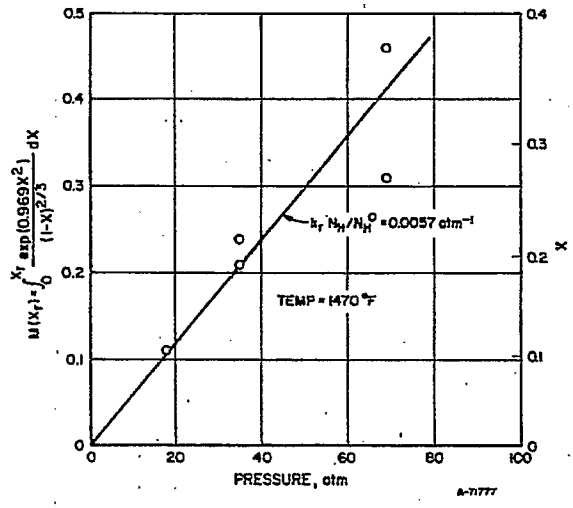

Figure 6d-19. CONSISTENCY OF HITESHUE et al.[7] DATA WITH KINETIC MODEL FOR RAPID-RATE METHANE FORMATION WITH HELIUM-PRETREATED HIGH-VOLATILE "A" BITUMINOUS COAL

$$\frac{k_r N_H}{N_H^o} = 0.0057 \text{ atm}^{-1}$$

If it is assumed that the value of k_r applicable to gasification of the char is the same as that for gasification of the coal from which the char was derived ($k_r = 0.0105$ atm^{-1}) where $N_H = N_H^o$, then the value of N_H/N_H^o obtained with the char is 0.54. This value is about 30% greater than a value of 0.41 computed with equation 10 using values of the kinetic parameters obtained with bituminous coal char.

6d.5 Low-Rate Gasification Kinetics

For practical purposes, char can be considered to undergo low-rate gasification only after devolatilization and rapid-rate methane formation reactions are completed. Results obtained on the thermobalance have indicated that at temperatures greater than about 1500°F, the char reactivity in the low-rate regime is substantially the same, whether the devolatilization occurs in nitrogen or in a gasifying atmosphere at the same conditions. This behavior was illustrated in Figure 6d-12 for gasification in hydrogen and in Figure 6d-7 for gasification in pure steam. Figure 6d-8 shows that there is no rapid-rate reaction with pure steam. Also shown is that weight loss vs. time characteristics are virtually identical for a test in which the coal is first devolatilized in nitrogen, and then reacted with steam, and in a test in which the coal is devolatilized in steam prior to low-rate gasification of the resultant char.

Therefore, the approach taken in this study to develop an overall model for the gasification of coal has been to treat low-rate char gasification as a process essentially independent of the devolatilization conditions, with one important exception. This exception is the temperature of devolatilization, since it has been shown in this study, as well as by Blackwood et al.[12] that the reactivity of a char at a given temperature, T, decreases with increasing pretreatment temperature, T°, when T° > T. This effect is quantitatively represented in the correlations discussed in this report. The model adopted does not, however, account for pretreatment effects on gasification rates during the initial stages of char gasification, which have been observed particularly at gasification temperatures less than about 1600°F.

A number of experimental investigations have been conducted to study char-gasification kinetics. In most studies, carbon gasification rates, R, are defined in terms of the expression –

$$R = \frac{dX}{dt} \Big/ (1 - X) \qquad (15)$$

where

X = carbon conversion fraction, mol/mol carbon initially present

t = time

The use of this form of expression, in which R is sometimes referred to as the "specific" carbon gasification rate, implies that the absolute rate of carbon gasified (moles of carbon gasified per time) is proportional to

the amount of carbon present at any time. The reason for this approach is that specific carbon gasification rates have often been found to be reasonably constant over limited initial ranges of carbon conversion, when constant gasifying conditions are maintained. An approach often taken in this circumstance for analysis of carbon gasification kinetics has been to determine the effects of gasifying conditions such as temperature, pressure, and gas composition on experimentally determined specific carbon gasification rates. The following example illustrates this approach:

$$R = \frac{dX}{dt} \Big/ (1 - X) = k p_{H_2} \qquad (16)$$

where

X = carbon conversion factor
t = absolute temperature
p_{H_2} = hydrogen partial pressure

and

$$k = k^{o} \exp\left(-\frac{E}{T}\right) \qquad (16a)$$

Here,

T = absolute temperature
k^{o},E = kinetic parameters

It has also been recognized, however, that specific carbon gasification rates are not constant over a wide range of carbon conversions but tend to decrease significantly at high levels of conversion. A typical effect obtained by Zielke and Gorin[8] for fluid-bed gasification of Disco char with steam-hydrogen mixtures is shown in Figure 6d-20. Although these investigators characterize their results in terms of specific carbon gasification rates, these rates are empirically represented as functions of the carbon conversion level.

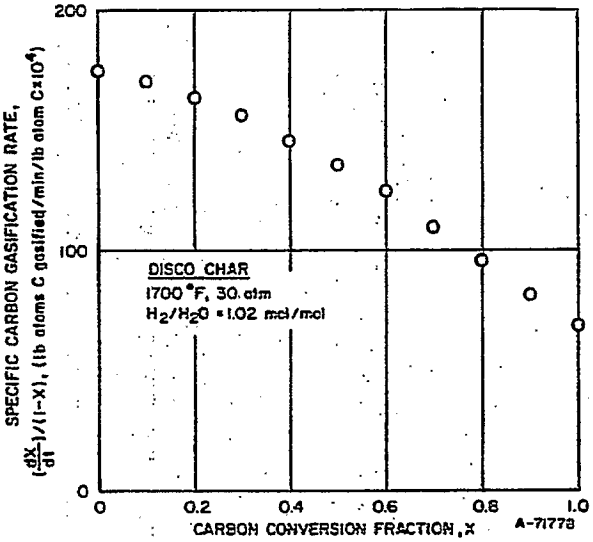

Figure 6d-20. TYPICAL VARIATION OF SPECIFIC CARBON GASIFICATION RATES WITH INCREASING CARBON CONVERSION

In the HYGAS-associated study reported here, a different approach was taken to characterize the effects of carbon conversion on gasification rates based on information obtained with the thermobalance and on the analysis of the differential gasification rate-information obtained by Zielke and Gorin,[9,8]

and Goring et al.[10,11] In the model adopted, the conversion rate, dX/dt, is represented by an expression of the form –

$$\frac{dX}{dt} = k\,(1 - X)^{2/3} \exp\,(-\beta X^2) \qquad (17)$$

Experimental justification for this form is presented below. The term $(1 - X)^{2/3}$ is considered to represent the effective internal surface area of elements within a coal particle, and the term $\exp\,(-\beta\,X^2)$ the reactivity per unit of effective internal surface area. The term k is a kinetic parameter dependent on a number of factors such as temperature, pressure, gas composition, coal type, and particle temperature history, but is independent of carbon conversion fraction. The term β has been correlated with gas composition and pressure.

The term $(1 - X)^{2/3}$ is equal to the relative surface area of a symmetrical volume element undergoing shrinkage in such a manner that the outer surface at any time remains parallel to the original surface. This model is sometimes referred to as the shrinking core model and has been applied to kinetic description of iron oxide reduction with hydrogen and/or carbon monoxide, using the following form of expression:

$$\frac{dY}{dt} = k\,(1 - Y)^{2/3} \qquad (18)$$

where –

Y = iron oxide reduction conversion fraction

k = kinetic parameter dependent on temperature, pressure, gas composition, iron oxide type, and particle size

Equation 18 is analogous in form with equation 17 with the exception of the exponential term. It is noteworthy, however, that iron oxide reduction of granular particles usually begins at the outer surface of a particle, forming an interface between an inner core of iron oxide and an outer shell of reduced iron oxide that moves inwardly into the particle as reduction proceeds. In such a situation, the parameter k is inversely proportional to the particle diameter, demonstrating that reduction rates increase with decreasing particle size. Essentially no effect of particle diameter on carbon gasification rates has been observed with coal particles under conditions where mass and heat transfer between individual particles and the exterior gaseous atmosphere do not affect overall gasification kinetics. Instead, gasification of base carbon in coal occurs essentially uniformly throughout the interiors of individual particles. This implies that if, indeed, coal does gasify via a shrinking core mechanism, coal particles consist of a large number of internally dispersed subelements that individually gasify via a shrinking core mechanism. Although gasification rates would then be inversely proportional to the initial diameter of the sub-elements, such rates would not depend on the overall particle diameter. With this model, the effective diameter of the sub-elements would then be reflective of one mode that characterizes the overall reactivity of a particular coal.

The suggestion that gasification rates are proportional to effective internal surface area of the reacting carbon is consistent with experimental results obtained by Blackwood et al.,[12] who estimated effective surface areas of pretreated chars by estimating saturation (CH_2) coverage. A direct correlation between char reactivity, varied by varying pretreatment temperatures, and estimated reactive surface area was obtained.

Results obtained on the thermobalance for gasification of Ireland mine bituminous coal char, devolatilized Montour No. 10 bituminous coal char, and a North Dakota lignite in pure steam have been correlated with an expression of the form given in equation 17, but where $\beta = 0$. For this condition, equation 17 can be integrated with respect to time to yield the expression —

$$3\left[1 - (1 - X)^{1/3}\right] = kt \qquad (19)$$

Figures 6d-21 and -22 show some examples of experimental results obtained where values of $3\left[1 - (1 - X)^{1/3}\right]$ are plotted vs. time, t. The significance of the applicability of the correlation, even at high values of carbon conversion, is illustrated in Figure 6d-23, which compares the different trends predicted by the use of a correlation assuming constant specific conversion rates to that given above.

The correlation form given in equation 19 does not describe experimental results obtained on the thermobalance for gasification of char in hydrogen or hydrogen-steam mixtures. With hydrogen-containing gases, conversion rates decrease more severely with increasing conversion than is accounted for by the term $(1 - X)^{2/3}$. This effect has been interpreted as corresponding to a decrease, in the presence of hydrogen, of the reactivity of the reacting interface. It is represented quantitatively by the term $\exp(-\beta X^2)$.

Equation 17 can be rearranged to

$$\ln \frac{\frac{dX}{dt}}{(1 - X)^{2/3}} = \ln k - \beta X^2 \qquad (20)$$

This equation has been used to correlate results obtained by Zielke and Gorin[9,8] and Goring et al.[11] for fluid-bed gasification of Disco char with steam-hydrogen mixtures at pressures of 1, 6, and 30 atm and temperatures of 1600° and 1700°F. Figure 6d-24 shows examples of the applicability of equation 20 to describe results of these investigators at various conditions. In the graph, the intercept of a given line at $X = 0$ corresponds to the value of k in equation 20, and the slope of the line corresponds to the value of β.

An integrated form of equation 20 was used to correlate data obtained on the thermobalance; that is —

$$M(X) = \int_0^X \frac{\exp(\beta X^2)\, dX}{(1 - X)^{2/3}} = kt \qquad (21)$$

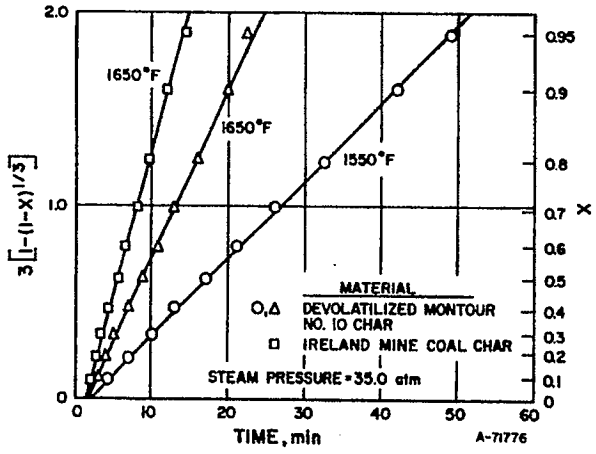

Figure 6d-21. CORRELATION OF DATA FROM BITUMINOUS COAL GASIFICATION WITH STEAM

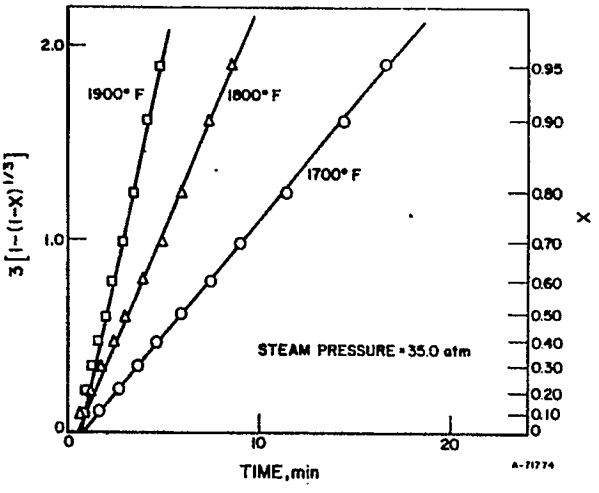

Figure 6d-22. CORRELATION OF DATA FROM GASIFICATION OF IRELAND MINE BITUMINOUS COAL CHAR WITH STEAM

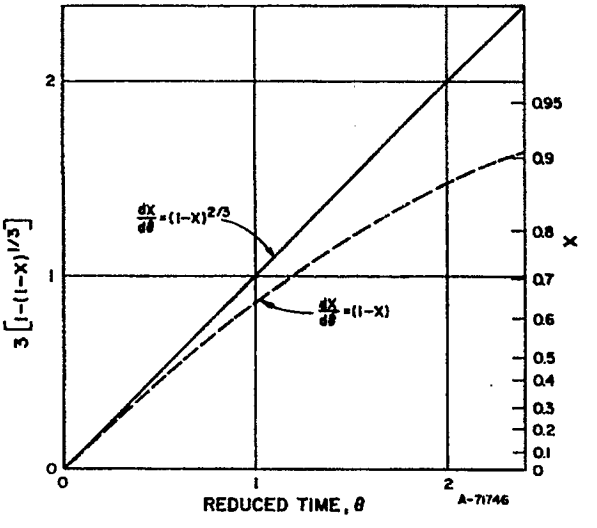

Figure 6d-23. COMPARATIVE EMPIRICAL TRENDS FOR DIFFERENT RATE EXPRESSIONS

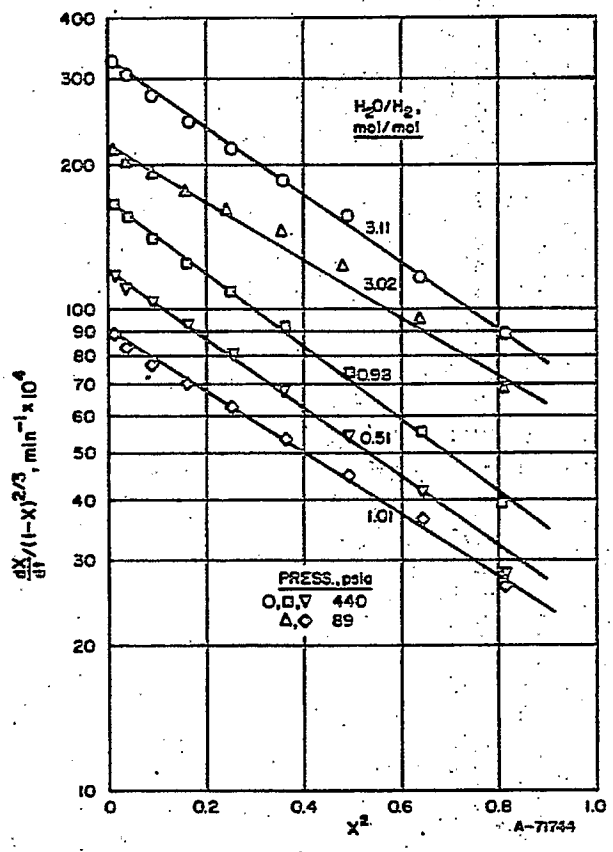

Figure 6d-24. CORRELATION OF DATA[8] FROM FLUID-BED GASIFICATION OF DISCO CHAR WITH STEAM-HYDROGEN MIXTURES

Figure 6d-25 shows plots of M(X) versus time t for data obtained with the thermobalance using steam-hydrogen mixtures. In computing values for M(X), a value of $\beta = 1.69$ was used for tests conducted with steam-hydrogen mixtures at high pressures, and a value of $\beta = 0.969$ was used for tests conducted with pure hydrogen. These values are consistent with a correlation developed from the data of Zielke and Gorin[9,8] and Goring et al.,[11] as well as data obtained on the thermobalance, which relates the value of β to steam and hydrogen partial pressure.

$$\beta = 0.969 + \frac{0.103\, p_{H_2}^{1/2}\, p_{H_2O}}{1 + 0.137\, p_{H_2}^{1/2} p_{H_2O}} \qquad (22)$$

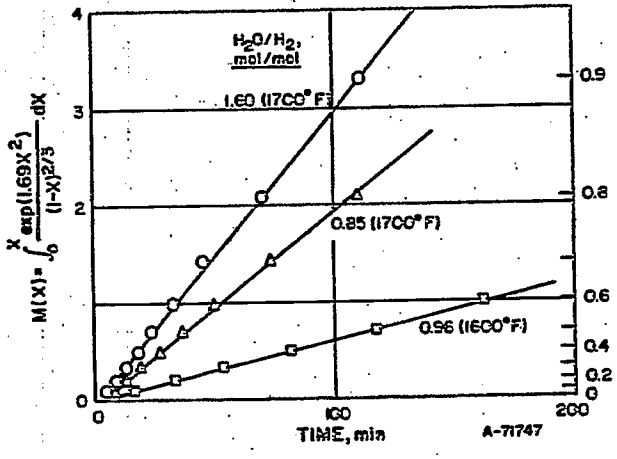

Figure 6d-25. CORRELATION OF DATA FROM GASIFICATION OF MONTOUR No. 10 BITUMINOUS COAL WITH STEAM-HYDROGEN MIXTURES USING THERMOBALANCE

Equation 22 is represented graphically in Figure 6d-26, which shows that only slight variations in values of β are exhibited at elevated pressures with steam-hydrogen mixtures. Although the value of $\beta = 0.969$, for pure hydrogen, is consistent with experimental results, equation 22 does not apply in pure steam or at very low hydrogen pressures since the value of β must approach zero as the hydrogen partial pressure approaches zero, consistent with results obtained in pure steam. This condition, however, is not of practical interest.

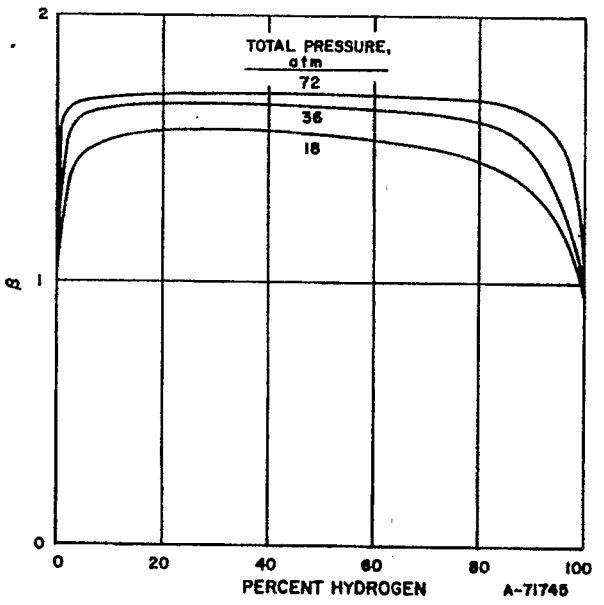

Figure 6d-26. RELATIVE INSENSITIVITY OF PARAMETER β WITH VARIATIONS IN GAS COMPOSITION FOR GASIFICATION WITH STEAM-HYDROGEN MIXTURES AT ELEVATED TEMPERATURES

The gasification data of Zielke and Gorin[9,8] and Goring et al.,[11] as well as a bulk of data obtained in HYGAS-associated studies with the high-pressure thermobalance and pilot-scale fluid beds, were used to evaluate parameters in a quantitative model developed to describe char gasification kinetics over a wide range of conditions. Three basic reactions were assumed to occur in gases containing steam and hydrogen:

$$H_2O + C \rightleftarrows CO + H_2 \qquad \text{Reaction I}$$

$$2H_2 + C \rightleftarrows CH_4 \qquad \text{Reaction II}$$

$$H_2 + H_2O + 2C \rightleftarrows CO + CH_4 \qquad \text{Reaction III}$$

Reaction I is the conventional steam-carbon reaction, which is the only reaction that would occur in pure steam at elevated pressures,* or essentially with gases containing steam, but at low pressure. Although, due to thermodynamic reversibility, steam conversion is rarely sufficiently high to decrease significantly the rate of this reaction, the reaction is severely inhibited by hydrogen. Some investigations have also noted inhibition by carbon monoxide and methane.

* Although some methane has been detected in gaseous reaction products when gasification is performed with pure steam, it is uncertain whether this methane results from direct reaction of steam with carbon, or from secondary reaction of hydrogen produced from the steam-carbon reaction with the carbon in the char.

Reaction II, which is the only reaction which would occur in pure hydrogen or in hydrogen-methane mixtures, has been found to greatly depend on hydrogen partial pressure. Many investigators have found that, at elevated pressures, the rate of this reaction is directly proportional to hydrogen partial pressure.[13,14]

The stoichiometry of Reaction III, limits its occurrence to systems in which both steam and hydrogen are present. Although this reaction is the stoichiometric sum of Reactions I and II, it is considered in this model to be a third independent gasification reaction. It was arbitrarily assumed to occur in the development of this model to facilitate correlation of the data, although Blackwood and McGrory[15] suggested that this type of reaction was required in such a system. Curran and Gorin[16] also assumed this reaction in order to correlate kinetic data for gasification of lignite at 1500°F in steam-hydrogen containing gases.

Initial development of the model was made from data obtained with hydrogen and steam-hydrogen mixtures where the gaseous reaction products CO, CO_2 and CH_4 were not present, and where pretreatment temperatures of the chars used were equal to the temperatures at which the chars were subsequently gasified. The correlation forms developed are described below:

$$\frac{dX}{dt} = fk_T (1 - X)^{2/3} \exp(-\beta X^2) \tag{23}$$

where —

$$k_T = k_I + k_{II} + 2k_{III} \tag{23a}$$

Here k_I, k_{II}, and K_{III} are rate constants for the invididual reactions considered. It is assumed that each of the three reactions occurs independently, but that the rate of each reaction is proportional to the same surface area and surface reactivity terms. These assumptions are inherent to the forms of expressions given in equations 23 and 23a.

The total gasification rate given in equation 23 is equal to the sum of formation rates of methane and carbon oxide, which can be individually represented as follows:

$$R_{CH_4}\left(\frac{\text{mol}}{\text{mol initial carbon} - \text{time}}\right) = f(k_{II} + k_{III})(1 - X)^{2/3} \exp(-\beta X^2) \tag{24}$$

$$R_{CO_x}\left(\frac{\text{mol}}{\text{mol initial carbon} - \text{time}}\right) = f(k_I + k_{III})(1 - X)^{2/3} \exp(-\beta X^2) \tag{25}$$

According to this model, then, the following relationship exists:

$$\frac{R_{CH_4}}{R_{CO_x} + R_{CH_4}} = \frac{k_{II} + k_{III}}{k_T} \qquad (26)$$

indicating that the ratio $R_{CH_4}/(R_{CO_x} + R_{CH_4})$ should not vary with increases in base carbon conversion fraction X at constant temperature, pressure, and gas composition. Although the data of Zielke and Gorin[9,8] and Goring et al.[11] do exhibit a consistent variation in the value of this ratio (Figure 6d-27), in evaluating kinetic parameters from their data we have assumed that the value of $R_{CH_4}/(R_{CO_x} + R_{CH_4})$ at X = 0 applies for all values of conversion. This assumption was made primarily because subsequent use of the quantitative model developed to predict methane and carbon oxide yields in integral fluid-bed gasification tests was generally successful. The possibility that variations in the $R_{CH_4}/(R_{CO_x} + R_{CH_4})$ ratio with increasing conversion was due to a catalytic reaction that occurred at some point downstream of the fluid bed employed by Zielke and Gorin and Goring et al. (promoted by certain ash constituents in coal particles blown out of the fluid bed) has recently been suggested.[16] In particular, iron in the ash is capable of catalyzing the reaction:

$$CO + 3H_2 \rightarrow CH_4 + H_2O$$

at the lower temperatures that would exist downstream of the fluid bed employed. It is reasonable to conclude that the observed experimental ratio of $R_{CH_4}/(R_{CO_x} + R_{CH_4})$ at low carbon conversions would be more representative of the ratio resulting solely from char gasification, since char fines would be expected to accumulate and have a greater relative effect with increasing time.

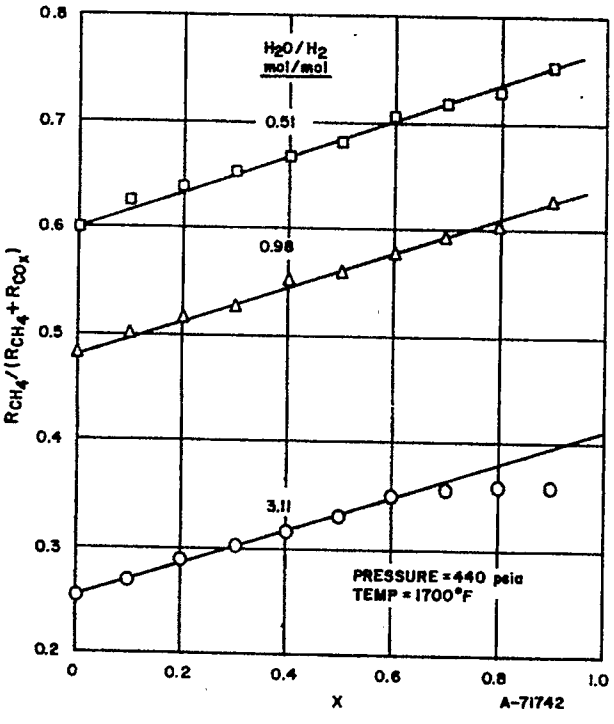

Figure 6d-27. VARIATION OF METHANE-CARBON OXIDES PRODUCT DISTRIBUTION DURING GASIFICATION OF DISCO CHAR WITH STEAM-HYDROGEN MIXTURES

Values for $k_{II}f$ were determined from results of tests conducted by Zielke and Gorin[9] in pure hydrogen, at pressures from 10 to 30 atm and at temperatures from 1600° to 1700°F, using the graphical approach illustrated in Figure 6d-24. An average value of $\beta = 0.969$ satisfactorily described these data, and intercept values at $X = 0$ were interpreted to be equal to $k_{II}f$ at a given hydrogen pressure and temperature. Values of $k_{II}f$, so obtained, were correlated with hydrogen partial pressure using the following form of correlation:

$$k_{II}f = k^{o}_{II}f\, p^{2}_{H_2}/(1 + K_{II}p_{H_2}) \qquad (27)$$

where k^{o}_{II} and K_{II} are temperature-dependent parameters empirically correlated with temperature based on results at 1600° and 1700°F using Arrhenius forms of expressions. The form of correlation given in equation 27 has been suggested by Zielke and Gorin[9] and is consistent with a form suggested by Blackwood.[17] He developed this form based on the following simple model:

$$H_2\,(\text{gas}) + \theta\,(\text{adsorption site on carbon surface}) \rightleftarrows H_2^{*}\,(\text{adsorbed species on carbon surface—may also be } CH_2 \text{ radical})$$

$$H_2^{*} + H_2\,(\text{gas}) \rightleftarrows CH_4\,(\text{gas}) + \theta$$

A relationship of the form given in equation 27 can be derived from the above model. It is interesting that this mechanism predicts the experimentally observed phenomenon that, when temperature is suddenly raised from one level to another in a system in which char is being gasified, there is a transient period at the higher temperature when the char reactivity decreases from some relatively high level to a steady-state level characteristic of the higher temperature. Conversely, when temperature is lowered to some level, a transient period exists during which the char reactivity increases to a level characteristic of the lower temperature. It should be noted that characteristic reactivity of the char at the lower temperature will be less when the char has been exposed to a higher temperature than when the char has not been exposed to a higher temperature because of the temperature history effect discussed previously.

By assuming that in steam-hydrogen mixtures values of $k_{II}f$ are unaffected by steam partial pressures, we were able to compute values of $k_{II}f$ corresponding to the conditions of the tests conducted by Zielke and Gorin[9,8] and Goring et al.[11] with steam-hydrogen mixtures, using the correlations developed from results obtained from gasification with pure hydrogen. By simultaneous solution of equations 24, 25 and 26 we were then able to compute values for the parameters $k_{III}f$ and k_If for each test

made with steam and hydrogen. These rate constants were correlated with steam and hydrogen partial pressures using the following forms of equations:

$$fk_I = \frac{f \cdot k_I^o}{\left(1 + \frac{K_I}{p_{H_2O}} + K_I' \frac{p_{H_2}}{p_{H_2O}}\right)^2} \tag{28}$$

$$fk_{III} = \frac{fk_{III}^o p_{H_2}^{1/2} p_{H_2O}}{(1 + K_{III} p_{H_2}^{1/2})} \tag{29}$$

where k_I^o, K_I, K_I', k_{III}^o, and K_{III} are kinetic parameters dependent on temperature. These parameters were empirically represented as functions of temperature using Arrhenius forms of expressions.

The quantitative predictions of the correlations developed in terms of total gasification rates are consistent with the results of a variety of tests made on the thermobalance at temperatures from 1600° to 1900°F and pressures up to 1000 psig. Values for the overall rate constant $f \cdot k_T$ were obtained from thermobalance data based on graphical representations consistent with the expression –

$$\int_o^X \frac{\exp(0.969 X^2)\, dX}{(1 - X)^{2/3}} = f \cdot k_T t \tag{30}$$

Values of the term fk_T, obtained for the particular chars used in thermobalance tests, were generally consistent with the predictions of the correlation, although a characteristic value of f was required for each particular type of char used. The materials used most extensively in the experimental program, whose kinetic behaviors were consistent with the trends predicted by the correlations, included Ireland mine coal char, Montour No. 10 coal, and North Dakota lignite, and, to a lesser extent, an Illinois No. 6 coal char. Results obtained with these materials, as well as results of just a few tests conducted with each of about 10 other coals of varying properties, have suggested that the correlations developed appear generally applicable to bituminous coals as well as to one lignite tested. However, results obtained in several tests with a Southwestern subbituminous coal indicated that the kinetic behavior exhibited by this particular material is more complex than that described by the relatively simplified model considered. Although the kinetic behavior exhibited during initial stages of conversion of this coal was reasonably consistent with the predictions of the correlations, at certain critical levels of conversion, depending on the gasifying conditions employed, reactivity for gasification suddenly diminished more rapidly than that predicted by the correlations. This decrease in reactivity was more severe with increasing hydrogen/steam ratios. This observed exception emphasizes the necessity to experimentally determine the applicability of the model developed to predict kinetic behavior of any particular coal.

The effects of pretreatment temperature on gasification rates have been studied by comparing the overall rate constants obtained with a particular coal in a gasifying atmosphere at constant conditions, but where the coal has been pretreated in nitrogen at various temperatures. Typical data obtained are shown in Figure 6d-28. The decrease in reactivity with increasing pretreatment temperature was interpreted as a decrease in the parameter f. This effect was empirically correlated with the expression —

$$f = f_o \exp\left(\frac{E_p}{T_p}\right) \qquad (31)$$

where —

f_o = reactivity factor dependent on inherent nature of coal
T_p = maximum pretreatment temperature prior to gasification
E_p = kinetic parameter = 8467°R

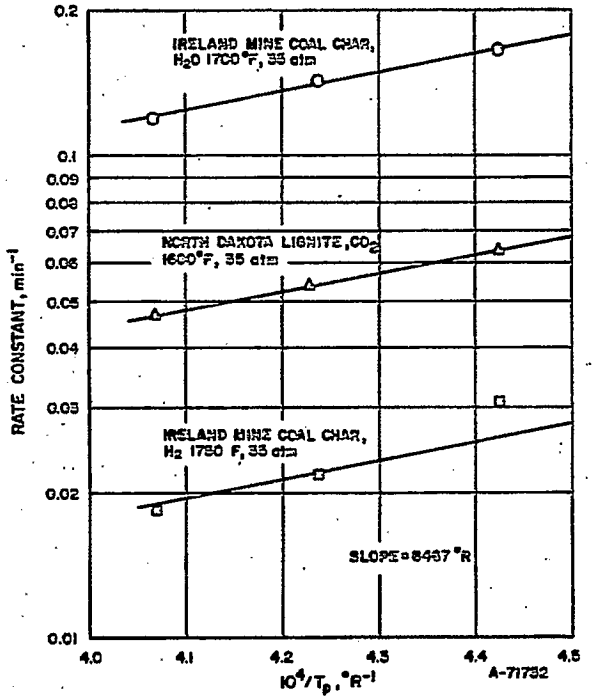

Figure 6d-28. EFFECT OF COAL-PRETREATMENT TEMPERATURE ON KINETICS OF SUBSEQUENT GASIFICATION

The value of E_p obtained with the coals tested in this study compares very well with a value of $E_p = 7848\,°R$ reported by Blackwood et al.[13] from the gasification of coconut and brown coal chars with hydrogen.

The effects of carbon monoxide and methane partial pressures on the rates of the three gasification reactions assumed were characterized using results of tests with the thermobalance at a variety of conditions and, somewhat, using results of integral fluid-bed tests. In the thermobalance test program, tests were frequently conducted at conditions in which the total gasification rates exhibited could be primarily attributed to gasification reactions postulated. In this way, the quantitative effects of carbon monoxide and methane concentrations on the individual rate parameters could be estimated. Preliminary quantitative representations of these effects were then evaluated based on consistency of the resulting correlations with integral fluid-bed results in which methane and carbon oxides yields could be directly measured. Deviations between predicted and calculated results were then used as a basis for modifying the effects assumed. The final correlations developed were generally consistent with both results of thermobalance tests as reflected by total carbon conversion values and with integral fluid-bed results as indicated by carbon monoxide and methane yields.

The quantitative expressions finally developed are summarized as follows:

$$\frac{dX}{dt} = f_o \exp\left(\frac{8467}{T_p}\right) \cdot (1 - X)^{2/3} \exp(-\beta X^2) \cdot k_T \tag{32}$$

$$k_T = k_I + k_{II} + 2k_{III} \tag{32a}$$

$$k_I = \frac{9380 \left\{\exp\left[-\frac{31705}{T}\right]\right\} \left(1 - \frac{p_{CO} p_{H_2}}{p_{H_2O} \cdot K_I^E}\right)}{\left\{1 + \left[\exp\left(-22.216 + \frac{44787}{T}\right)\right] \frac{1}{p_{H_2O}} + 16.35 \frac{p_{H_2}}{p_{H_2O}} + 43.5 \frac{p_{CO}}{p_{H_2O}}\right\}^2}, \text{ min}^{-1} \tag{33}$$

$$k_{II} = \frac{16.5\, p_{H_2}^2 \left[\exp\left(-\frac{33076}{T}\right)\right] \left(1 - \frac{p_{CH_4}}{p_{H_2}^2 K_{II}^E}\right)}{\left\{1 + p_{H_2} \left[\exp\left(-10.4520 + \frac{19976}{T}\right)\right]\right\}}, \text{ min}^{-1} \tag{34}$$

$$k_{III} = \frac{p_{H_2}^{1/2} \cdot p_{H_2O}\left[\exp 11.8794 - \frac{44{,}544}{T}\right]\left(1 - \frac{p_{CO}p_{CH_4}}{p_{H_2}p_{H_2O} \cdot K_{III}^{E}}\right)}{\left\{1 + \left[\exp\left(-6.6696 + \frac{15198}{T}\right)\right]\left(p_{H_2}^{1/2} + 0.85\, p_{CO} + 18.6\frac{p_{CH_4}}{p_{H_2}}\right)\right\}^2}, \text{ min}^{-1} \quad (35)$$

$$\beta = 0.969 + \frac{0.103\, p_{H_2}^{1/2} p_{H_2O}}{1 + 0.137\, p_{H_2}^{1/2} p_{H_2O}} \quad (36)$$

where –

K_I^E, K_{II}^E, K_{III}^E = equilibrium constants for Reactions I, II, and III, considering carbon as graphite

T = reaction temperature, °R

p_{H_2}, p_{H_2O}, p_{CO}, p_{CH_4} = partial pressures of H_2, H_2O, CO, and CH_4, atm

T_p = maximum temperature to which char has been exposed prior to gasification, °R

(If $T_p < T$, then a value of $T_p = T$ is used in equation 32.)

Values of f_o obtained in this study were based on the definition that $f_o = 1$ for char derived from Ireland mine coal.

The consistency of the expressions given above with results on the thermobalance for gasification of Ireland mine bituminous coal char with gases containing steam, hydrogen, carbon monoxide, carbon dioxide, and methane is illustrated in Figure 6d-29.

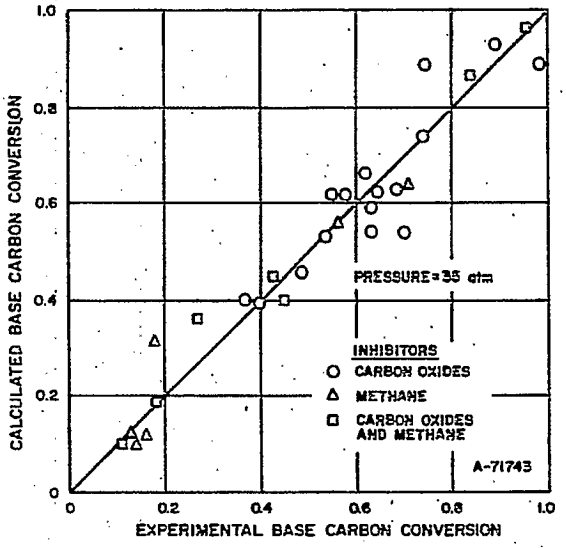

Figure 6d-29. CONSISTENCY BETWEEN CALCULATED AND EXPERIMENTAL RESULTS FROM GASIFICATION OF IRELAND MINE BITUMINOUS COAL CHAR (Thermobalance Data: 1500°-1750°F)

6d. 6 Consistency of Kinetic Model with Moving- and Fluidized-Bed Data

The consistency of the predictions of the correlations developed, with pilot-plant-scale moving- and fluid-bed data obtained in experimental programs associated with HYGAS, are illustrated in Figures 6d-30 through -32. In making estimates of carbon oxides and methane yields for these integral systems, it was necessary to assume models for the physical nature of gas solids contacting. For the moving-bed systems, gases were fed to the bottom of the moving bed at a point where the solids left the reactor. Gases moved upward countercurrent to the downward moving solids leaving the bed into a dilute solids phase zone above the bed where solid particles rained down from a solids feed point at the top of this zone. The gas exited from the reactor at a point near the top of the dilute solid phase zone. In the moving bed, it was assumed that both gas and solid were in plug flow. In the dilute solids phase zone, the gas and solids were also assumed to be in countercurrent flow. It was further assumed that, when coal or coal char containing volatiles were the feed, both devolatilization and rapid-rate methane formation occurred in the dilute solids phase zone above the

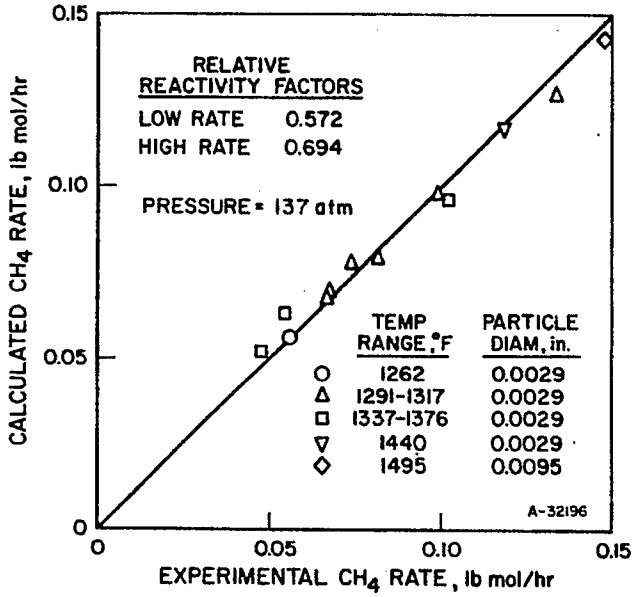

Figure 6d-30. CONSISTENCY BETWEEN CALCULATED AND EXPERIMENTAL METHANE YIELDS OBTAINED FOR MOVING BED GASIFICATION OF MONTOUR No. 10 COAL WITH HYDROGEN (IGT)

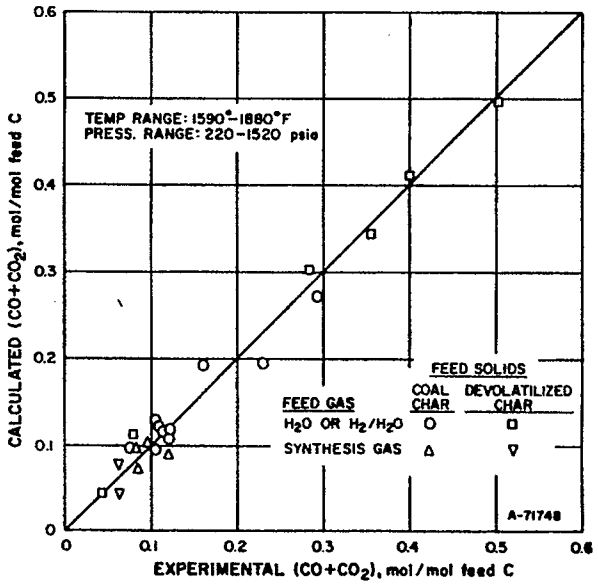

Figure 6d-31. CONSISTENCY BETWEEN CALCULATED AND EXPERIMENTAL CARBON OXIDES YIELDS FROM FLUID-BED GASIFICATION OF IRELAND MINE BITUMINOUS COAL AND CHAR (IGT)

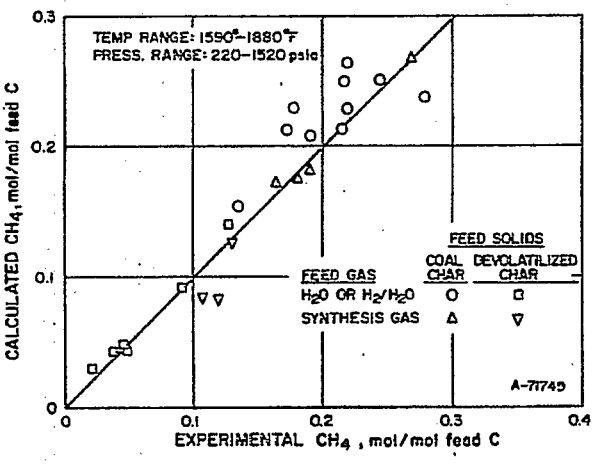

Figure 6d-32. CONSISTENCY BETWEEN CALCULATED AND EXPERIMENTAL METHANE YIELDS FROM FLUID-BED GASIFICATION OF IRELAND MINE BITUMINOUS COAL CHAR AND DEVOLATILIZED CHAR (IGT)

moving bed, and that only low-rate gasification occurred in the moving bed itself. In making predictions, we estimated devolatilization yields from empirical correlations based on statistical averages of yields obtained in several of the tests conducted. Estimates of coal conversions due to rapid-rate methane formation were based on the correlations discussed previously for reaction in this regime; coal conversions in the moving bed were estimated from the correlations developed to describe low-rate gasification kinetics.

A similar procedure was used to estimate behavior in fluid beds, except that ideal gas and solids mixing were assumed to occur in the fluid bed itself. The assumption of gas mixing was verified with experimental observations. In each of several tests, gas samples taken at various points in the fluid bed were essentially of the same composition, but product gas analyses for a given test showed a significantly different composition from that in the fluid bed. This was interpreted as the result of apparent devolatilization and rapid-rate methane formation primarily above the bed.

For both moving- and fluid-bed systems, the hydrogen partial pressure in the product gas was used to compute rapid-rate methane formation, since hydrogen partial pressure does not change significantly in the space above the bed. This is due to the compensating effects of hydrogen evolution from the coal resulting from devolatilization and hydrogen reaction to form methane. It was also assumed in all calculations that the water gas shift reaction was in equilibrium at reaction temperatures.

For the simplified models assumed to describe gas-solids contacting in the moving- or fluid-bed systems, the important conditions characterizing a particular test include: coal (or char) feed rate, coal (or char) composition, particle residence time in the bed, bed temperature and pressure, and feed gas composition and flow rate. Reactivity factors used to compute the low- and rapid-rate gasification regimes were experimentally determined from tests on the thermobalance with the particular coals used.

The results in Figures 6d-30 through -32 show generally good agreement between calculated and experimental rates. It is of interest that the moving-bed data in Figure 6d-30 has been previously analyzed by Wen and Huebler[18]

in terms of a kinetic model in which mass transfer between gas and solids was assumed to be the rate-controlling factor. The large amount of experimental kinetic information obtained with the thermobalance since that previous analysis was made, however, indicates that the assumption of mass transfer rate control is not valid, particularly since the same data considered can be well predicted using quantitative correlations developed from data in which mass transfer was definitely not a rate-controlling factor.

The correlations described above for low-rate gasification were also used to predict carbon oxides and methane formation rates obtained by May et al.[19] for batch gasification of Disco char in a fluid bed. Again, in computing values for carbon oxides and methane yields, it was assumed that the fluid bed was completely backmixed with respect to gas and solids. The reactivity factor for Disco char determined from data of Zielke and Gorin[8,9] and Goring et al.[11] was also used in calculations. Figures 6d-33 and -34 show the generally good consistency between computed and experimental results.

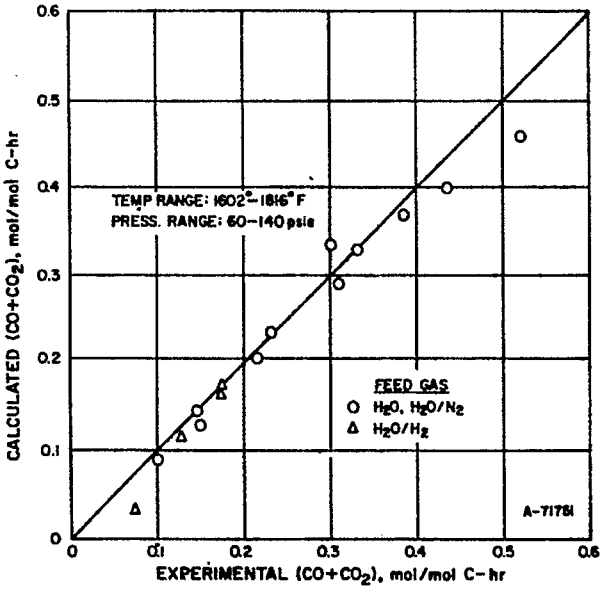

Figure 6d-33. CONSISTENCY BETWEEN CALCULATED AND EXPERIMENTAL CARBON OXIDES YIELDS FROM FLUID-BED GASIFICATION OF DISCO CHAR (May et al.[19])

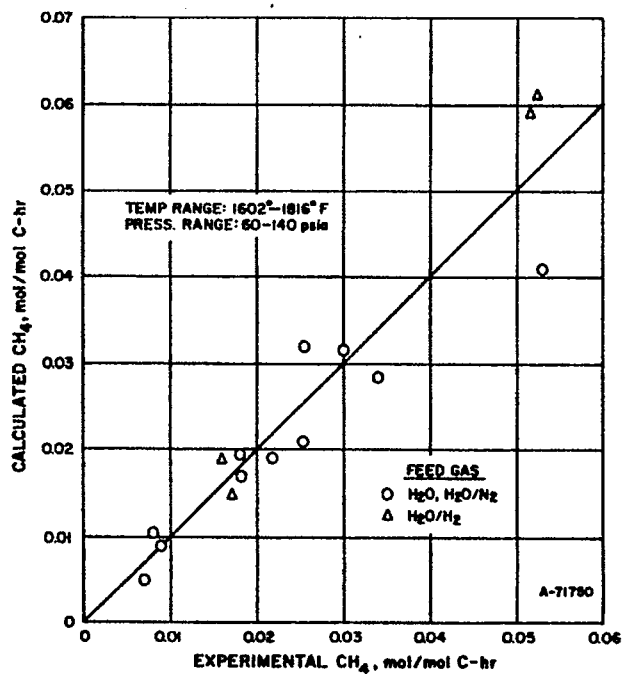

Figure 6d-34. CONSISTENCY BETWEEN CALCULATED AND EXPERIMENTAL METHANE YIELDS FROM FLUID-BED GASIFICATION OF DISCO CHAR (May et al.[19])

Although the model developed appears applicable for kinetically describing gasification behavior for a variety of coals in steam-hydrogen containing gases, systematic variations between predicted and calculated methane yields have been noted when oxygen is used in the feed gas. Although carbon oxides yields have been adequately predicted for the systems examined, experimental methane yields obtained by May et al.[19], as well as in HYGAS-associated tests, are generally higher than predicted. Whether this is due to some activating process that occurs when char undergoes combustion with oxygen, or whether it is due to some experimental difficulty in defining fluid-bed temperature in such a system has not been determined.

The assumption of Reaction III in the model proposed results in interesting behavior of gasification systems in terms of the methane yields predicted under certain conditions. Frequently it has been noted that the $p_{CH_4}/p^2_{H_2}$ ratio in product gases from integral fluid-bed systems for gasification of coal or char with steam-hydrogen containing gases is greater than the equilibrium constant for the graphite-hydrogen-methane system. This has often been interpreted as corresponding to a situation in which the coal or char has a thermodynamic activity greater than unity with respect to graphite. The model proposed in this report offers two explanations for this phenomenon. When coal is used as a feed material, a rapid-rate methane reaction occurs; the methane yield resulting from this step is kinetically determined, independent of methane partial pressure. Under certain conditions, then, values of the ratio $p_{CH_4}/p^2_{H_2}$ greater than that corresponding to equilibrium with respect to the graphite-hydrogen-methane system can result. Values of the $p_{CH_4}/p^2_{H_2}$ ratio greater than that corresponding to the equilibrium considered can also occur during low-rate gasification of coal char according to the model. This is illustrated in Figure 6d-35, where gas yields in a hypothetical fluid bed for char gasification with a pure steam feed gas have been computed using the model developed. The reason for the behavior illustrated is that at intermediate values of hydrogen partial pressure, the rate of Reaction III, which produces methane, is greater than the rate of Reaction II in which methane is consumed when a potential for carbon deposition via this reaction exists. The partial pressure dependencies defined in the correlations developed are such, however, that at sufficiently high hydrogen partial pressure Reaction II dominates, and equilibrium for this reaction is approached.

The qualitative trends exhibited in Figure 6d-35, and even the magnitudes of these trends, bear a striking resemblence to a similar plot given by Squires[20] to correlate activities of coals and chars for equilibrium of the char-hydrogen-methane system with temperature and pressure.

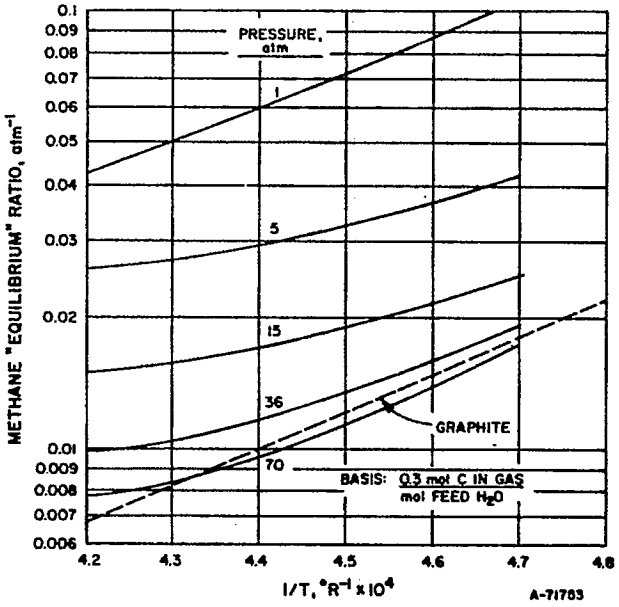

Figure 6d-35. CALCULATED VARIATIONS OF THE METHANE "EQUILIBRIUM" RATIO ($p_{CH_4}/p_{H_2}^2$) FROM GASIFICATION OF CARBON WITH STEAM IN A BACK-MIXED REACTOR

6d.7 References Cited

1. Feldkirchner, H. L. and Johnson, J. L., "High Pressure Thermobalance," Rev. Sci. Instrum. 39, 1227-29 (1968) August.

2. Blackwood, J. D. and McCarthy, D. J., "The Mechanism of Hydrogenation of Coal to Methane," Aust. J. Chem. 19, 16-33 (1958) February.

3. Feldkirchner, H. L. and Linden, H. R., "Reactivity of Coals in High-Pressure Gasification With Hydrogen and Steam," I&EC Process Des. Dev. 2, 153-62 (1963) April.

4. Moseley, F. and Paterson, D., "The Rapid High-Temperature Hydrogenation of Coal Chars. Part 1: Hydrogen Pressures Up to 100 Atmospheres," J. Inst. Fuel 38, 13-23 (1965) January; Part 2: "Hydrogen Pressures Up to 1,000 Atmospheres," ibid., 378-91 (1965) September.

5. Zahradnick, R. L. and Glenn, R. A., "Direct Methanation of Coal," Paper presented at 158th National Meeting of the American Chemical Society, Division of Fuel Chemistry, New York, September 7-12, 1969.

6. Birch, T. J., Hall, K. R. and Urie, R. W., "Gasification of Brown Coal With Hydrogen in a Continuous Fluidized-Bed Reactor," J. Inst. Fuel 33, 422-35 (1960) September.

7. Hiteschue, R. W., Friedman, S. and Madden, R., "Hydrogasification of a High-Volatile A Bituminous Coal," U. S. Bur. Mines Rep. Invest. No. 6376 (1964).

8. Zielke, C. W. and Gorin, E., "Kinetics of Carbon Gasification," Ind. Eng. Chem. 49, 396-403 (1957) March.

9. Zielke, C. W. and Gorin, E., "Kinetics of Carbon Gasification. Interaction of Hydrogen With Low Temperature Char at 1500° to 1700°F," Ind. Eng. Chem. 47, 820-25 (1955) April.

10. Goring, G. E. et al., "Kinetics of Carbon Gasification by Steam. Effect of High Temperature Pretreatment on Reactivity of Low Temperature Char to Steam and Carbon Dioxide," Ind. Eng. Chem. 44, 1051-57 (1952) May.

11. Goring, G. E. et al., "Kinetics of Carbon Gasification by Steam. Mechanism of Interaction of Low Temperature Char and Steam-Hydrogen Mixtures at 1600°F," Ind. Eng. Chem. 45, 2586-91 (1953) November.

12. Blackwood, J. D., Cullis, B. D. and McCarthy, D. J., "Reactivity in the System Carbon-Hydrogen-Methane," Aust. J. Chem. 20, 1561-70 (1967) August.

13. Blackwood, J. D., "The Reaction of Carbon With Hydrogen at High Pressure," Aust. J. Chem. 12, 14-28 (1959) February.

14. Sastry, N. V. S., Mallikarjunan, M. M. and Vaidyeswaran, R., "Kinetic Investigations of Hydrogasification of Semicoke in an Integral Reactor," Brennst.-Chem. 50, 363-67 (1969) December (German test).

15. Blackwood, J. D. and McGrory, F., "The Carbon-Steam Reaction at High Pressure," Aust. J. Chem. 11, 16-33 (1958) February.

16. Curran, G. P. and Gorin, E., "Phase II, Bench-Scale Research on CSG Process — Laboratory Physico-Chemical Studies, U. S. Office of Coal Research R&D Report No. 16, Interim Report No. 3, Book 2, Washington, D. C.: U. S. Government Printing Office, 1970.

17. Blackwood, J. D., "The Kinetics of the System Carbon-Hydrogen-Methane," Aust. J. Chem. 15, 397-408 (1962) August.

18. Wen, C. Y. and Huebler, J., "Kinetic Study of Coal Char Hydrogasification," I&EC Process Des. Dev. 4, 147-54 (1965) April.

19. May, W. G., Mueller, R. H. and Sweetser, S. B., "Carbon-Steam Reaction Kinetics From Pilot Plant Data," Ind. Eng. Chem. 50, 1289-96 (1958) September.

20. Chambers, R. P. and Boudart, M., "Lack of Dependence of Conversion on Flow Rate in Catalytic Studies," J. Catal. 6, 141-45 (1966) August.